CLIMATE EXTREMES OVER THE MID-ATLANTIC STATES: A REGIONAL APPROACH

by

Emily K. Aiken

A thesis submitted to the Faculty of the University of Delaware in partial fulfillment of the requirements for the degree of Master of Science in Geography

Winter 2018

CLIMATE EXTREMES OVER THE MID-ATLANTIC STATES: A REGIONAL APPROACH

by

Emily K. Aiken

Approved: ____

Sara Rauscher, Ph.D.
Professor in charge of thesis on behalf of the Advisory Committee

Approved: ____

Delphis Levia, Ph.D.
Chair of the Department of Geography

Approved: ____

Estella Atekwana, Ph.D.
Dean of the College of Earth, Ocean, and Environment

Approved: ____

Ann L. Ardis, Ph.D.
Senior Vice Provost for Graduate and Professional Education

ACKNOWLEDGMENTS

I wish to thank the North American Regional Climate Change Assessment Program (NARCCAP) for providing the data used in this paper. NARCCAP is funded by the National Science Foundation (NSF), the U.S. Department of Energy (DoE), the National Oceanic and Atmospheric Administration (NOAA), and the U.S. Environmental Protection Agency Office of Research and Development (EPA). I acknowledge the World Climate Research Programme's Working Group on Regional Climate, and the Working Group on Coupled Modelling, former coordinating body of CORDEX and responsible panel for CMIP5. I also thank the climate modelling groups (listed in Table 2.2 of this paper) for producing and making available their model output. I also acknowledge the Earth System Grid Federation infrastructure an international effort led by the U.S. Department of Energy's Program for Climate Model Diagnosis and Intercomparison, the European Network for Earth System Modelling and other partners in the Global Organisation for Earth System Science Portals (GO-ESSP). I also wish to thank Dr. Park Williams of Columbia University, who generously shared his PDSI code and data. This publication was made possible by the National Science Foundation EPSCoR Grant No. IIA-1301765 and the State of Delaware.

On a personal note, I would like to thank my advisor, Dr. Sara Rauscher, for her endless patience and unflagging support. I would like to thank my other committee members, Dr. Dana Veron and Dr. Tobias Kukulka, for generously sharing their time and expertise. I owe thanks as well to the entire Geography Department at the

University of Delaware, all of whom have provided support and encouragement in a thousand small ways. And I would like to thank my fiancé Erin, whose love turned a dream into reality.

TABLE OF CONTENTS

LIST OF TABLES

LIST OF FIGURES

ABSTRACT

Much of our current risk assessment, especially for extreme events and natural disasters, comes from the assumption that the likelihood of future extreme events can be predicted based on the past. However, as global temperatures rise, established climate ranges may no longer be applicable, as historic records for extremes such as heat waves and floods may no longer accurately predict the changing future climate. To assess extremes (present-day and future) over the contiguous United States, I used NOAA's Climate Extremes Index (CEI), which evaluates extremes in maximum and minimum temperature, extreme one-day precipitation, days without precipitation, and the Palmer Drought Severity Index (PDSI). The CEI is a spatially sensitive index that uses percentile-based thresholds rather than absolute values to determine climate "extremeness," and is thus well-suited to compare extreme climate across regions. I used regional climate model data from the North American Regional Climate Change Assessment Program (NARCCAP) and the Coordinated Regional Downscaling Experiment (CORDEX) to compare a late 20th century reference period to a mid-21st century business as usual (RCP8.5 and SRES A2) greenhouse gas-forcing scenario. Additionally, I used CMIP3 and CMIP5 data to compare regional climate model data to its global climate model boundary forcings, to see what added value the regional climate models provide in the Mid-Atlantic region. Results show a universal increase in extreme temperatures across all models, with annual average maximum and minimum temperatures exceeding historic 90th percentile thresholds over more than 90% of the area assessed by 2068. Results for precipitation indicators have greater

spatial variability from model to model, but indicate an overall movement towards less frequent but more extreme precipitation days in the future.

Chapter 1

INTRODUCTION

Anthropogenic climate change is a complex global issue with repercussions for virtually every facet of human life, from public health to economics to ecology. Understanding and effectively communicating about climate extremes is one of the most important problems that climate scientists face. One major problem is the issue of nonstationarity: much of our understanding of weather-related risk is based on historic trends, but climate is neither static nor stationary (Barros 2014). As climatic mean and variance change, so will the probability of extreme climate hazards such as heat waves.

Climate scientists often express climate change in terms of changes in mean and variance. For example, Diffenbaugh et al. (2008) identified climate-change "hot-spots" over the US using mean temperature and precipitation. While changes in mean conditions across the United States are well-documented in climate literature, this has not always been accompanied by an equal understanding of changes in extremes (Gleason 2008). For instance, the first iterations of the Intergovernmental Panel on Climate Change (IPCC) Assessment report addressed climate change primarily through trend analysis of changes in mean conditions (SAR; Houghton et al. 1995). Some analysis of extremes and climate variability was added in the Third (TAR; Houghton et al. 2001) and Fourth Assessment reports (AR4; Solomon et al. 2007) but in keeping with the global focus of the IPCC reports, these analyses were primarily done on a continental or global scale, not a regional one. While changes in mean conditions are useful metrics for detecting climate change signal and expressing change, they do not show the entire picture, as extreme events have the greatest impact on natural and human systems (Peterson et al. 2008).

In addition, many climate extremes have no clear universal definition or threshold. What counts as an ordinary day in Florida could be a severe heat warning in New England, so any metric must by necessity be spatially sensitive and relative to historic ranges. The questions that matter to our colleagues outside of climate science are often measures of extremes: how many more extreme heat waves per year should we expect, with associated heat-related hospitalizations and fatalities? How many more droughts and floods, how severe, and where will they occur? In short, when we ask what the natural and human impacts of climate change will be, often we are asking "what changes in climate extremes can we expect?"

This work will address the following research questions:

1. What patterns in climate extremes (heat waves, flood, drought, etc.) are currently observable over the continental US (CONUS)?

2. In particular, what patterns in climate extremes (heat waves, flood, drought, etc.) are currently observable over the Mid-Atlantic region?

3. What changes in climate extremes are projected by climate models to occur in the future?

4. Do regional climate models (RCMs) produce different spatial trends than high-resolution global climate models (GCMs)? If so, what trends exist, and what causes might we attribute to the difference?

The objectives of the proposed research are:

1. Calculate the U.S. Climate Extremes Index (CEI) for both the CONUS and the Mid-Atlantic, over two time periods: one late twentieth century, and one mid-21st century;

2. Create map series for each of the individual components of the CEI, highlighting spatial trends and changes over time;
3. Compare the CEI (both calculated index and components) using regional model simulations from the North American Regional Climate Change Assessment Program (NARCCAP) and global climate model simulations from the Coupled Model Intercomparison Project version 3 (CMIP3);
4. Compare these results to selected high-resolution models from the Coupled Model Intercomparison Project version 5 (CMIP5) to evaluate how the continuously evolving field of climate modeling – and our continuously evolving understanding of climate change – affects projections of future scenarios.

1.1 Extreme Heat in the United States

Episodes of extreme heat and cold can have serious impacts on society, agriculture, and health. In particular, extreme heat is the number one cause of weather-related death, with hundreds of fatalities annually, and contributes to even more heat-related illnesses (National Weather Services 2012). High temperatures can also exacerbate cardiovascular and respiratory illness; children, the elderly, people with chronic illnesses, and urban populations in poverty are all at especially high risk (Habeeb et al. 2015). High temperatures at night have an even more pronounced correlation to heat-related mortality, because the body does not get a reprieve to regulate temperature during the cooler nighttime (Serofim et al. 2016). Increased heat waves will put even more stress on aging infrastructure in many urban areas, especially along the heavily urbanized Atlantic corridor from Washington, D.C. to New York City (Horton et al. 2014).

The effects of changing temperature variance can have indirect health and ecological impacts as well. Seasonal temperature extremes can impact the spread of invasive species, as well as vector-borne illnesses such as Lyme disease (Canning-clode et al. 2011, Monaghan 2015). Lyme disease is concentrated heavily in the Northeast, especially in the region from Maryland to Connecticut, and is the most commonly reported vector-borne illness in the United States (CDC 2015). On the other end of the spectrum, episodic events of extreme cold can serve as a critical ecological 'reset' mechanism, offsetting the effects of increasing mean temperature. Transient cold spells along the mid-Atlantic coastline have been shown to limit the range expansion of marine invasive species from the Caribbean, despite warming average ocean temperatures (Canning-clode et al. 2011).

Observations dating back to 1900 show that the 21^{st} century has the largest spatial extent of record-breaking and extreme monthly minimum and maximum temperatures (Wuebbles et al. 2014). Heat wave temperatures in the CMIP5 RCP8.5 scenario are projected to increase from 5 to 7 degrees Celsius across the continental U.S. by the end of the 21^{st} century (Wuebbles et al. 2014). CMIP5 projections using the RCP8.5 scenario also found that current annual maximum temperature extremes are projected to occur every year over the entire U.S., excluding parts of Alaska (Wuebbles et al. 2014). However, these projections show little spatial variance, with temperatures increasing consistently across large swaths of the continent. By including regional climate models, in addition to the global CMIP3 and CMIP5 data, I will examine spatial trends in greater detail.

1.2 Extreme Precipitation in the United States

Out of all the natural hazards the United States is faced with, flooding has the potential to cause the greatest harm, both in terms of economic and property damage, and by endangering the safety and wellbeing of human communities (Brody et al. 2007). It is estimated that flooding causes billions of dollars in economic harm annually, and this number only continues to rise (Brody et al. 2007). In terms of potential socioeconomic impacts, intensified storms and extreme precipitation events could contribute to floods which threaten urban coastal areas. Several studies have already identified the Delmarva region as a potential hotspot for accelerated sea level rise, which can have a synergistic effect with extreme precipitation events to increase the intensity of flooding (Ezer and Atkinson 2014, Sallenger et al. 2012). Current estimates suggest that between 450,000 and 2.3 million people in the Mid-Atlantic are at risk from sea level rise alone over the next century, not counting the increased risk from storm surges and heavy precipitation (CCSP 2009). Additionally, many coastal cities, including New York and Philadelphia, use combined sewer and stormwater systems that are vulnerable to flooding, increasing the risk of waterborne illness (NCA 2014). A study of stormwater infrastructure around Washington, D.C. found evidence that as future precipitation intensifies, current stormwater retention basins will likely not be able to keep up with the increased load (Moglen & Vidal 2014).

While the majority of the United States shows little change in the frequency of flood events, there are some exceptions. Complicating any examination of hydrological trends are changes in anthropogenic land use and management, which can affect the frequency of floods, independent of changes to precipitation patterns (Peterson et al. 2013). Current observational data indicates that flooding is increasing in parts of the Midwest, and decreasing in the Southwest (Peterson et al. 2013). Additionally, increasing trends in flood magnitude over the eastern half of the United States have been observed in multiple studies, especially in the area of the northern Appalachian Mountains up to New England (Peterson et al. 2013, Collins 2008, Villarini and Smith 2010, Smith et al. 2010, Hodgkins 2010, Hirsch and Ryberg

2012). However, the exact magnitude and causes of these changes are still poorly understood.

Analysis of CMIP5 data shows an increasing trend in both the frequency and intensity of precipitation events and the fraction of annual total precipitation that falls during the heaviest 1% of daily precipitation events (Wuebbles et al. 2014). By the end of the century, the fraction of annual precipitation falling during extreme events is projected to increase by 50% in the RCP4.5 scenario, and by 90% in the RCP8.5 scenario. This change is especially noticeable over the eastern and western coastal regions, with the central U.S. showing a smaller percent increase (Wuebbles et al. 2014). In general, confidence in model predictions of precipitation is lower than confidence in model predictions of temperature; the standard deviation between models is often greater than the signal when examining extreme precipitation events (Wuebbels et al. 2014).

While model simulations predict an overall increase in precipitation over the next century, estimates of magnitude and seasonal timing of these changes vary considerably between models (Najjar 2000). Recent studies indicate that some of this uncertainty may be linked to the influence of multidecadal climatic cycles, such as the Atlantic Multidecadal Oscillation and El Niño Southern Oscillation, on extreme precipitation events (Curtis 2007, Ning 2015). Spatial heterogeneity is also a factor; an examination of multiple global precipitation indices showed that changes in precipitation patterns were much more spatially heterogeneous than temperature changes (Donat et al. 2013). However, multiple studies agree that the frequency of days with heavy precipitation have been increasing across the eastern United States, especially in New England (Peterson et al. 2013, Karl et al. 2009, Kunkel et al. 2013).

1.3 Study Area

Two primary study areas were taken into consideration in this analysis, at two different scales: first, the CEI was calculated over the entire continental United States (CONUS). Then, the CEI was calculated again, but solely over the Mid-Atlantic region. This two-pronged approach has multiple advantages; calculating the CEI over the full CONUS allows for any changes to the Mid-Atlantic CEI to be put into perspective, and also allows for examination of any synoptic-scale spatial trends. There is no singular universal definition for the boundaries of the Mid-Atlantic region, and many studies fold the Mid-Atlantic states into the Northeast and Southeast regions (Najjar et al. 2000, Polsky et al. 2000, NCA 2014, Karl and Koss 1984). For this study, I used the regional boundaries specified by Polsky et al. (2000), specifically inclusive of Delaware, Maryland, Pennsylvania, Virginia, West Virginia, the District of Columbia, and parts of New York, New Jersey, and North Carolina.

The 2014 National Climate Assessment of the Northeast region (which overlaps heavily with the Mid-Atlantic region defined above as a study area) characterizes the region as a high-density urban corridor along the Atlantic coast, and one of the most heavily developed environments in the world (NCA 2014). Physically, the Mid-Atlantic region encompasses a broad range of physiographic regions and land cover types, from coastal plain up to the Appalachian plateau (Polsky et al. 2000). Intra-regional climate variation reflects the influences of latitude, elevation, and physiography: the southern states are relatively low-latitude and low-elevation, experiencing warmer temperatures and greater precipitation. In contrast, the northernmost part of the region is comparatively high-elevation and high-altitude, experiencing cooler average temperatures and precipitation more strongly influenced by lake effects (Polsky et al. 2000).

The Mid-Atlantic is notably underserved by current regional climate research. While there have been many studies in the past few years focusing on the influence of specific teleconnections, many overview papers focusing on the Mid-Atlantic regional climate date back over 15 years – prior to the release of the IPCC Third Assessment Report, while we are now on the Fifth (Najjar et al. 2000, Polsky et al. 2000). A previous study of climate change hotspots identified the southwestern United States as an area of primary concern, with the Mid-Atlantic showing relatively mild response to climate change (Diffenbaugh et al. 2008). However, there are several reasons why further analysis could be valuable. First, the fact that climate change may be *more* severe in some areas does not negate potential climate impacts elsewhere, and local officials and planners still need to be informed on the magnitude of changes they should likely expect. Second, the Diffenbaugh et al. 2008 paper used only monthly CMIP3 data and a single high-resolution nested model, whereas now we have access to CMIP5 data as well as a range of regional climate models, integrating multiple metrics at different time scales. Finally, the goal of Diffenbaugh et al. was to quantify sensitivity to climate change by calculating hotspots using seasonal mean and standard deviation. The Climate Extremes Index, by contrast, is explicitly focused on changes to the tails of the climate distribution, rather than on mean values for temperature and precipitation.

1.4 The U.S. Climate Extremes Index

The U.S. Climate Extremes Index (CEI) was developed by Thomas Karl of NCDC, as a tool to quantify climate change as changes in extremes, rather than changes in mean conditions (Gleason et al. 2008). The CEI is a percentile-based index, calculated at each gridpoint based on historic climate values. In other words, it measures relative change at each gridpoint, rather than using fixed thresholds to define heat wave, drought, etc. The original CEI was developed in 1996, based on an aggregate set of climate indicators in an attempt to produce a single, nonparametric index of how the climate is becoming more extreme (Karl et al. 1996). It was later revised by NOAA in 2008, to include additional data not available at the time of the original index's publishing, and to modify the way that certain components were calculated (Gleason et al. 2008).

Developing indices of "extremeness" is a difficult task: quantifying extremeness will produce different results when calculated based on arbitrary thresholds, defined events such as hurricanes, or socioeconomic impact (Gallant et al. 2014). Other extremes, such as heavy precipitation or heat waves, are defined primarily by their place on the tails of the normal climate distribution (Peterson et al. 2013). None of these approaches can be deemed objectively wrong, but all have different applications. The CEI is not a universal index of all climate extremes; it does not attempt to quantify changes in natural disasters such as floods or tornadoes (Gallant et al. 2014). However, as a broad assessment of multidecadal changes in both temperature and precipitation extremes, it has successfully been applied in the United States, Europe, and Australia to identify consistent trends, especially towards widespread heat extremes (Gallant et al. 2014).

The CEI's primary strength is also its primary weakness: it is a simple, nonparametric index that aims to distil a large amount of complex climate information into a single score that represents whether an area is becoming more or less "extreme" (Gallant et al. 2014). However, since the CEI includes extremes from both tails of the distribution, the index itself does not convey the sign of these changes. Nor does it indicate which temperature or precipitation metrics are contributing most of the extremeness. Therefore, in accordance with NOAA's recommendations on interpretation of the CEI, I have included analysis of each individual component of the CEI separately, to supplement the combined index (Gleason et al. 2008).

Additionally, I have added a new component to my analysis. The standard CEI as computed by NOAA is an area average, and thus produces a single annual or seasonal score for the entire area over which the CEI is calculated. NOAA currently produces an annual and seasonal report of regional CEI using the nine U.S. Standard Regions as defined by Karl and Koss (1984, Fig. 1.1). While these regions are broadly used in climate analyses, changes in climate trends along the whole of the East Coast may not necessarily be applicable to the Mid-Atlantic. For example, intensified hurricane activity in Florida may not reach as far north as Virginia, and expected winter conditions in New England are very different from coastal Maryland and Delaware. A more specific spatial analysis, one that is not aggregated by region, could highlight fine-scale detail and processes that are otherwise lost. To complement the standard CEI, which calculates area average at each time step, I calculated the average CEI over time at each grid point to create a series of CEI maps. This allows for inclusion of spatial trend analysis, which is absent from traditional calculations of the CEI.

1.5 Approach

In order to assess how climate extremes will change in the future, we turn to climate models. There is an impressive body of work dedicated to projections of global change, including recent IPCC reports; however, the ability to accurately represent smaller-scale regional changes is a relatively recent development. As computational power advances and climate models become more sophisticated, higher-resolution calculations become possible. Increasing climate model resolution by a factor of two results in a factor of ten increase in required computing power, so in order to keep computational costs from becoming prohibitive, global climate models are by necessity limited in resolution (UCAR 2011). As of the Intergovernmental Panel on Climate Change (IPCC) Fourth Assessment Report (AR4), average resolution for global climate models was roughly 110 km per grid cell (UCAR 2011). For reference, the entire state of Delaware is roughly 154 km in length (delaware.gov). Therefore, one of the primary challenges of regional climate assessment is a matter of scale, as many important climate processes cannot be adequately represented at a global grid scale.

Climate modelers have developed multiple downscaling techniques in order to simulate local and regional processes with greater accuracy than global climate models alone can provide. One such downscaling technique, statistical downscaling, relies on a combination of large-scale climate factors and local physiographic features to create a statistical model, into which global simulation data can be fed to estimate local climate characteristics (TAR 2001). Statistical downscaling is computationally inexpensive, but relies on the assumption that present-day statistical relationships will continue to hold true under future climate forcings (TAR 2001). An alternative, potentially more robust but also more computationally expensive, is to use regional climate models (RCMs). RCMs take their boundary conditions from global climate simulations, but then use those boundary conditions to calculate effects of sub-GCM grid scale forcings and atmospheric variables (TAR 2001). Because regional models are run over a small area of interest, reducing the total number of grid points, they are less computationally expensive than a global model run at equivalent resolution, and thus can be run at a finer grid scale. Ideally, regional climate models provide a more accurate dynamic simulation of small-scale climate forcings under varying conditions than statistical downscaling, while being less computationally expensive than high-resolution global modeling. As part of this study, we will compare output from North American Regional Climate Change Assessment Program (NARCCAP) regional climate models to the global climate models from which they take their boundary conditions, to assess what fine-scale trends in extremes the regional models highlight.

Global climate models can capture synoptic-scale climatic features such as the jet stream and mid-latitude cyclones, but are not necessarily equipped to accurately resolve mesoscale features such as tropical storms, lake effects, and land-sea interactions. Nor is model grid scaling solely a matter of finer detail, like zooming in on an image. Better resolution of these small-scale phenomena can reveal enhanced climate responses: one study of future changes in snowmelt-driven runoff timing over the western US showed that a high-resolution model, which better represented topographic complexity, also showed an amplified snow-albedo feedback which significantly changed the temperature response (Rauscher et al. 2008). Specifically in the case of mid-Atlantic climate, a study using empirical downscaling methods showed that appropriate application of downscaling generally reduced inter-GCM uncertainty, showing the same increases in precipitation as the raw GCM projections but with a much smaller magnitude (Ning et al. 2012). This mid-Atlantic study used empirical downscaling based on self-organizing maps, but empirical downscaling does not change the underlying physics of the models used or resolve small-scale phenomena. Using regional climate models, such as those used in the NARCCAP and CORDEX data sets, could potentially highlight even further detail at the mesoscale.

Figure 1.1: U.S. Standard Regions for Temperature and Precipitation (Karl and Koss, 1984)

Chapter 2

DATA AND METHODS

2.1 Observations

Table 2.1 List of observational datasets to be used in the analysis.

Variables	Source	Resolution	Type	Time Period
Temperature, precipitation	Maurer et al. (2002)	1/8° x 1/8°	Gridded	1949-2010

The current NOAA-produced CEI report uses data from NCEI's nClimGrid, as of October 2016. Prior to October 2016, the CEI was calculated using station data from the U.S. Historical Climatology Network (USHCN) for temperature data, and from the Global Historical Climatology Network (GHCN) for daily precipitation (NOAA 2015). These station data points are then averaged into 1° × 1° grid cells and evaluated for completeness, to ensure that at least 90% of grid cells contain at least one station (Gleason 2008).

Due to limited temporal coverage and availability of observational data at comparable resolutions, only one observational data set was used in this analysis: a set of gridded observational data produced by Maurer et al. of Santa Clara University, and provided to the public at http://www.engr.scu.edu/~emaurer/gridded_obs/index_gridded_obs.html. While observational uncertainty is a factor, the CEI I calculated from this observational data was validated against the CEI as calculated by NOAA, publicly available on their website at https://www.ncdc.noaa.gov/extremes/cei/graph.

2.2 Models

For the purposes of this analysis, I used regional model projections from NARCCAP and CORDEX, as well as global climate model data from CMIP3 and CMIP5. This climate model data is already gridded, so the completeness evaluation used for observational data above was not necessary. However, all model data was regridded bilinearly onto a common 1/8° x 1/8° grid to allow for easier direct comparison and ensemble means. Two multidecadal time periods were compared: a late 20th century period, from 1968 to 1998, and a mid-21st century period, from 2038 to 2068. The exception to this rule was CMIP3 data, whose mid-21st century period was run from 2046 to 2065 due to data availability. These time periods were selected for maximum overlap between various observational and model outputs, as certain projects such as NARCCAP were run over limited time slices. See Table 2.2 below for a list of all models used in this analysis.

Table 2.2 List of models used in the analysis

Project	Model	Type	Organization	Experiment	Horizontal Resolution	Data Access
CMIP3	CCSM3	GCM	NCAR	SRES A2	1.4°x1.4°	Public via ESGF
CMIP3	CGCM3.1	GCM	CCCMA	SRES A2	1.9°x1.9°	Public via ESGF
CMIP3	GFDL-CM2.1	GCM	NOAA-GFDL	SRES A2	2.0°x 2.5°	Public via ESGF
NARCCAP	CRCM	RCM	OURANOS/UQAM	SRES A2	50km	Public
NARCCAP	ECPC/ECP2	RCM	UC San Diego/Scripp	SRES A2	50km	Public
NARCCAP	HRM3	RCM	Hadley Centre	SRES A2	50km	Public
NARCCAP	MM5I	RCM	Iowa State University	SRES A2	50km	Public
NARCCAP	RCM3	RCM	UC Santa Cruz	SRES A2	50km	Public
NARCCAP	WRFP/WRFG	RCM	Pacific Northwest Nat'l Lab	SRES A2	50km	Public
CMIP5	EC-EARTH	GCM	ENES	RCP 8.5	1.1215°x1.125°	Public via ESGF
CMIP5	CanESM2	GCM	CCCMA	RCP 8.5	2.81°x2.79°	Public via ESGF
CORDEX	HIRHAM5	RCM	DMI	RCP 8.5	0.44°x0.44°	Public via ESGF
CORDEX	RCA4	RCM	SMHI	RCP 8.5	0.44°x0.44°	Public via ESGF

All project data used in this experiment (CMIP3, CMIP5, NARCCAP, CORDEX) are made available with a full suite of climate variables; a full list of variables with standard output for CMIP can be found at http://www-pcmdi.llnl.gov/ipcc/standard_output.html. For this project, the variables used were maximum temperature (tasmax), minimum temperature (tasmin), daily precipitation (pr), and mean surface temperature (tas). Mean surface temperature was not used directly in the analysis, but indirectly to estimate PET during PDSI calculations.

2.2.1 CMIP3

The Coupled Model Intercomparison Project, or CMIP, was a joint effort by the Working Group on Coupled Modelling (WGCM) under the World Research Climate Programme. The project began in 1995, with the majority of CMIP data archived on the Program for Climate Model Diagnosis and Intercomparison website (PCMDI) for use by climate scientists and other researchers. CMIP3 is the third phase of the project, and provided much of the material underlying the IPCC Fourth Assessment Report (CMIP 2010).

CMIP3 includes “realistic” scenarios as defined by the IPCC Special Report Emissions Scenarios; there are a total of 40 SRES storylines, representing a comprehensive range of possible futures. However, a majority of these scenarios are slight variations of one another, exploring different assumptions in energy technology (Nakićenović 2000). In brief, the scenarios fall along two axes: economic-environmental, and global-regional, and in doing so can be said to fall into four archetypes, also referred to as the four “families” of storylines (Nakićenović 2000). The economic-environmental axis represents the degree to which policy and public opinion favor economic growth at the cost of environmental factors. The global-regional axis represents the degree to which developing technology continues to foster globalization; this can also be read as whether technology is assumed to be largely homogeneous or heterogeneous worldwide in the future. For this analysis, I focused on the A2, or regional-economic storyline: this assumes a heavy emphasis on economic growth and limited movement of ideas and people across regions, with resultant high emissions.

2.2.2 CMIP5

CMIP5 is the most recent iteration of the Coupled Model Intercomparison Project, completed for the IPCC Fifth Assessment Report. Between the time of CMIP3 and CMIP5, the IPCC discontinued use of the Special Report Emissions Scenarios, replacing them with Representative Concentration Pathways, or RCPs. Rather than acting as specific socioeconomic scenarios, the RCPs represent a broad range of climate outcomes, and are defined by total radiative forcing (IPCC 2014). No exact one-to-one comparison can be made between the SRES scenarios and the RCP pathways; for instance, it would be misleading to say that SRES A2 is “equivalent” to RCP 8.5, as the two were derived by wholly different methodologies. However, for purposes of this analysis, we will be using the RCP 8.5 scenario. Like the SRES A2 storyline, it represents the most extreme climate forcings out of its scenario set, and most closely resembles the current path of observed trends; thus, using A2 and RCP 8.5 allows for the best possible parallel between CMIP3 and CMIP5 results.

2.2.3 NARCCAP

NARCCAP is an ensemble of dynamically downscaled regional climate simulations, using 50 km grid spacing over North America. Figure 2.1 shows the complete NARCCAP domain; for the purposes of this analysis, ocean gridpoints were masked, and only the continental U.S. was taken into consideration. All NARCCAP data is based on the A2 scenario from the IPCC Special Report Emissions Scenarios; this scenario is at the higher end of the emissions scenarios, and roughly tracks with current trajectory of emissions, provided no major policy changes or dramatic shifts towards renewable energy are enacted (NARCCAP 2008). NARCCAP simulations exist for a 20th century historical simulation (1968-1998) and a mid-21st century future simulation (2038-2068).

Table 2.3: GCM-RCM pairings in NARCCAP. RCMs are on the vertical axis, GCMs on the horizontal.

	CCSM	CGCM3	GFDL	HadCM3
CRCM	X	X		
ECP2			X	X
HRM3			X	X
MM5I	X			X
RCM3		X	X	
WRFG	X	X		

The NARCCAP project uses twelve GCM-RCM pairings, from 6 different RCMs and 4 different GCMs for boundary conditions. The GCMs used as boundary conditions for NARCCAP are all taken from CMIP3 (NARCCAP 2008). See Table 2.3 above for available pairings. All twelve NARCCAP pairings were used in this analysis; however, HadCM3 had to be excluded from the CMIP3 analysis, as future projections were only available for the end of 21st century (2071-2100) period.

2.2.4 CORDEX

Like NARCCAP, CORDEX is a regional climate downscaling project, using boundary conditions from GCMs to drive RCMs. However, there are two important distinctions between CORDEX and NARCCAP. Where NARCCAP was specifically North American, CORDEX is an international coordinated project, with teams of scientists working on common domains all over the globe; this project focuses on the North American domain, but CORDEX data also exists for most major land areas. CORDEX is also more recent – in fact, as of 2017, CORDEX is still ongoing and receiving regular updates (CORDEX.org). Where NARCCAP uses CMIP3 data, CORDEX uses the more updated CMIP5. As above, this analysis will focus on the RCP 8.5 scenario, which is the closest analogue to the SRES A2 scenario, and will also represent the most dramatic (while still realistic) potential climate forcing for future simulation.

Table 2.4: GCM-RCM pairings in CORDEX. RCMs are on the vertical axis, GCMs on the horizontal.

	EC-EARTH	CCCma-CanESM2
HIRHAM5	X	
RCA4	X	X

The CORDEX project is still in progress; over 50 different RCMs have been officially registered with CORDEX as of July 2016 (CORDEX.org). However, not all models provide simulations yet, and there is no single central CORDEX archive or master list of available simulations. For this project, I used all currently available CORDEX simulations for the North American domain; as of December 2016, only three GCM-RCM pairings had all the requisite variables in the appropriate time scales.

This data was provided by the same ESGF data hub as the CMIP3 and CMIP5 data. See Table 2.4 above for available GCM-RCM pairings.

2.3 The U.S. Climate Extremes Index

The CEI, as calculated by NOAA, is the arithmetic mean of five indicators:

1. the sum of (a) percentage of the United States with maximum temperatures much below normal and (b) percentage of the United States with maximum temperatures much above normal;

2. the sum of (a) percentage of the United States with minimum temperatures much below normal and (b) percentage of the United States with minimum temperatures much above normal;

3. the sum of (a) percentage of the United States in severe drought based on the Palmer Drought Severity Index (PDSI) and (b) percentage of the United States with severe moisture surplus based on the PDSI;

4. twice the value of the percentage of the United States with a much greater-than-normal proportion of precipitation derived from extreme 1-day precipitation events;

5. the sum of (a) percentage of the United States with a much greater-than-normal number of days with precipitation and (b) percentage of the United States with a much greater-than-normal number of days without precipitation. (Gleason 2008)

NOAA provides a plot of the historic CEI going back to 1910 at https://www.ncdc.noaa.gov/extremes/cei/. For each period within the study timeframe (typically monthly data for an annual calculation, or daily values for precipitation) NOAA grids observed station temperatures into 1° x 1° cells, and the resulting values for each grid cell are averaged together with all other monthly values during the study timeframe. For my analysis, only gridded data was used, so the intermediary step of converting station temperatures into gridded cells was not necessary. I also used a finer resolution: 1/8° x 1/8° rather than 1° x 1° cells. From this distribution of monthly means, 90^{th} and 10^{th} percentile values are calculated, and any period falling above the 90^{th} percentile or below the 10^{th} percentile is classified as an “extreme” temperature value. Figure 2.2 shows an example graph from NOAA, showing historic values of the CEI for the maximum temperature component.

PDSI is assessed using NOAA’s PDSI database, which includes data from 1900 to the present day. As with temperature, monthly PDSI values are averaged for the period of interest, then sorted and ranked to identify the 90^{th} and 10^{th} percentile values. For each grid cell, any values falling outside those boundaries are marked as extreme. I calculated PDSI for model data using monthly minimum temperature, monthly maximum temperature, and daily precipitation. For further details on how the PDSI was treated in this analysis, refer to the following section for an extended methods discussion.

Extreme precipitation is assessed using the same method as temperature, except that only the 90^{th} percentile is taken into consideration. For purposes of the CEI, “extreme precipitation” is defined as the proportion of total annual precipitation that falls on days where the daily precipitation total is extremely high (above the 90^{th} percentile). In other words, this indicator is not a measure of total precipitation, but of proportionally how much precipitation falls in the form of extreme one-day events. To keep this indicator weighted consistently with the other indicators, the value is then doubled. For the fifth indicator, daily precipitation data is tallied, and total number of days with/without precipitation are calculated annually over the entire period of record. As with temperature and precipitation above, the 90^{th} and 10^{th} percentile are calculated, and values falling outside those values are considered extreme (Gleason 2008). For the purposes of this analysis, trends in each of the above indicators will be discussed. Figure captions will use a consistent shorthand: for instance, components TMAX10 and TMAX90 refer to the 10th and 90th percentile components of maximum temperature, respectively. Likewise, TMIN represents minimum temperature, TDD total dry days, EPD extreme precipitation days, and PDSI is the Palmer Drought Severity Index. Note that, unlike the other variables, EPD only assesses the 90th percentile, making for a total of nine indicator values.

Each of the indicator values is then expressed as a percentage of the study area experiencing an extreme climate event: for instance, for monthly maximum temperatures, the percentage of grid cells with extreme (above 90th percentile) maximum temperatures would be calculated and then summed over the analysis period. The CEI itself is simply the arithmetic mean of all five indicators, producing a single value that expresses the relative proportion of the study area which experienced extreme climate events during the study period. However, the CEI alone, being a broad index of multiple variables, does not evaluate to what degree each individual variable contributes to the final score. Therefore, in addition to the CEI itself, this thesis will include individual analysis and spatial mapping of each component, to determine which are the strongest factors in observed and projected regional climate extremes.

2.3.1 The Palmer Drought Severity Index

Four of the CEI metrics can be easily calculated using monthly maximum and minimum temperature and daily precipitation. The model data used in this project includes temperature and precipitation data available on daily or 3-hourly time slices, which can easily be converted into daily precipitation and monthly maximum and minimum temperatures. In contrast to the other four metrics, the Palmer Drought

Severity Index (PDSI) is itself a calculated index value, making it essentially a two-step process.

The PDSI, first published in 1965, is one of the most widely-used drought indices (Jacobi et al. 2013, Heim 2002, Wells et al. 2003). It was originally developed by meteorologist Wayne Palmer, in 1965 (Palmer 1965). The PDSI was among the first drought indices to analyze precipitation and temperature as part of a water balance model, rather than simply defining drought as an unusual shortage of rainfall (Heim 2002). Unlike comparable drought indices such as the Standardized Precipitation Index, which only tracks precipitation, the PDSI incorporates moisture supply and demand into a hydrologic budget, thereby incorporating both meteorological and hydrological drought (Heim 2002). In 2004, an updated version of the PDSI was developed at the University of Nebraska: the self-calibrating PDSI, or scPDSI (Wells et al. 2004). The self-calibrating PDSI uses a very similar procedure to Palmer's original index, but takes into account the accessibility of modern computing resources that were unavailable at the time that the original index was developed. The self-calibrating PDSI can also be used to compare values between diverse climatological regions, a common criticism leveraged against the original PDSI (Wells et al. 2004). As regional analysis is a crucial component to this study, all PDSI calculations herein are done using the self-calibrating method.

The PDSI is a widely used drought index, but it has been criticized for its lack of transparency, and is notoriously difficult for researchers to calculate independently (Jacobi et al. 2013). An abbreviated explanation of the PDSI calculation will be provided here; for a more thorough step-by-step process, refer to Palmer 1965 and Wells et al. 2004.

For each month of the year, eight values are computed: evapotranspiration (ET), potential evapotranspiration (PE), recharge (R), potential recharge (PR), runoff (RO), potential runoff (PRO), loss (L), and potential loss (PL). The PDSI itself uses a "bucket" model of soil moisture, in which the top layer is assumed to hold one inch of moisture, and the remaining water holding capacity is based on geology as inputted by the user. The four potential values are then weighted to form the water-balance coefficients, α, β, γ, and δ. These coefficients are also referred to as climatically appropriate for existing conditions, or CAFEC, and reflect the variance in "normal" conditions between climatically different regions. These values are then combined to produce the CAFEC precipitation value, $\hat{P}$, using the following equation:

$$\hat{P} = \alpha_i PE + \beta_i PR + \gamma_i PRO - \delta_i PL$$

The difference *d* is then calculated by subtracting CAFEC precipitation from actual precipitation, and then weighted using the climatic characteristic K. This is where the self-calibrated PDSI departs: the original PDSI used an empirical constant K calculated by Palmer, while the self-calibrated PDSI automatically calculates values of K based on historic climate data (Wells et al. 2004). The end result of the process produces a range of nonparametric values, with anything below -4 representing severe drought, and anything above 4 representing severe moisture surplus.

The PDSI values used by NOAA are based on observed station data, not gridded model simulations, and are provided by the National Climatic Data Center of NOAA already calculated. MATLAB and FORTRAN tools for calculating PDSI exist, requiring four inputs: temperature, precipitation, latitude, and available water capacity of the soil (Jacobi et al. 2013). Temperature, precipitation, and latitude data were already acquired to calculate the other metrics, and AWC is entered into the calculation as a constant (Jacobi et al. 2013). One concern, however, is that any AWC data acquired will be representative of the present-day, and will not account for any changes in future soil capacity, e.g. urbanization, land use change, impervious surfaces, etc. For purposes of this study, Dr. Park Williams of Columbia University generously provided both his MATLAB tool for calculating PDSI, and his gridded soil capacity data, both of which were invaluable for completing this research.

An additional challenge was posed by the calculation of potential evapotranspiration (PET), a necessary component of the PDSI. There are at least 50 different methods or models used to estimate PET; however, these can be roughly divided into temperature-based methods, radiation-based methods, and combination methods (Lu et al. 2005). Previous studies utilizing the PDSI with GCM data have used the modified Hargreaves or Thornthwaite methods – two of the most commonly-used temperature-based methods – to transform GCM outputs into monthly potential evapotranspiration data, then followed procedures outlined by Palmer to generate PDSI from those monthly PET values (Strzepek et al. 2010, Wang 2014). The Thornthwaite method in particular has been commonly used due to its ease of calculation, requiring only average temperature and latitude to produce an estimate of PET, and was used in the original version of the PDSI calculation (Wells et al. 2004). However, because the Thornthwaite method assumes a largely linear relationship between temperature and PET, recent studies have expressed concern that it may result in overestimations of PET in future warming scenarios (Sheffield et al. 2012, Hoerling et al. 2012). Recent studies generally agree that the Penman-Monteith method is the gold standard for future estimates of PET (Cook et al. 2014, Sheffield et al. 2012, Hoerling et al. 2012). On the other hand, as a combined temperature-based and radiation-based method, the Penman-Monteith calculation requires a large number of variables, including wind and solar radiation, which are not available for all models and observational data sets.

In order to maximize the number of simulations used in this study, I employed the Thornthwaite method, taking into account several factors. First, this is not a hydrology study, and evapotranspiration itself is not the primary focus of the research. PET is being calculated solely as an intermediate step in calculating the Palmer Drought Severity Index, which is in turn only a one-fifth component in a larger climate index. Second, it is important to remember that the CEI is a relative index: "extremeness" in the CEI is not determined based on any absolute value of dryness or wetness, but is a percentile-based value calculated from historic climate conditions. Therefore, even if the PDSI was overestimated in some areas, this bias would still be accounted for in the percentile-based thresholds.

Several studies indicate that the method of PET calculation may not have a dramatic impact. Lu et al. (2005) directly compared six different PET calculations, including Thornthwaite, and found that they were all highly correlated (Pearson's R values of .85 to 1.00). Another study directly compared PDSI values calculated using Thornthwaite and Penman-Monteith, and concluded that they were "very similar, in terms of correlation, regional averages, trends, and in terms of identifying extremely dry or wet months" (Schrier et al. 2011). Schrier et al. concluded that the PDSI is primarily a reflection of heterogeneity in precipitation inputs, and that it is largely insensitive to the use of one PET calculation method over another. This conclusion was made specifically in reference to the self-calibrating PDSI, the version used in this study (Schrier et al. 2011).

To test the assumption that PET would not be a significant factor in final calculations, I also ran a set of sample data through the PDSI calculation twice: once using the Penman-Monteith method, and once using Thornthwaite. Ultimately I found that while the scPDSI calculated using Thornthwaite had a slightly higher variance (4.91 versus 4.82), the Willmott Index of Agreement between the two was very high, at 0.945. The Index of Agreement was designed as a standardized measure for evaluating model performance, by calculating the degree of difference between observed and simulated values (Willmott 1981). In this case, the Penman-Monteith values stood in for the observations, and the Thornthwaite for the simulated. A value of 1 indicates perfect agreement, while 0 indicates no agreement at all. The index of agreement is calculated by the following formula:

$$d = 1 - \left(\frac{\Sigma(obs - sim)^2}{\Sigma(\left|sim - \overline{obs}\right| + |obs - \overline{obs}|)^2} \right)$$

A scatterplot of the two sample data sets is provided in Figure 2.2 below, for reference. In light of this close correlation between the PDSI calculated with Thornthwaite and Penman-Monteith, the Thornthwaite method was used in order to maximize the number of data sets that could be incorporated into the analysis.

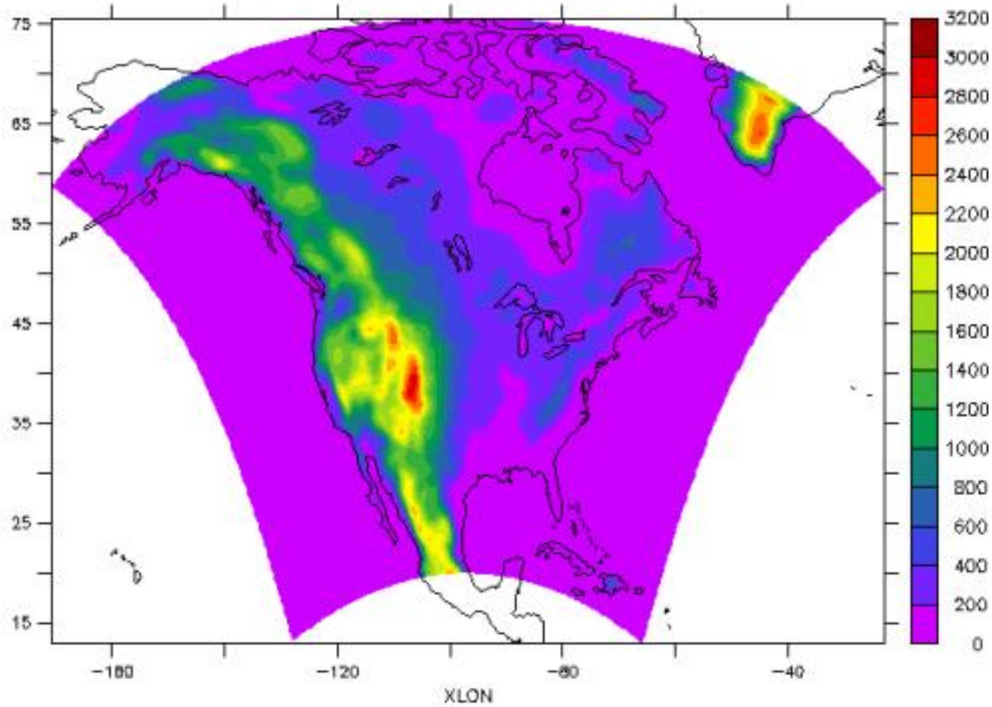

Figure 2.1: NARCCAP domain, showing coverage of the full CONUS. Reprinted from http://www.narccap.ucar.edu/

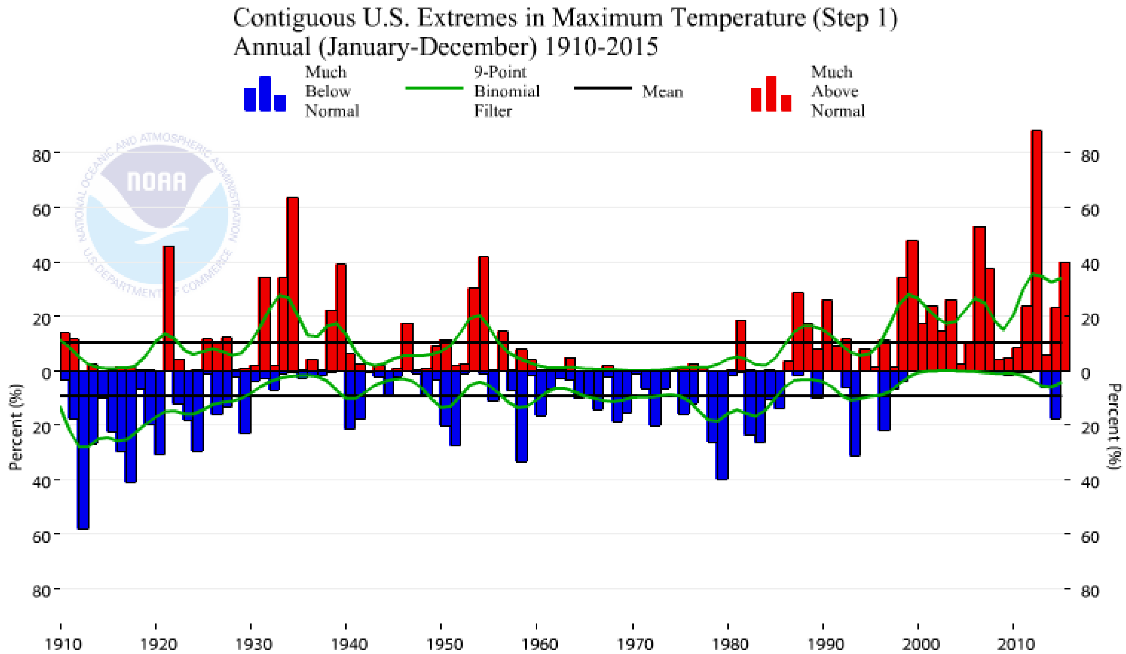

Figure 2.2: Climate Extremes Index, Indicator 1: Extremes in Maximum Temperature. Plot represents percentage of continental U.S. with maximum temperatures above the 90th percentile (red) or below the 10th percentile (blue) from 1910 to 2016, based on gridded observational data. Reprinted from https://www.ncdc.noaa.gov/extremes/cei/

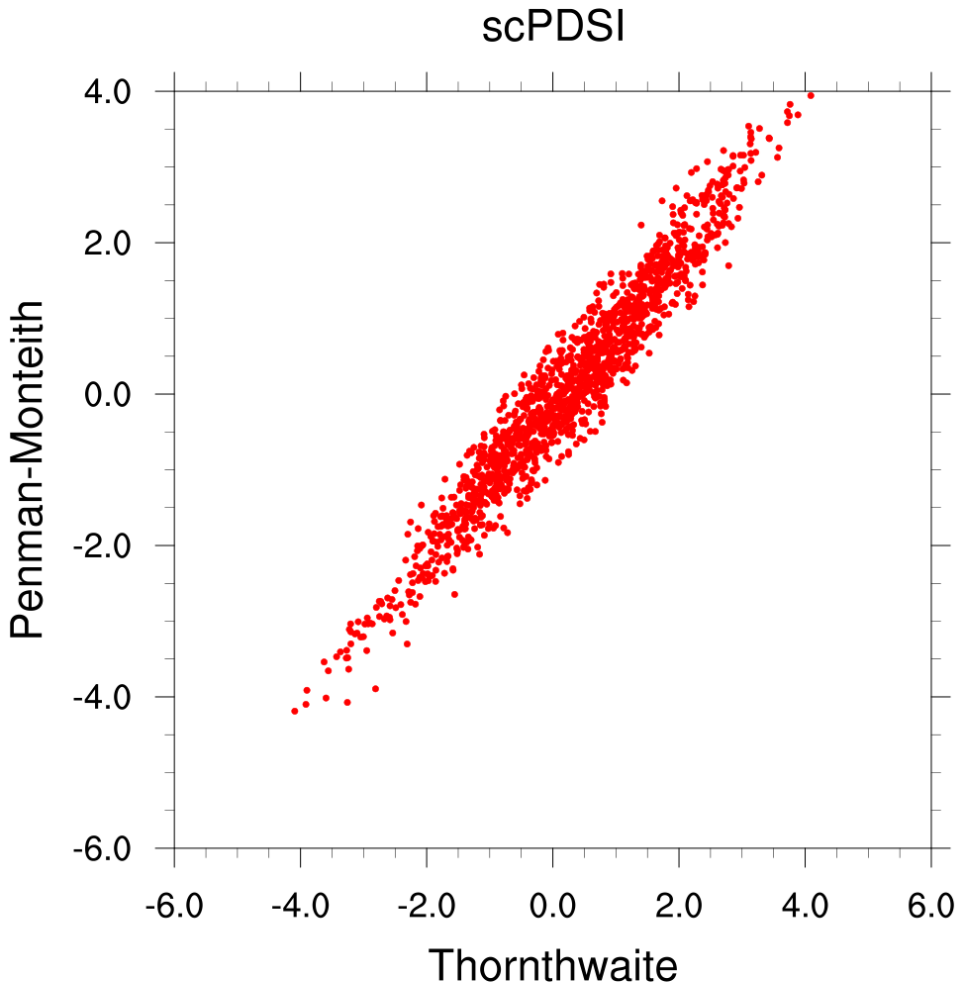

Figure 2.3: A scatterplot of sample self-calibrated Palmer Drought Severity Index (scPDSI) data, calculated using both the Penman-Monteith and Thornthwaite methods for estimating potential evapotranspiration, showing strong agreement.

Chapter 3

RESULTS

In the following chapters, we separate our analysis into the temporal and spatial dimensions of the CEI. First we examine the standard CEI, shown as a time series, which shows the **percentage of the contiguous U.S. in each year that is experiencing climate extremes**. While the index provides a snapshot of the U.S. as a whole, and an effective means of comparing changes over time, it does not on its own provide information on where those changes are occurring. The spatial patterns of the CEI will be addressed in Chapter 4.

Traditionally, the CEI is calculated based on gridded observation data, not from model data. Therefore, the first step is to calculate the CEI using observed data, to validate the methods used against expected values of the index. We then calculate the CEI using models over the historical period, to provide a baseline for comparison between the historical and mid-21st century periods. Finally, we turn our attention to the future period, to examine the type and degree of expected changes in extreme temperature and precipitation. For both the historical and future periods of the model data, we will first examine the CEI as a whole, then individually examine each component.

3.1 Observational Data

Figure 3.1 shows the results of CEI calculations on observational data from the period of 1949 to 2010. The area for these line plots is the whole CONUS, to provide a better comparison with existing NOAA data. Note that the black line on Figure 3.1 represents the index as calculated from data provided by Maurer et al., while the red dashed line indicates data calculated by NOAA from nClimGrid data, and downloaded from the NCDC website. The nClimGrid data was not used for analysis; it is included here for validation purposes, and to show strong agreement between my calculation methods and NOAA's. Small differences between the two can be attributed to observational uncertainty, as they were calculated using wholly different observational datasets.

Note also that the blue line represents an expected value of 0.2 for the complete index. The expected value for each individual indicator is 0.1, indicating that 10% of the study area falls into the 10^{th} percentile, and 10% into the 90^{th} percentile, at any given time. As the final index is calculated by combining the 10^{th} and 90^{th} percentile components in each category, and then averaging them together, the expected value for a completely climatologically average year would be 0.2. **Values above 0.2 indicate a more extreme climate over the CONUS (i.e., more of the CONUS than we would expect is experiencing extremes), while values below 0.2 represent a less extreme climate, overall.** As expected, the historical observation data shows variation from year to year, but overall stays close to 0.2.

Figure 3.2 shows each individual component of the CEI, as calculated from the gridded observation data. These individual components will be explained in more depth in the next section.

3.2 Model Data for the Historical Period

Figure 3.3 shows the complete Climate Extremes Index, calculated for all four model groups under consideration: NARCCAP, CMIP3, CORDEX, and CMIP5. For ease of comparison, the regional climate models (NARCCAP and CORDEX) are on the left-hand side, while their associated global climate models (CMIP3 and CMIP5) are on the right-hand side. Ensemble means for the full CONUS are shown in black, while individual models are shown in red. The green line represents the ensemble mean for just the Mid-Atlantic region. It is clear that there is a large amount of variation between models, but all of them adhere fairly closely to expected values around 0.2: there are very few spikes higher than 0.4 in this historical analysis, and all of them are single-model peaks.

The first component of the CEI is maximum temperature. Figure 3.4 indicates the frequency with which the maximum temperatures for each year fell below the 10th percentile value; values close to 1 indicate that maximum temperatures are unusually cool at every grid cell, while values close to 0 indicate that maximum temperatures never fall below the 10th percentile, suggesting an unusually warm year. The first thing to note is that all of the extreme temperature indicators show dramatic spikes from year to year, even in the historic data; this indicates that extreme temperatures are highly variable on an interannual time scale, although the multidecadal mean still averages out to 0.1. Additionally, some similar year-to-year patterns can be seen between ensemble means, with high values at the beginning of the study period and lower values from 1985 to 1990.

Figure 3.5 represents the frequency with which maximum temperatures exceeded the 90th percentile threshold. For this component, values close to 1 indicate that maximum temperatures are unusually warm at every grid cell, while values close to 0 indicate that maximum temperatures are unusually cool at every grid cell. Even in this late 20^{th} century study period, there are already excursions above the expected value of 0.1, indicative that more of the CONUS is experiencing maximum temperature extremes over the 31-year period. There are several very large single-model spikes, especially in the earlier NARCCAP and CMIP3 data; it is more difficult to evaluate the CORDEX and CMIP5 data due to the smaller number of ensemble members.

The second component of the CEI is minimum temperature. Similar to the maximum temperature components, Figure 3.6 shows the frequency with which minimum temperatures fall below the 10^{th} percentile over the CONUS. Higher values indicate a cooler year over more of the CONUS, while lower values indicate an unusually warm year. As with the maximum temperature indicator, these values are highly variable from year to year, with NARCCAP in particular showing some dramatic single-model peaks. However, as with the maximum temperature indicator, there are already signs of warming, with peaks more common towards the beginning of the study period, and dropping off towards the end.

Figure 3.7 shows the frequency with which minimum temperatures exceed the 90^{th} percentile value. As with the previous indicators, this is the inverse of the 10^{th} percentile, which higher values indicating unusually warm temperatures, and lower values indicating unusually cool temperatures. Once again we see high variability from year to year, and a subtle tendency towards more of the CONUS experiencing higher minimum temperatures, although this is slightly less pronounced in the NARCCAP data, which has high inter-model variability and spikes as high as 0.5 across the whole study period.

Next we move on to the precipitation-based components of the CEI, beginning with the Palmer Drought Severity Index. Strong negative values of the PDSI (shown in Figure 3.8) indicate drought conditions, while strong positive values (Fig. 3.9) indicate a moisture surplus. Therefore, the 10^{th} percentile of the PDSI is associated with extreme dryness, while the 90^{th} percentile is associated with extreme wetness. With all the historical precipitation indicators, we see less year-to-year variability than with the temperature indicators, with values hovering much closer to the expected value of 0.1.

Figure 3.10 represents extreme precipitation above the 90^{th} percentile. Recall from the methods section that extreme precipitation is defined, for the purposes of the CEI, as the proportion of total precipitation per year that falls during extreme ($>90^{th}$ percentile) one-day precipitation events. It can be inferred that higher values of the index mean more of the country experiences more intense precipitation events, while lower values mean fewer extreme precipitation events. Note that this is not a measure of change in total precipitation; this is not an indicator of *how much* total rainfall an area is receiving, but *how* it is receiving that rainfall. Of all nine individual components of the CEI, this one shows by far the least variance, rarely showing either values of zero or values higher than 0.2. For historical data, the standard deviation for ECP90 was generally 0.04 or lower, in contrast to standard deviations of 0.15 or higher for the temperature indicators, for an index with an expected value of 0.1. This suggests that the proportion of extreme precipitation events is ordinarily extremely stable from year to year, when averaged over the CONUS as a whole. Because of the spatial averaging inherent in the CEI, however, this statement only applies to the

CONUS as a whole; as will be seen in the next chapter, precipitation is much more spatially heterogeneous than temperature.

The final component of the CEI is total dry days, defined as the total number of days in a given year where the total precipitation is less than a certain trace threshold. To match the methodology cited by Gleason et al. (2008), the minimum precipitation threshold used in this analysis was 0.01 inches, or 0.254 mm. Figure 3.11 represents greater than normal days with precipitation, while Figure 3.12 represents greater than normal days without precipitation. As with the extreme precipitation metric, precipitation is more spatially heterogeneous than temperature; however, total dry days showed much more interannual variance than extreme precipitation. This indicates that the frequency of precipitation events is more variable from year to year.

3.3 Model Data for Mid-21st Century

3.3.1 Composite CEI

Already, simply from a cursory visual examination of Figure 16, it is clear that the mid-21st century climate is much more extreme. At no point in any year do any individual models fall below the expected value of 0.2, and at no point do any of the ensemble means fall below 0.4. Only three NARCCAP models have minimum values below 0.3, and only one CORDEX model has a minimum value below 0.4. Ensemble mean values are 0.53 for NARCCAP, 0.53 for CMIP3, 0.55 for CORDEX, and 0.56 for CMIP5. This means that over half the CONUS is experiencing a more extreme climate. However, simply examining the overall index does not tell us which components are contributing the most to this increase in extremeness, or how much. For that, we must examine them individually.

3.3.2 Maximum Temperature

Already, with the first indicator, there are signs of obvious change. Figure 3.14, representing maximum temperatures much below normal, clearly shows that the most common value across all models is zero. This indicates that historically low maximum temperatures almost never occur between 2038 and 2068. For NARCCAP and CMIP3, most models show only one or two years with any maximum temperatures below the 10^{th} percentile, and CMIP5 show none at all.

Figure 3.15 in turn shows maximum temperatures exceeding the historic 90^{th} percentile almost every year, and at almost every grid cell. While greater uncertainty exists for the earlier part of the future simulation, all models agree that extreme temperatures will increase drastically from the historical baseline. For all models and all years in the future scenario, at no point did any of them approach the expected value of 0.1, and virtually all models have at least one value of 1.0 – representing a year in which every grid point experienced record high temperatures. The ensemble mean for NARCCAP is 0.87, 0.91 for CMIP3, 0.96 for CORDEX, and 0.97 for CMIP5, suggesting that on average the CMIP5-based model groups predict even more severe temperature increase.

Considerable inter-model variability exists, especially in the earlier part of the period; some pairings show consistently high extreme values across the entire period of interest, while others project a steep upward slope over the 31-year period. NARCCAP pairings that used the CCSM or CGCM3 for boundary forcings appear to be more stable over time, while the GFDL pairings have a steeper slope, with HadCM3 more or less variable depending on RCM. What is consistent is a dramatic increase in historic warm temperatures. By 2068, all models groups are in agreement that over 90% of the country will be experiencing historic 90th percentile temperatures on a yearly basis.

3.3.3 Minimum Temperature

As seen in Figure 3.16, minimum temperature values are just as extreme or more so than the maximum temperature values, with a majority of models showing values at or near zero. This indicates that minimum temperatures between 2038 and 2068 virtually never fall below the historic 10th percentile. Both CMIP3 and CMIP5 have no values above 0, while NARCCAP and CORDEX models have only one or two years with any historic low temperatures.

Likewise, Figure 3.17 shows that by the end of the 31-year future period, a majority of models report minimum temperatures above the historic 90th percentile by 2068. As with maximum temperature above, NARCCAP shows an upward slope over the 31-year period, while CORDEX and CMIP5 start out with values already close to the maximum, indicating that warming is already too extreme to fall within historic normals. The ensemble mean for NARCCAP is 0.94, 0.98 for CMIP3, 0.98 for CORDEX, and 0.99 for CMIP5, even higher than for maximum temperature. Clearly, the two 90th percentile temperature indicators are strong contributors to the rise in overall CEI.

In a nonstationary climate, there are three potential sources of changes in climate extremes: the distribution itself can shift, the variance of the distribution can change, or the skewness of the distribution can change, or a combination of any of the above (Gallant et al. 2014, Field et al. 2012, Seneviratne et al. 2012). The CEI alone does not provide enough diagnostic data to definitively assert how the temperature distribution as a whole is changing. However, it is clear that certain patterns are emerging. Both tails of the distribution are shifting drastically warmer across the entire CONUS, to the point where historic percentile thresholds are no longer useful diagnostic tools; once the CEI reaches its maximum value of 1.0, it cannot detect any further changes. This change is happening at roughly equal rate and magnitude for both maximum and minimum temperature, where historic warm temperatures happen yearly and historic cool temperatures are vanishingly rare. This suggests that the distribution itself is shifting, both for maximum and minimum temperature.

3.3.4 PDSI

Overall, signals in the precipitation indicators are less extreme than those seen in the temperature indicators, and also show less overall agreement between models. Figure 3.18 shows strong negative values of the PDSI, indicating severe drought, while Figure 3.19 shows strong positive values, indicating severe moisture surplus. Looking at the 10^{th} percentile component of the PDSI, indicating severe drought conditions, ensemble means are 0.14 for NARCCAP, 0.13 for CMIP3, 0.12 for CORDEX, and 0.13 for CMIP5. For comparison, the ensemble mean for the 20^{th} century was 0.097 for all four model groups. There appears to be a small increase in drought conditions over the mid-21^{st} century period, with the NARCCAP and CMIP3 ensembles in particular showing higher values by 2068. However, with standard deviations of between 0.06 and 0.09 across all model groups, none of these ensemble mean values are likely to be statistically significant deviations from the expected value of 0.1.

A lack of significant increase or decrease in the PDSI metric does not necessarily mean that no changes in precipitation or drought are occurring. Because of the spatial averaging of the CEI, if parts of the CONUS are becoming wetter while others are becoming drier, the overall index will result in something close to the expected value. While temperature changes are universally positive all over the CONUS, precipitation changes vary by region. Thus, a lack of change in the PDSI metric means that whatever changes in extreme drought are occurring, they are occurring at a regional scale rather than across the whole CONUS. Spatial trends in precipitation will be examined in more detail in Chapter 4.

3.3.5 Extreme Precipitation

Extreme precipitation requires some context: as seen earlier in the historical graphs, it shows very little year-to-year variance when compared with the other indicators, and stays extremely close to the expected value of 0.1. While the increase shown in Figure 3.20 is small in magnitude, it is consistent across all model groupings. The ensemble mean for NARCCAP is 0.16, 0.14 for CMIP3, 0.15 for CORDEX, and 0.16 for CMIP5. The average difference between the future and historical values is 0.06 for NARCCAP, 0.05 for CMIP3, 0.05 for CORDEX, and 0.07 for CMIP5. However, unlike with PDSI above, the standard deviations are respectively 0.02, 0.03, 0.04, and 0.05. A paired t-test comparing future vs historical values for NARCCAP (chosen due to the largest sample size of models) shows statistical significance at $p<0.01$.

It is important to recall in this context that an increase of 0.1 to 0.15, while appearing less dramatic than the temperature indicators, still represents a 50% increase from its historic value. In real-world terms, the percentage of the CONUS experiencing extreme precipitation in any given year is projected to increase by half. This value has a relatively small impact on the overall CEI score, in relation to the more extreme changes seen in the temperature indicators. However, this underscores why it is important to examine each metric of the CEI individually, as explained in Gallant et al. 2014. Given that this metric is related to the proportion of extreme precipitation, and thus represents a potential increase in severe precipitation events, it may also have a disproportionate impact on human and biological systems. The CEI itself is not a diagnostic tool for detecting the cause of changing precipitation patterns, but it is consistent with CMIP5 analysis showing both an increase in extreme precipitation and an overall intensification of the hydrological cycle, driven by increased temperatures (Wuebbles et al. 2014).

3.3.6 Days With/Without Precipitation

Figure 3.21 represents greater than normal days with precipitation, while Figure 3.22 represents greater than normal days without precipitation. For days with precipitation, the ensemble mean value is 0.08 for NARCCAP, 0.11 for CMIP3, 0.12 for CORDEX, and 0.14 for CMIP5. The average difference between the future and historical values is -0.02 for NARCCAP, 0.02 for CMIP3, 0.02 for CORDEX, and 0.05 for CMIP5. None of these differences are larger than the standard deviation for their respective model groups. This indicates that the CONUS as a whole is not becoming more or less extreme in respect to years with a very high number of precipitation events.

For days without precipitation, the ensemble mean is 0.24 for NARCCAP, 0.18 for CMIP3, 0.16 for CORDEX, and 0.14 for CMIP5. The average difference between future and historical values is 0.14 for NARCCAP, 0.08 for CMIP3, 0.06 for CORDEX, and 0.04 for CMIP5. Paired t-tests indicate statistical significance at $p<0.01$ for all model groupings except CMIP5. This could be attributed to the lower sample size of CMIP5 models, or to the lower average difference between the historical and future values. Regardless, three of four model groups show a small but significant increase in the frequency of years with unusually low number of precipitation events.

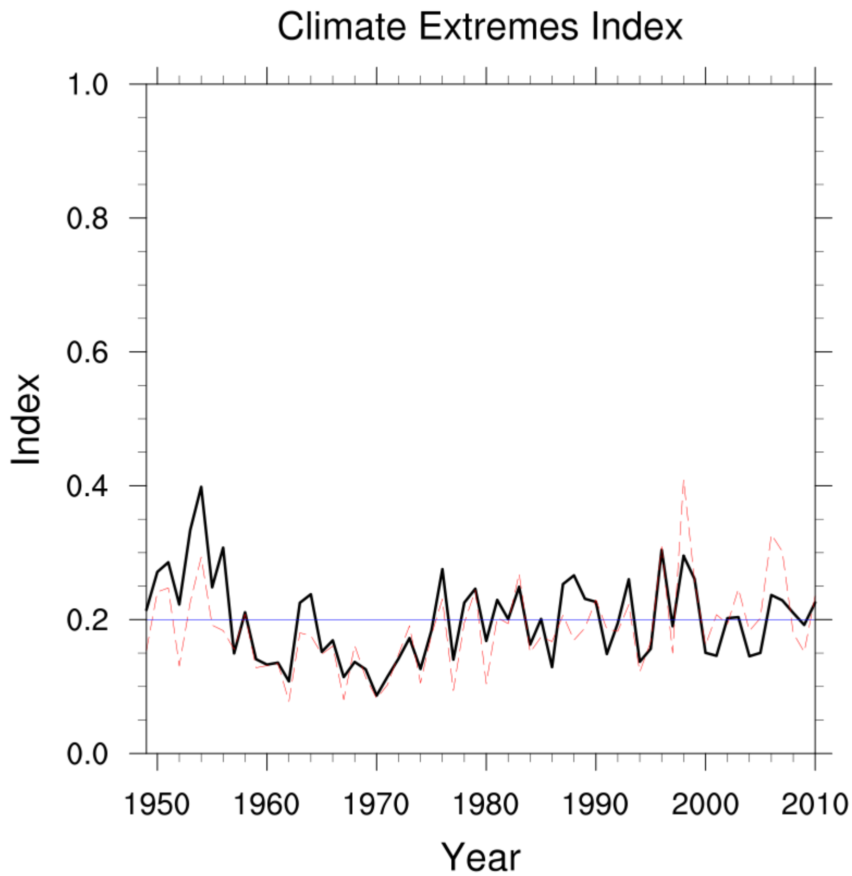

Figure 3.1: Climate Extremes Index (CEI) calculated from observation data. The date range is 1949 to 2010. The black line indicates index values calculated from gridded observation data provided by Maurer et al. (2002). The red line indicates CEI values calculated by NOAA using nClimGrid data. The blue line indicates the expected value of the index (0.2) for a stationary climate.

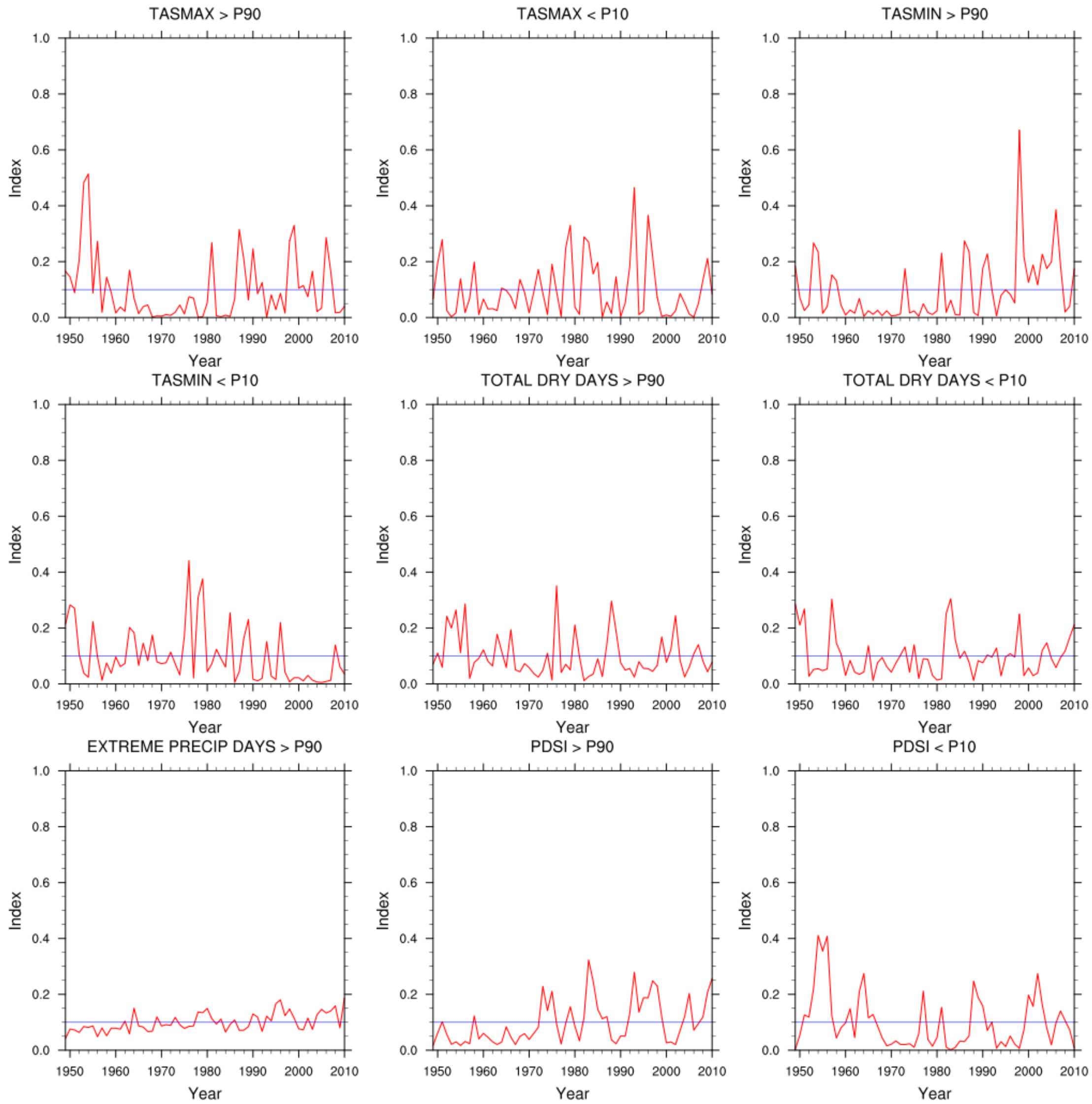

Figure 3.2: Individual components of the CEI. The date range is 1949 to 2010. The black line indicates index values calculated from gridded observation data provided by Maurer et al. (2002). The blue line indicates the expected value of each component (0.1) for a stationary climate.

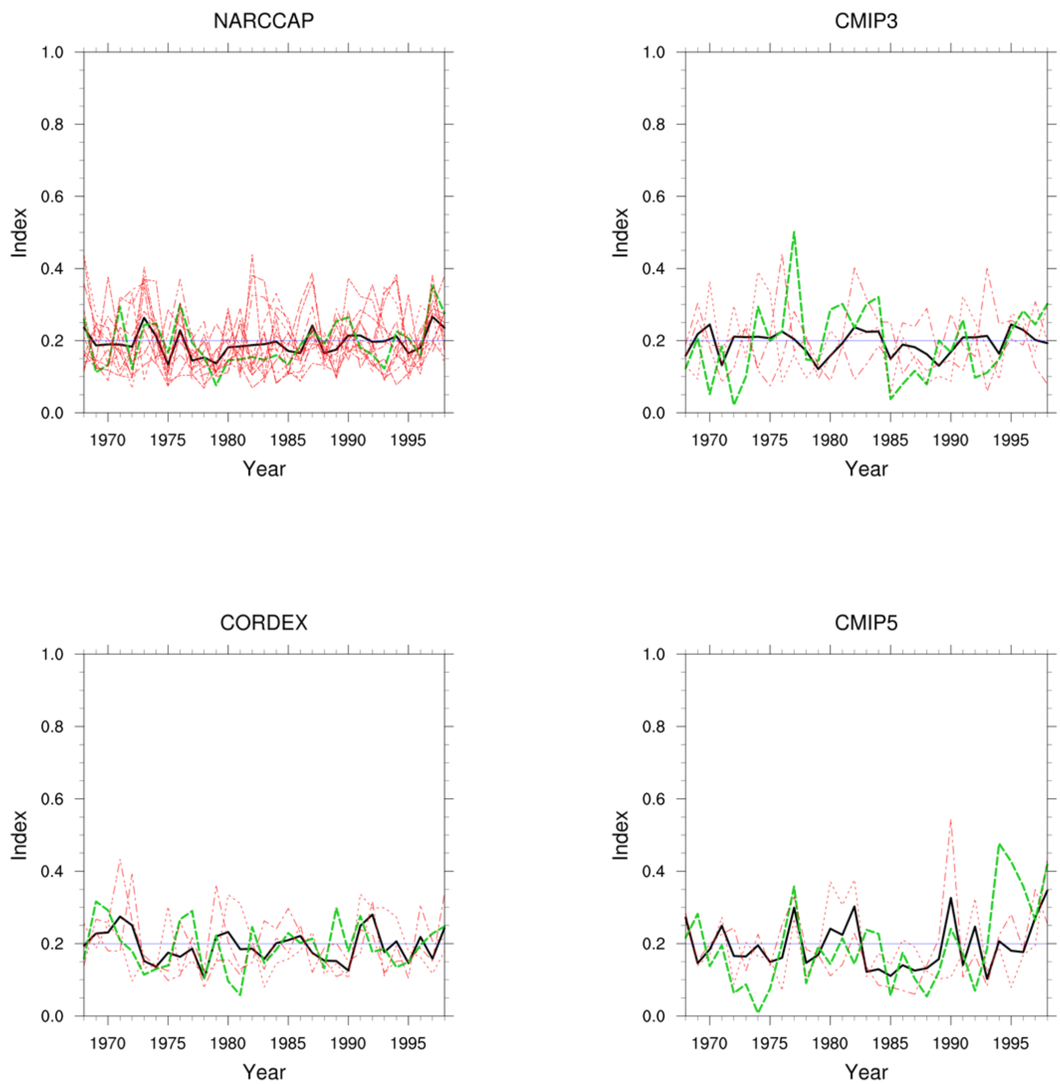

Figure 3.3: Climate Extremes Index (CEI) calculated from model data. The date range is 1968 to 1998. Black lines indicate ensemble mean values for the CONUS, while red lines indicate individual models. The green line represents the ensemble mean for just the Mid-Atlantic region. The blue line indicates the expected value of the index (0.2) for a stationary climate.

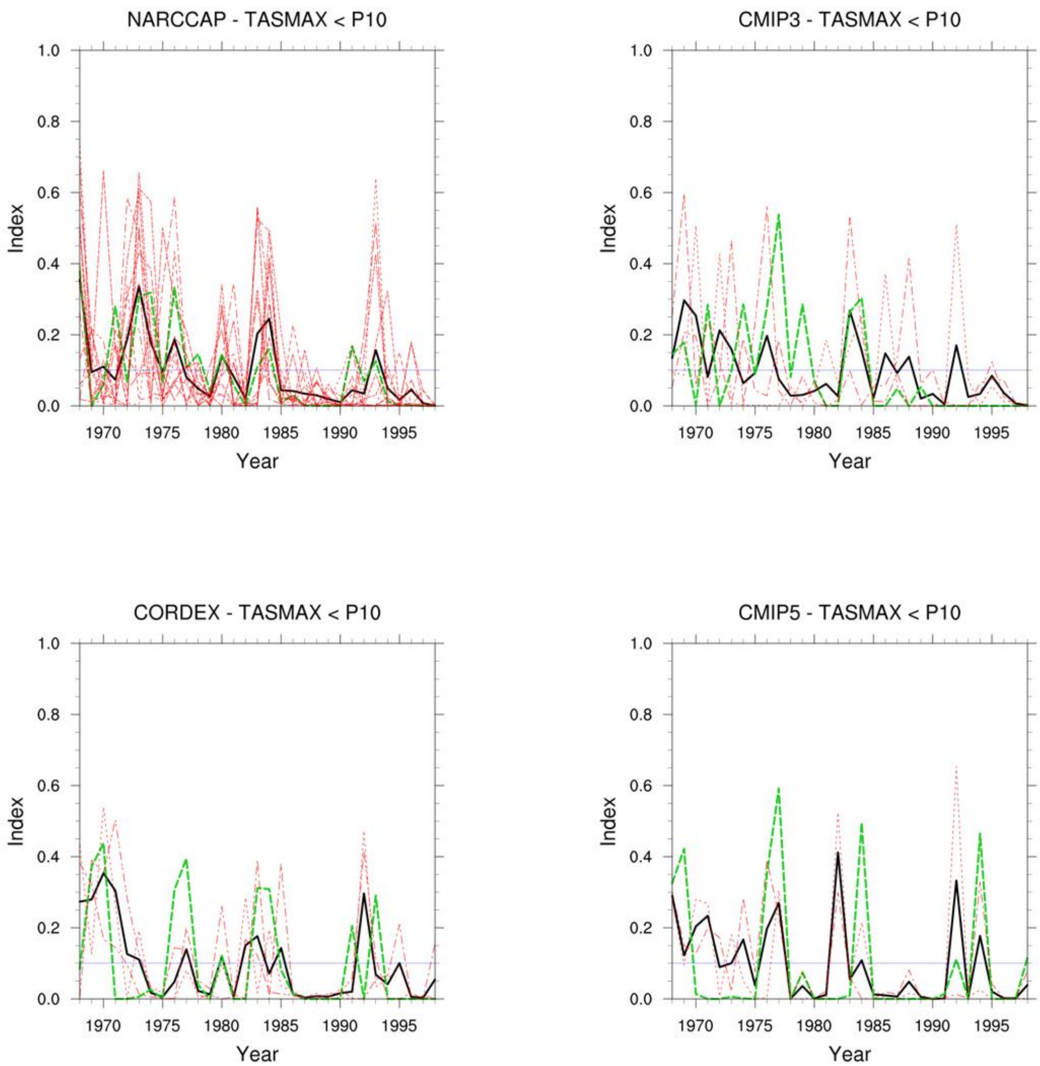

Figure 3.4: Climate Extremes Index (CEI) component TMAX10: maximum temperatures much below normal. The date range is 1968 to 1998. Black lines indicate ensemble mean values for the CONUS, while red lines indicate individual models. The green line represents the ensemble mean for just the Mid-Atlantic region. The blue line indicates the expected value of the component (0.1) for a stationary climate.

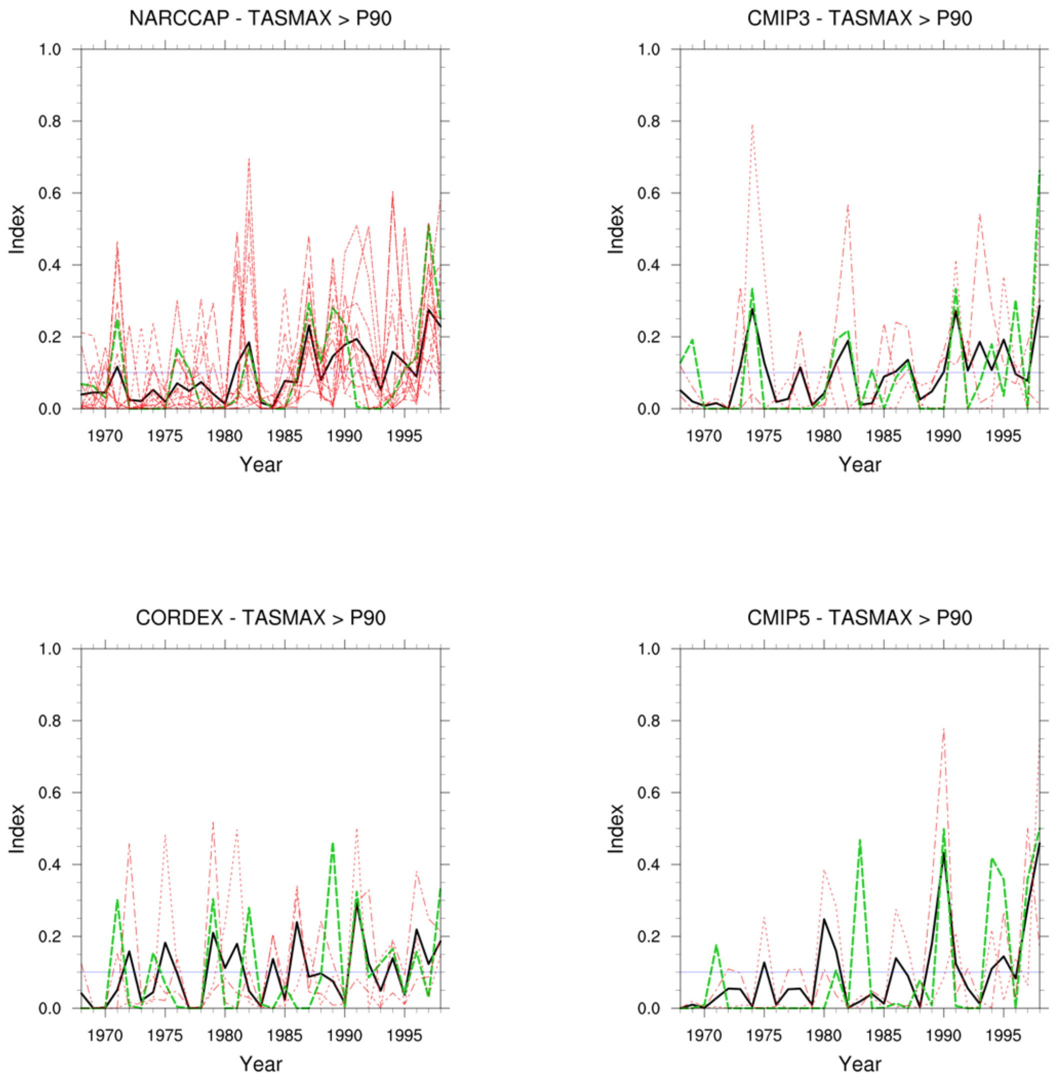

Figure 3.5: Climate Extremes Index (CEI) component TMAX90: maximum temperatures much above normal. The date range is 1968 to 1998. Black lines indicate ensemble mean values for the CONUS, while red lines indicate individual models. The green line represents the ensemble mean for just the Mid-Atlantic region. The blue line indicates the expected value of the component (0.1) for a stationary climate.

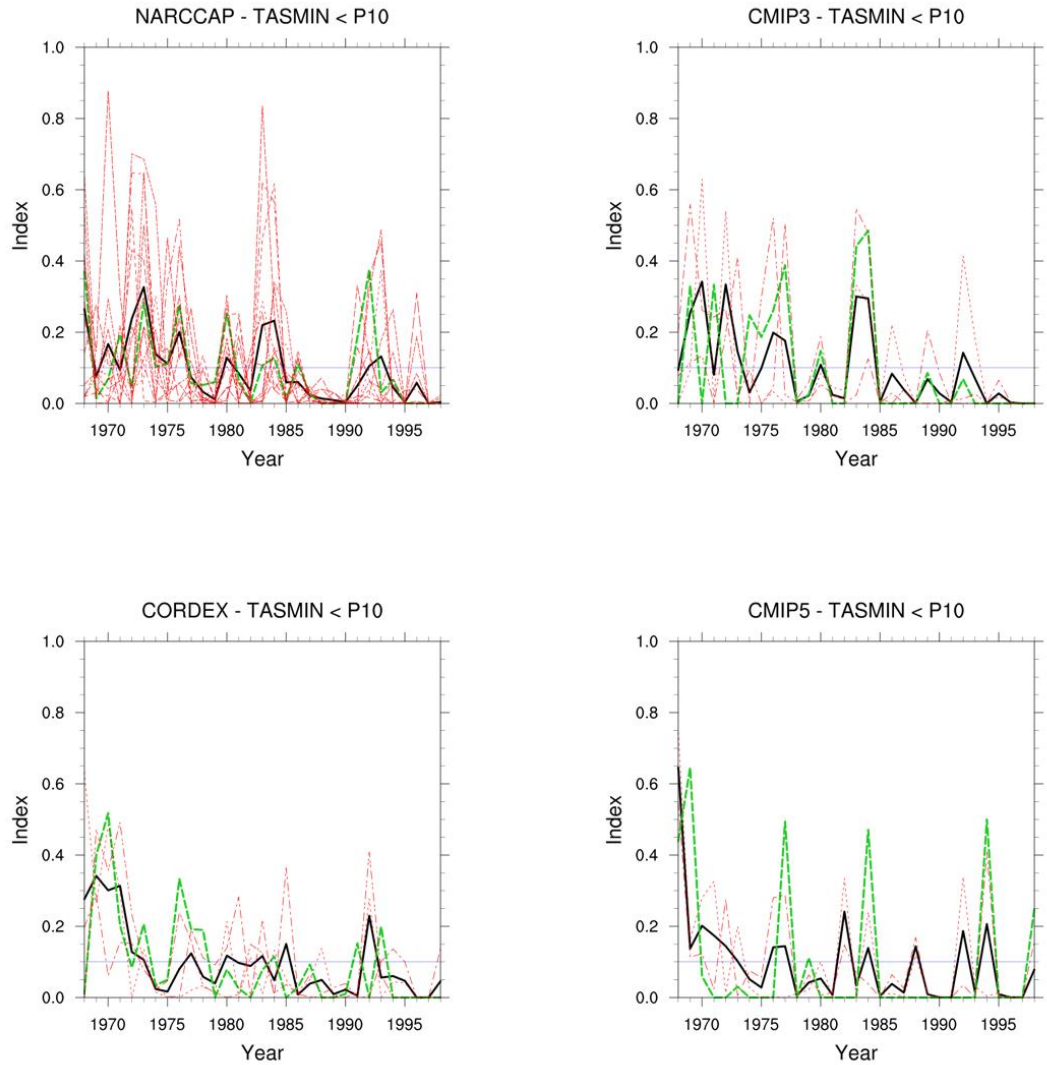

Figure 3.6: Regional Climate Extremes Index (rCEI) component TMIN10: minimum temperatures much below normal. The date range is 1968 to 1998. Black lines indicate ensemble mean values for the CONUS, while red lines indicate individual models. The green line represents the ensemble mean for just the Mid-Atlantic region. The blue line indicates the expected value of the component (0.1) for a stationary climate.

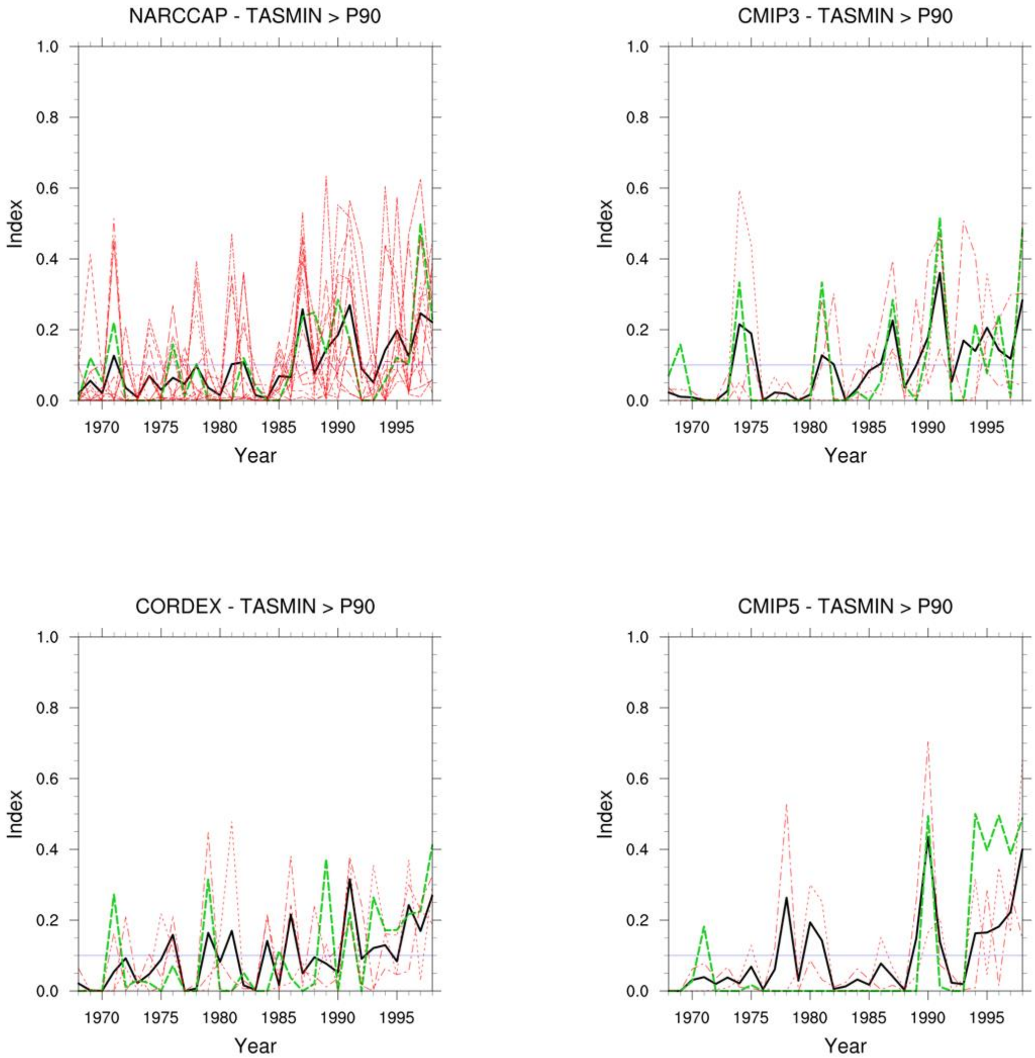

Figure 3.7: Climate Extremes Index (CEI) component TMIN90: minimum temperatures much above normal. The date range is 1968 to 1998. Black lines indicate ensemble mean values for the CONUS, while red lines indicate individual models. The green line represents the ensemble mean for just the Mid-Atlantic region. The blue line indicates the expected value of the component (0.1) for a stationary climate.

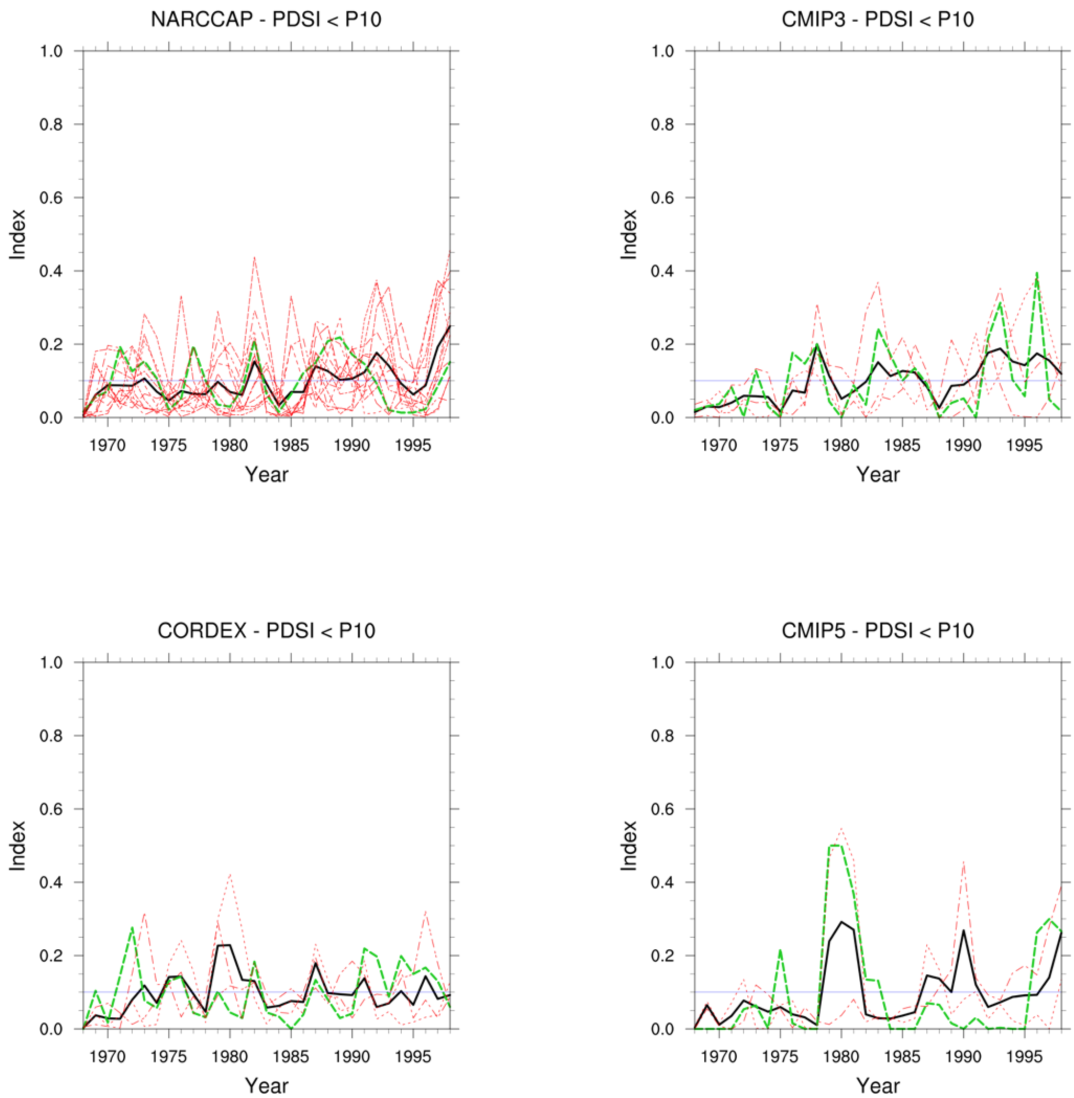

Figure 3.8: Climate Extremes Index (CEI) component PDSI10: strong negative values of the PDSI (indicating severe drought). The date range is 1968 to 1998. Black lines indicate ensemble mean values for the CONUS, while red lines indicate individual models. The green line represents the ensemble mean for just the Mid-Atlantic region. The blue line indicates the expected value of the component (0.1) for a stationary climate.

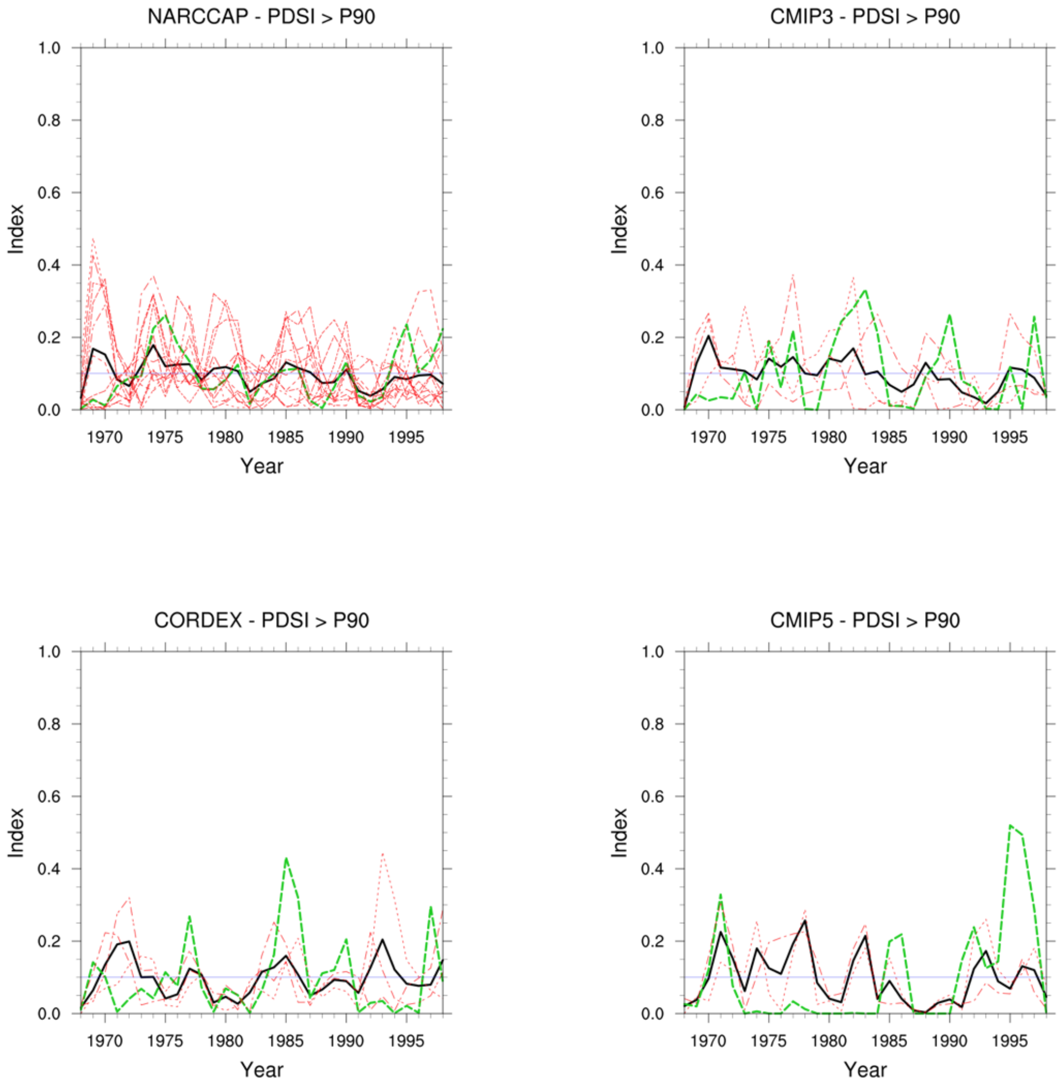

Figure 3.9: Climate Extremes Index (CEI) component PDSI90: strong positive values of the PDSI (indicating severe moisture surplus). The date range is 1968 to 1998. Black lines indicate ensemble mean values for the CONUS, while red lines indicate individual models. The green line represents the ensemble mean for just the Mid-Atlantic region. The blue line indicates the expected value of the component (0.1) for a stationary climate.

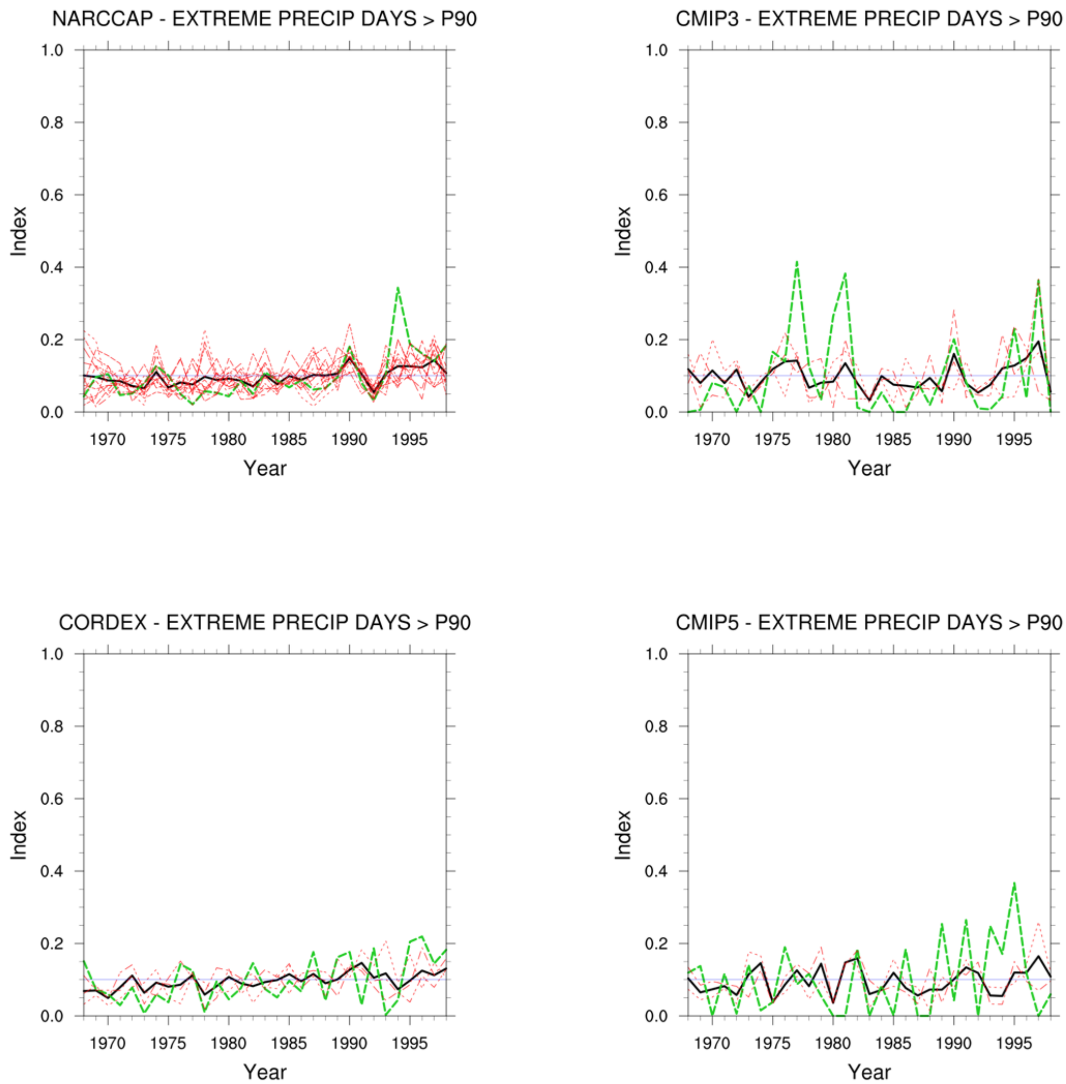

Figure 3.10: Climate Extremes Index (CEI) component EPD90: precipitation derived from extreme 1-day precipitation events. The date range is 1968 to 1998. Black lines indicate ensemble mean values for the CONUS, while red lines indicate individual models. The green line represents the ensemble mean for just the Mid-Atlantic region. The blue line indicates the expected value of the component (0.1) for a stationary climate.

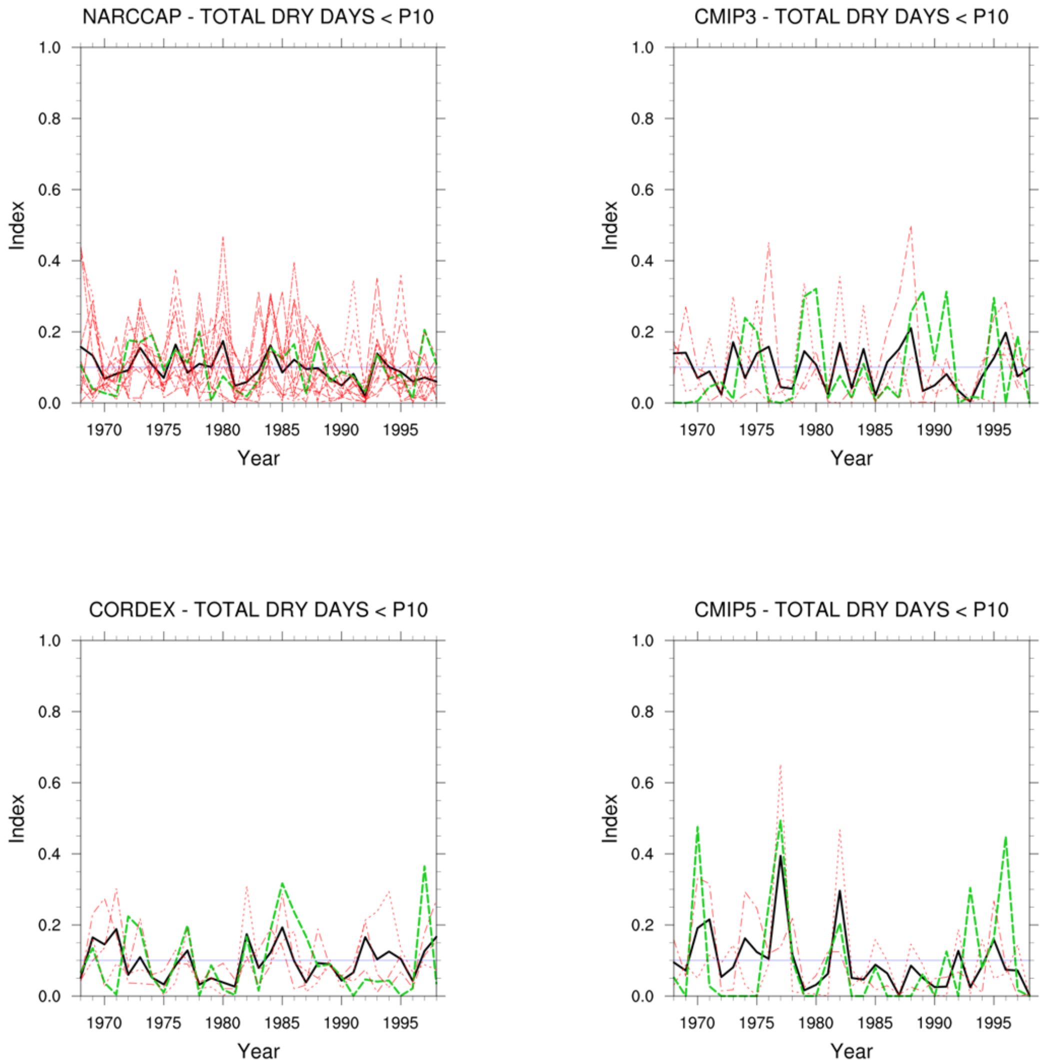

Figure 3.11: Climate Extremes Index (CEI) component TDD10: greater than normal days with precipitation. The date range is 1968 to 1998. Black lines indicate ensemble mean values for the CONUS, while red lines indicate individual models. The green line represents the ensemble mean for just the Mid-Atlantic region. The blue line indicates the expected value of the component (0.1) for a stationary climate.

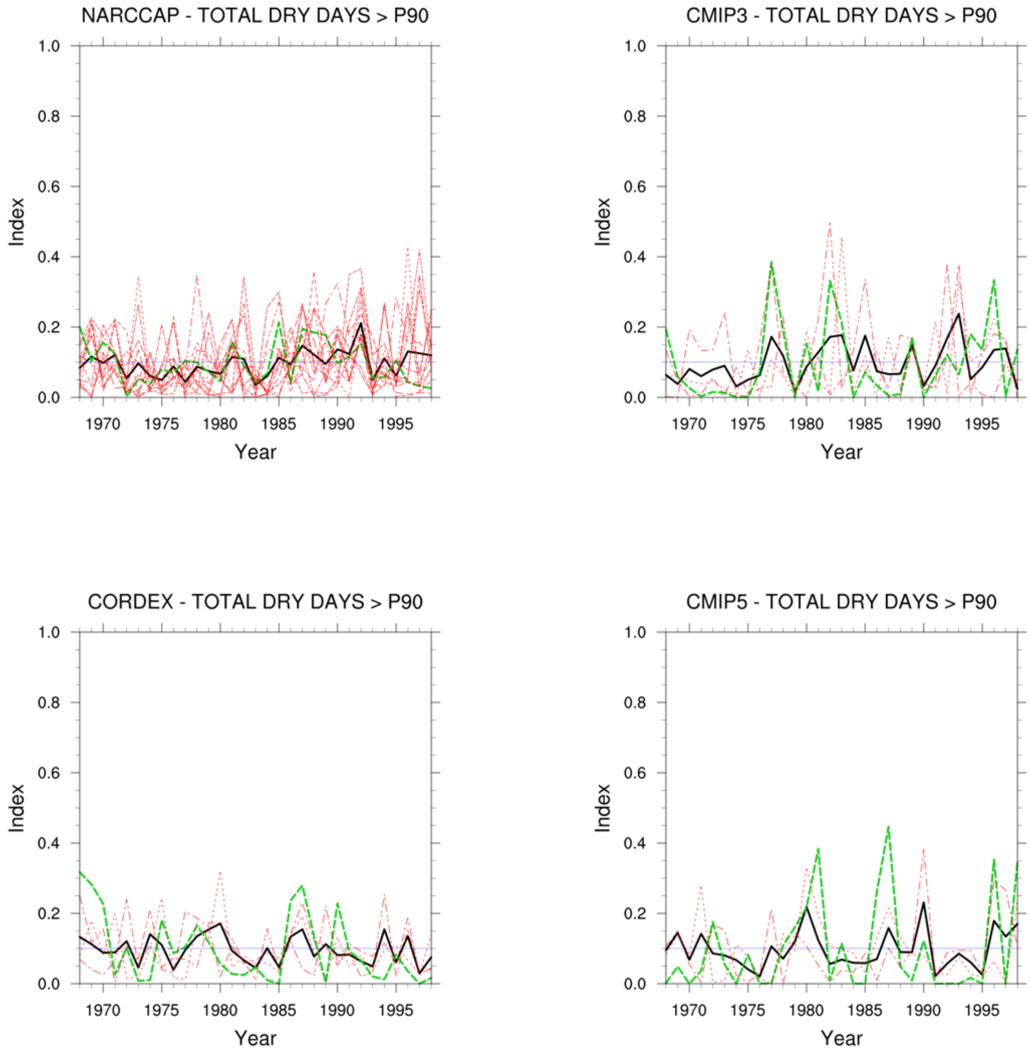

Figure 3.12: Climate Extremes Index (CEI) component TDD90: greater than normal days without precipitation. The date range is 1968 to 1998. Black lines indicate ensemble mean values for the CONUS, while red lines indicate individual models. The green line represents the ensemble mean for just the Mid-Atlantic region. The blue line indicates the expected value of the component (0.1) for a stationary climate.

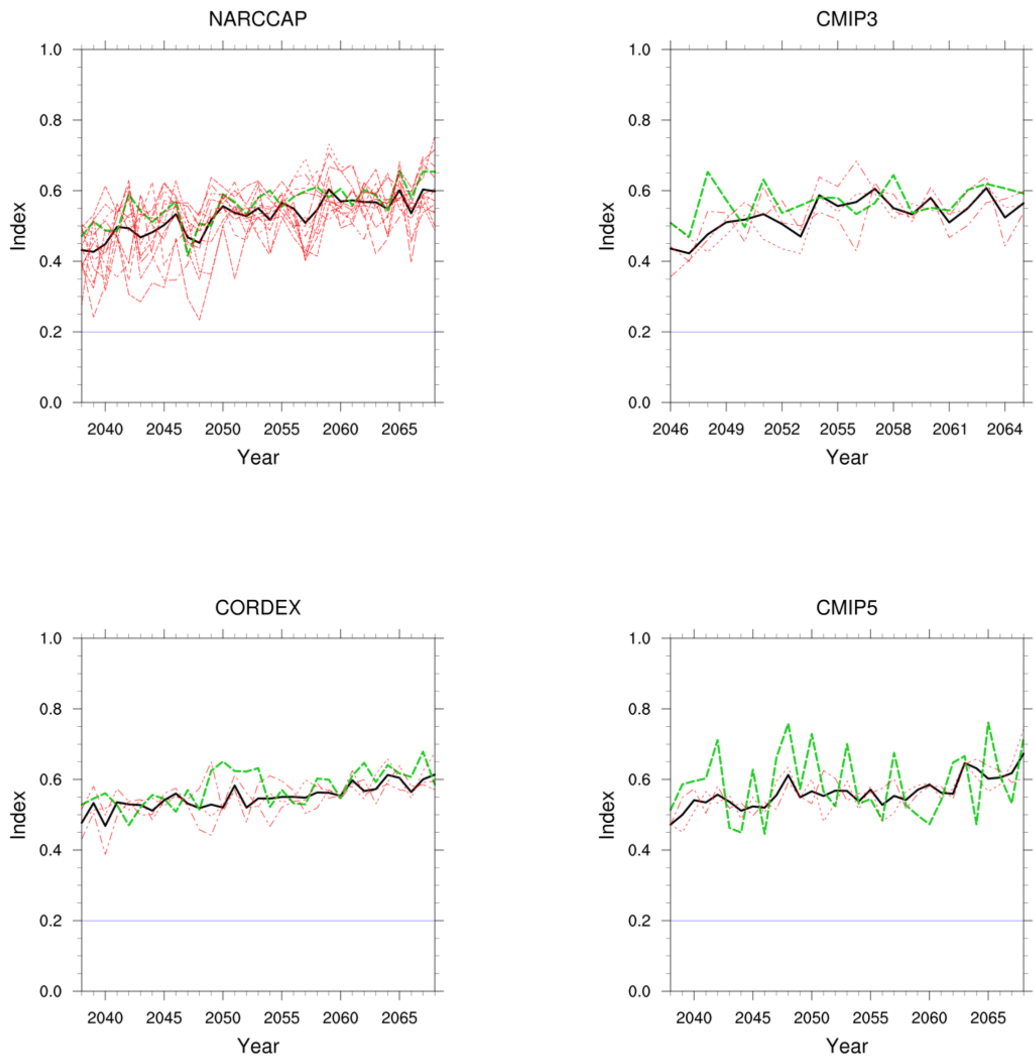

Figure 3.13: Climate Extremes Index (CEI) calculated from model data. The date range is 2038 to 2068, except for CMIP3, where the date range is 2046 to 2065. Black lines indicate ensemble mean values for the CONUS, while red lines indicate individual models. The green line represents the ensemble mean for just the Mid-Atlantic region. The blue line indicates the expected value of the index (0.2) for a stationary climate.

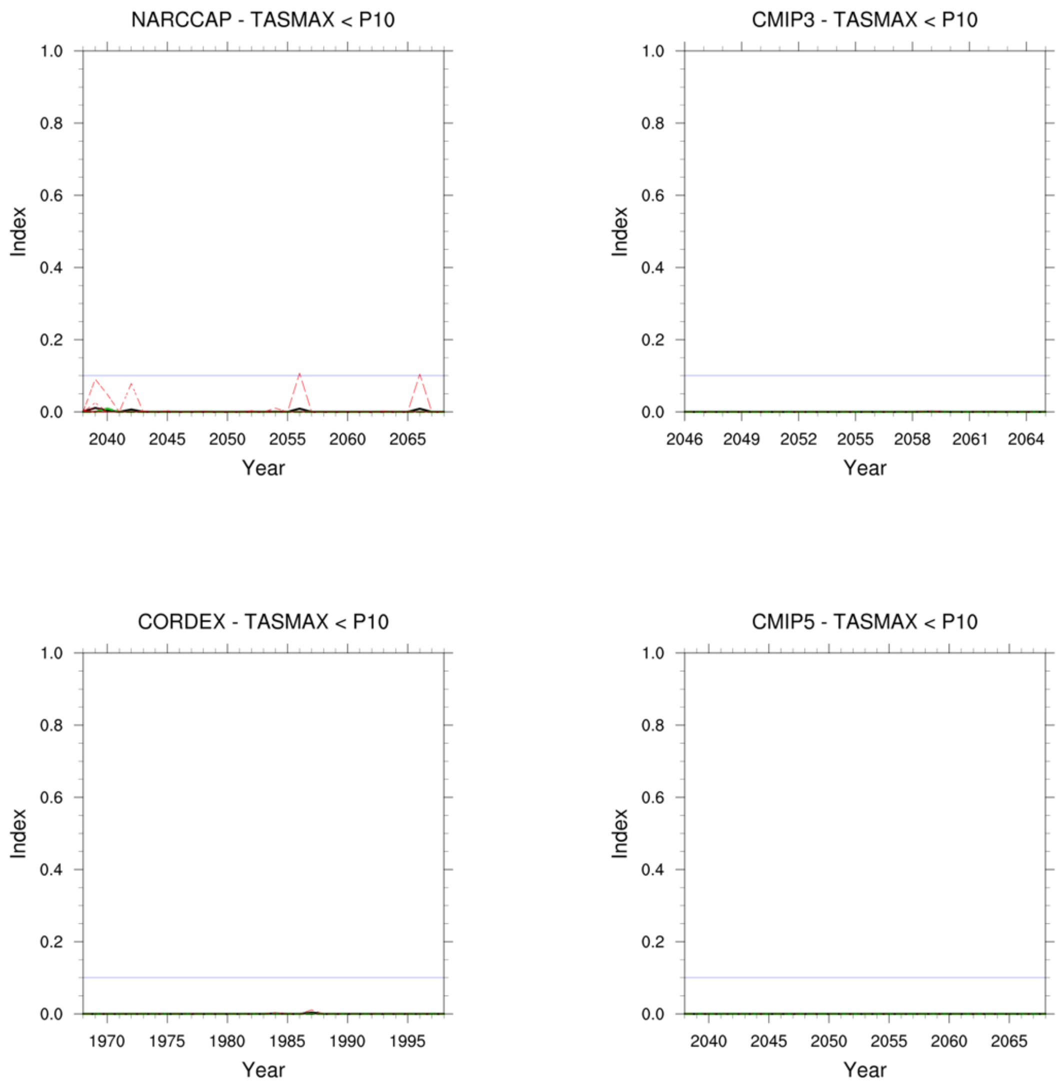

Figure 3.14: Climate Extremes Index (CEI) component TMAX10: maximum temperatures much below normal. The date range is 2038 to 2068, except for CMIP3, where the date range is 2046 to 2065. Black lines indicate ensemble mean values for the CONUS, while red lines indicate individual models. The green line represents the ensemble mean for just the Mid-Atlantic region. The blue line indicates the expected value of the component (0.1) for a stationary climate.

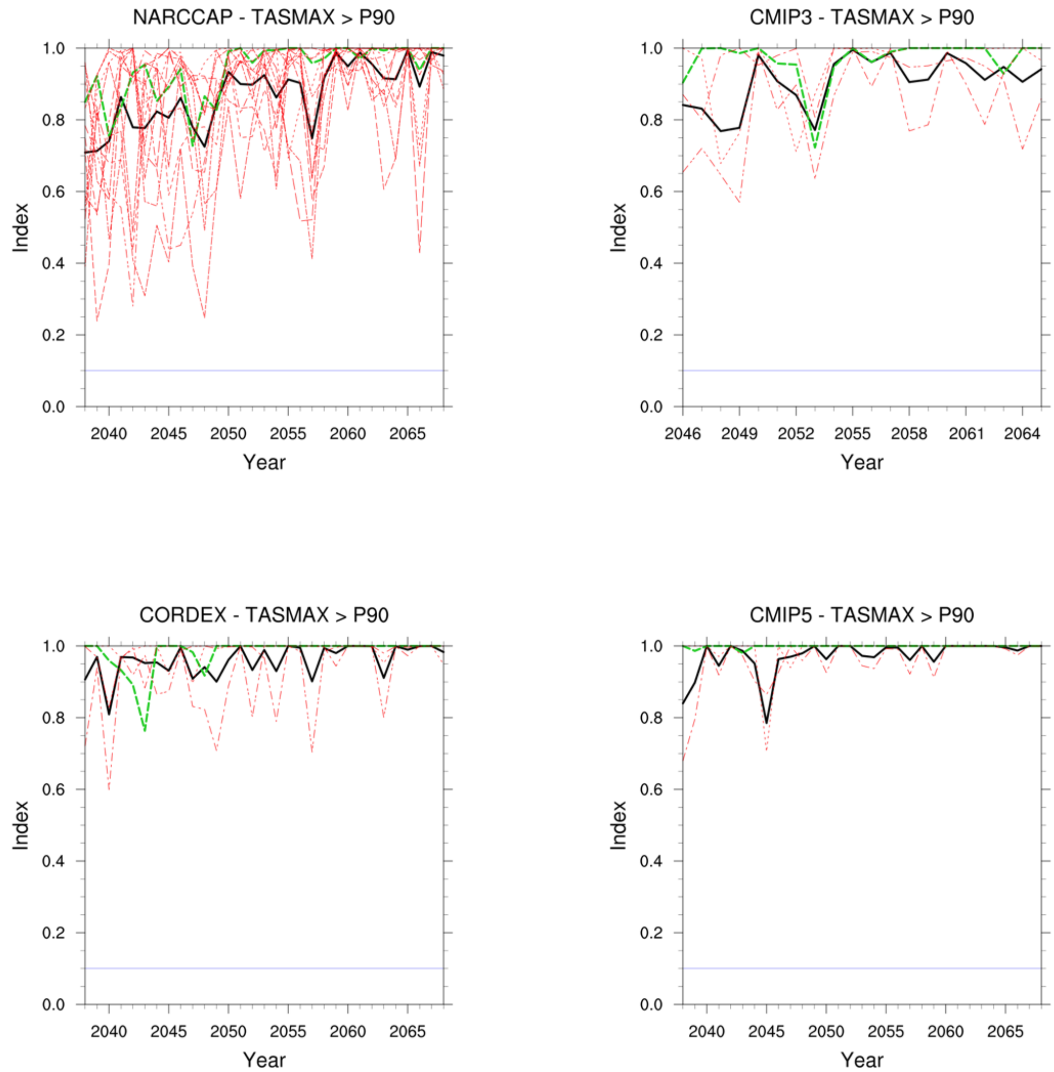

Figure 3.15: Climate Extremes Index (CEI) component TMAX90: maximum temperatures much above normal. The date range is 2038 to 2068, except for CMIP3, where the date range is 2046 to 2065. Black lines indicate ensemble mean values for the CONUS, while red lines indicate individual models. The green line represents the ensemble mean for just the Mid-Atlantic region. The blue line indicates the expected value of the component (0.1) for a stationary climate.

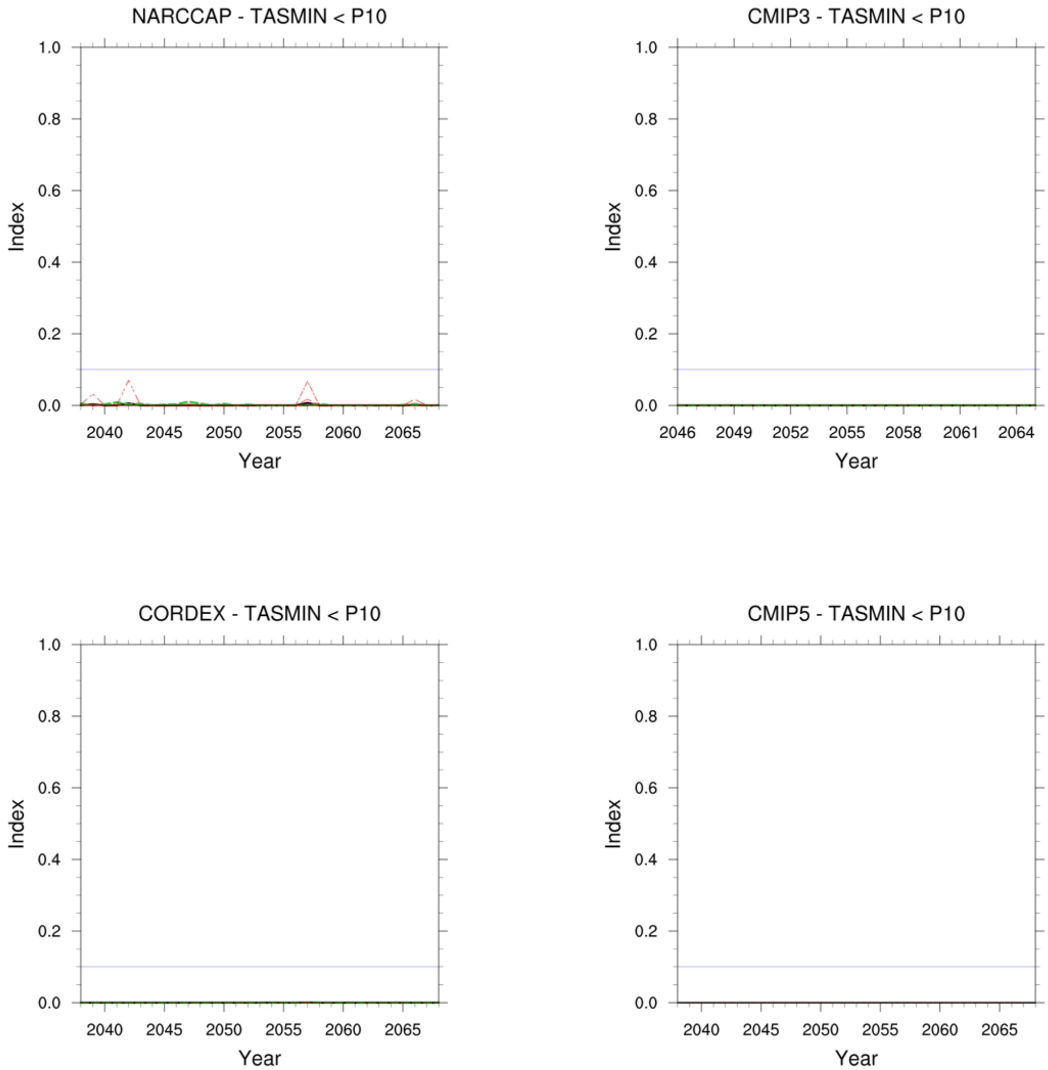

Figure 3.16: Regional Climate Extremes Index (rCEI) component TMIN10: minimum temperatures much below normal. The date range is 2038 to 2068, except for CMIP3, where the date range is 2046 to 2065. Black lines indicate ensemble mean values for the CONUS, while red lines indicate individual models. The green line represents the ensemble mean for just the Mid-Atlantic region. The blue line indicates the expected value of the component (0.1) for a stationary climate.

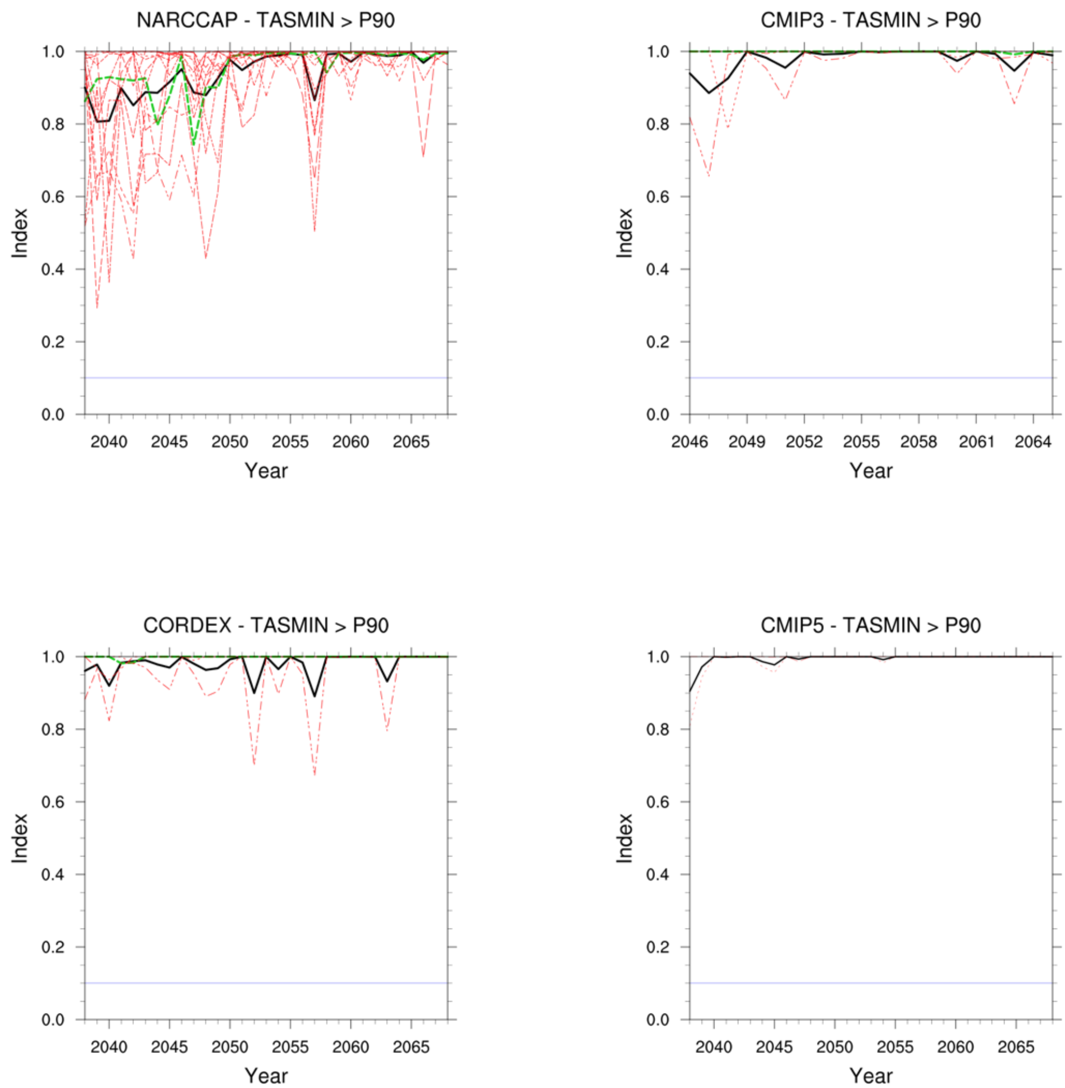

Figure 3.17: Climate Extremes Index (CEI) component TMIN90: minimum temperatures much above normal. The date range is 2038 to 2068, except for CMIP3, where the date range is 2046 to 2065. Black lines indicate ensemble mean values for the CONUS, while red lines indicate individual models. The green line represents the ensemble mean for just the Mid-Atlantic region. The blue line indicates the expected value of the component (0.1) for a stationary climate.

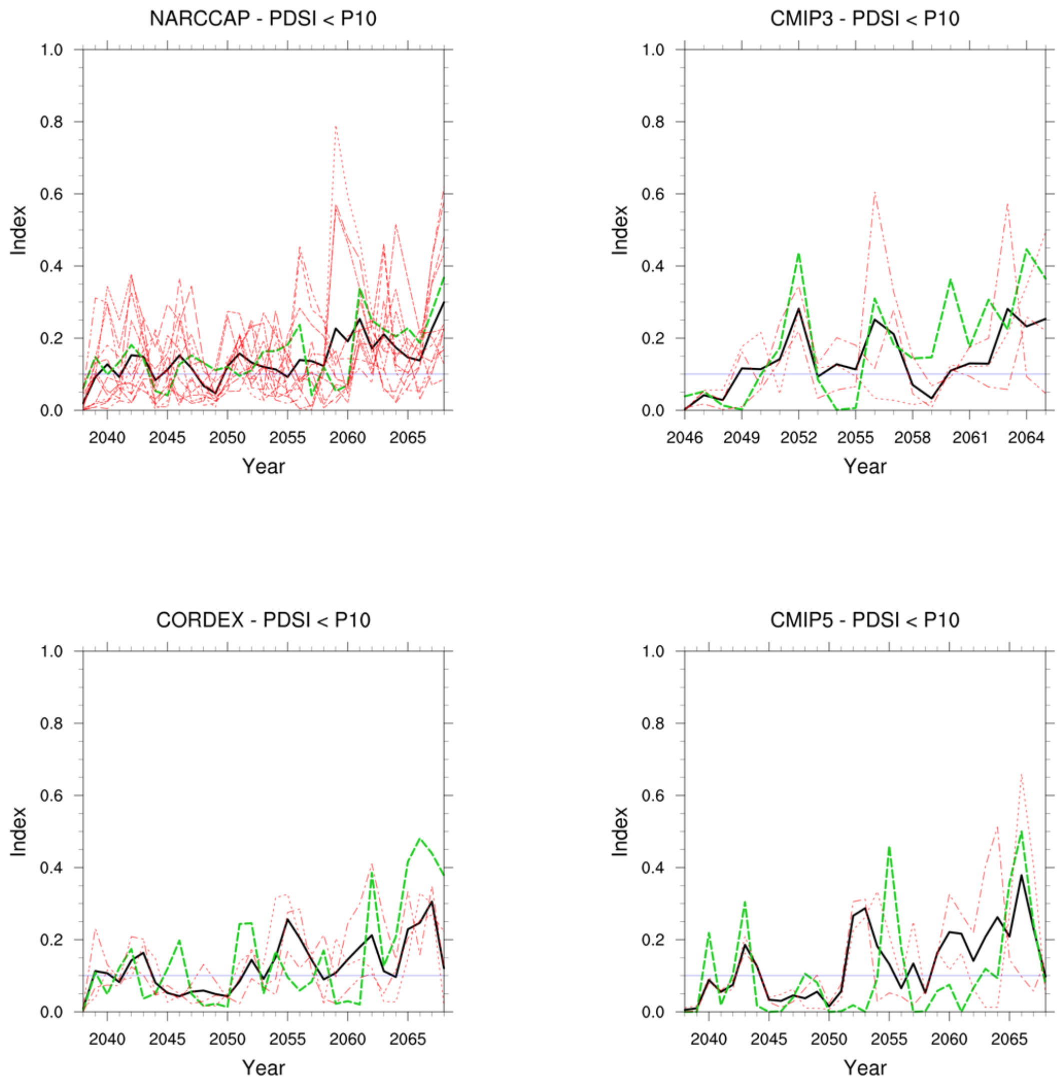

Figure 3.18: Climate Extremes Index (CEI) component PDSI10: strong negative values of the PDSI (indicating severe drought). The date range is 2038 to 2068, except for CMIP3, where the date range is 2046 to 2065. Black lines indicate ensemble mean values for the CONUS, while red lines indicate individual models. The green line represents the ensemble mean for just the Mid-Atlantic region. The blue line indicates the expected value of the component (0.1) for a stationary climate.

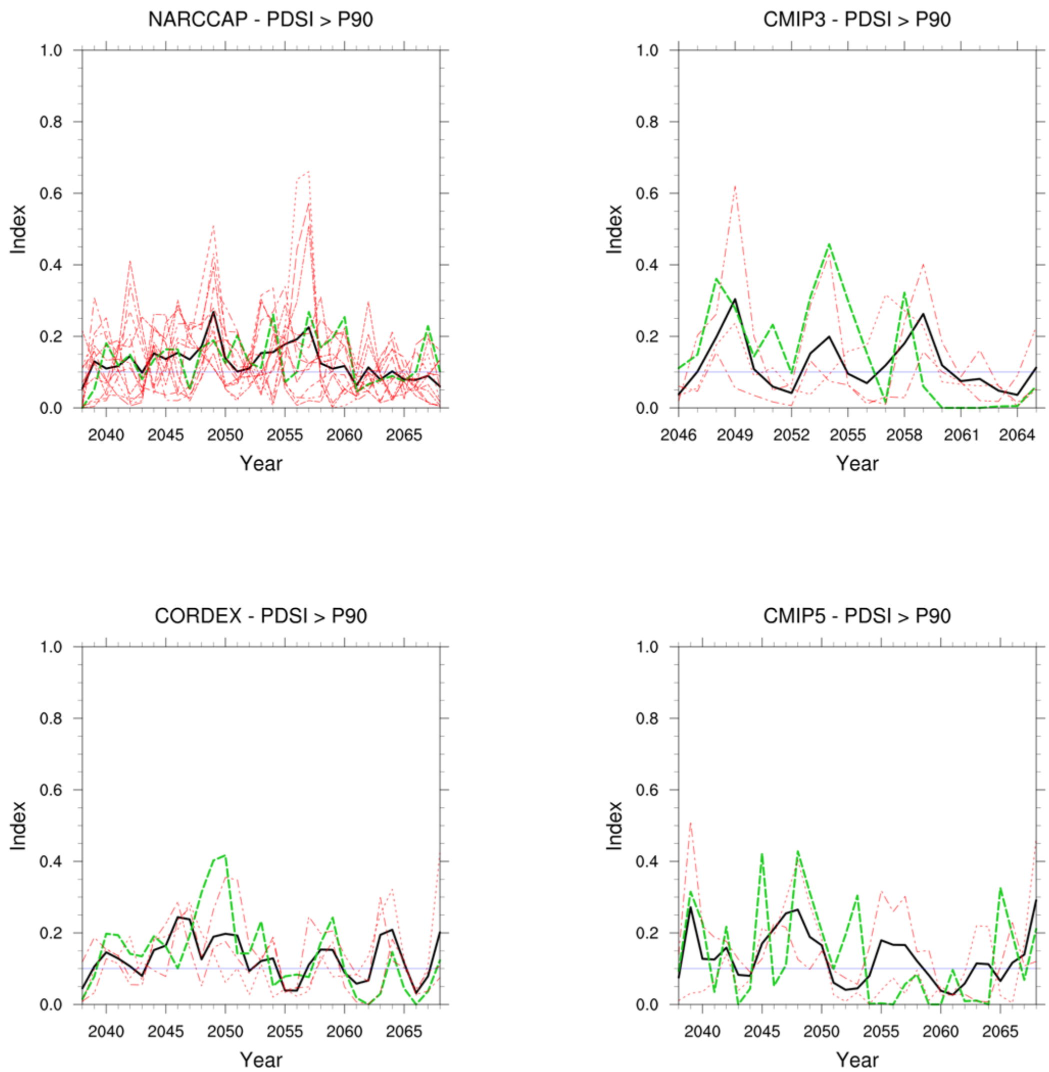

Figure 3.19: Climate Extremes Index (CEI) component PDSI90: strong positive values of the PDSI (indicating severe moisture surplus). The date range is 2038 to 2068, except for CMIP3, where the date range is 2046 to 2065. Black lines indicate ensemble mean values for the CONUS, while red lines indicate individual models. The green line represents the ensemble mean for just the Mid-Atlantic region. The blue line indicates the expected value of the component (0.1) for a stationary climate.

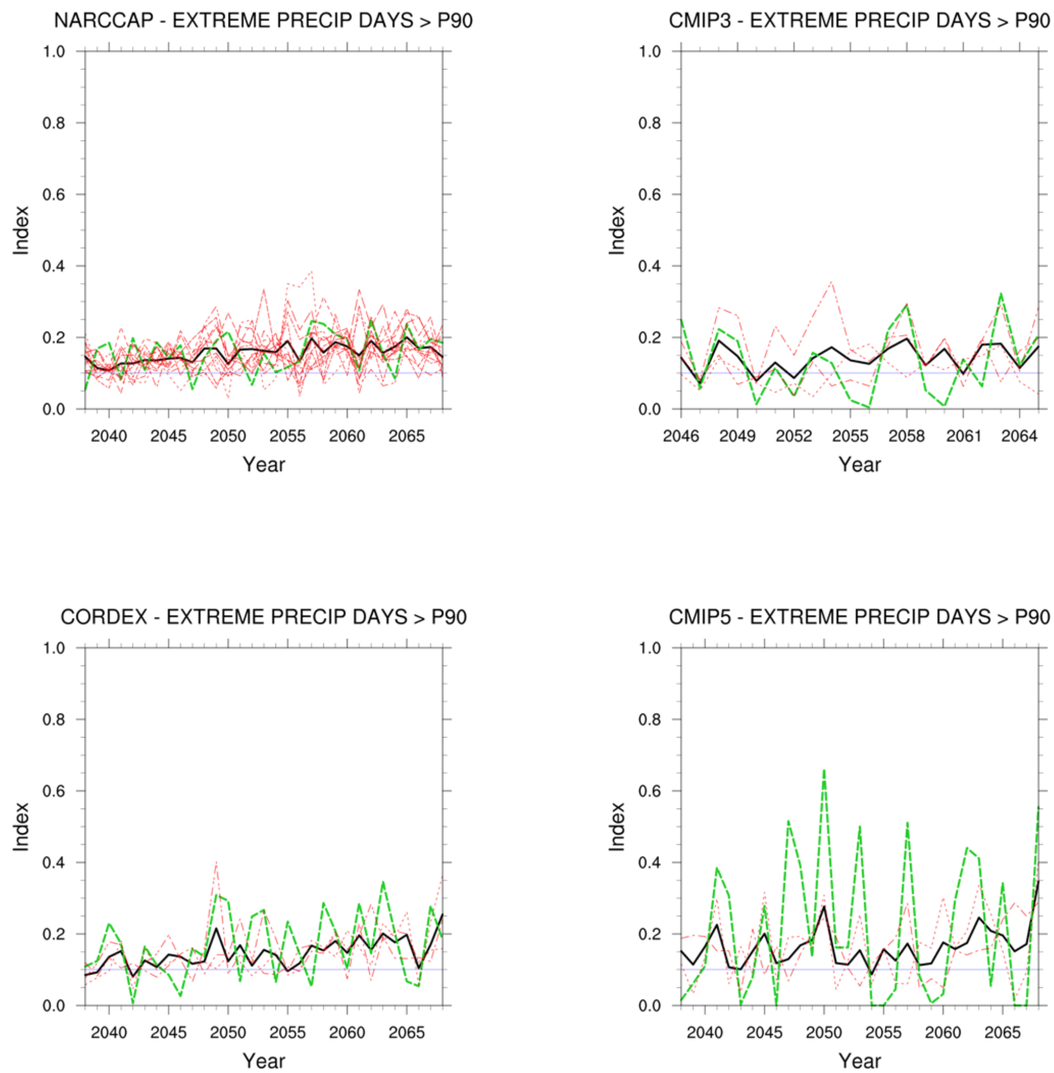

Figure 3.20: Climate Extremes Index (CEI) component ECP90: precipitation derived from extreme 1-day precipitation events. The date range is 2038 to 2068, except for CMIP3, where the date range is 2046 to 2065. Black lines indicate ensemble mean values for the CONUS, while red lines indicate individual models. The green line represents the ensemble mean for just the Mid-Atlantic region. The blue line indicates the expected value of the component (0.1) for a stationary climate.

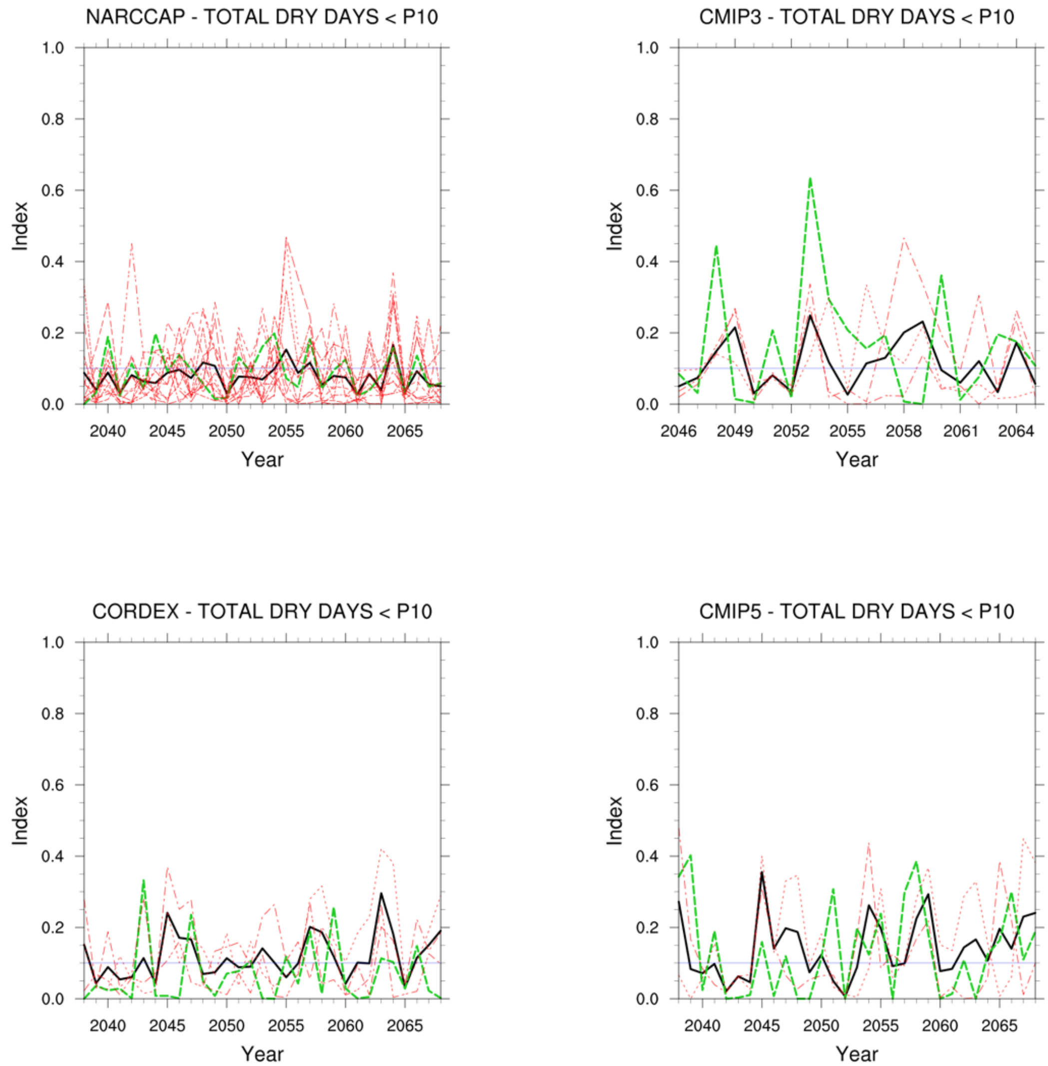

Figure 3.21: Climate Extremes Index (CEI) component TDD10: greater than normal days with precipitation. The date range is 2038 to 2068, except for CMIP3, where the date range is 2046 to 2065. Black lines indicate ensemble mean values for the CONUS, while red lines indicate individual models. The green line represents the ensemble mean for just the Mid-Atlantic region. The blue line indicates the expected value of the component (0.1) for a stationary climate.

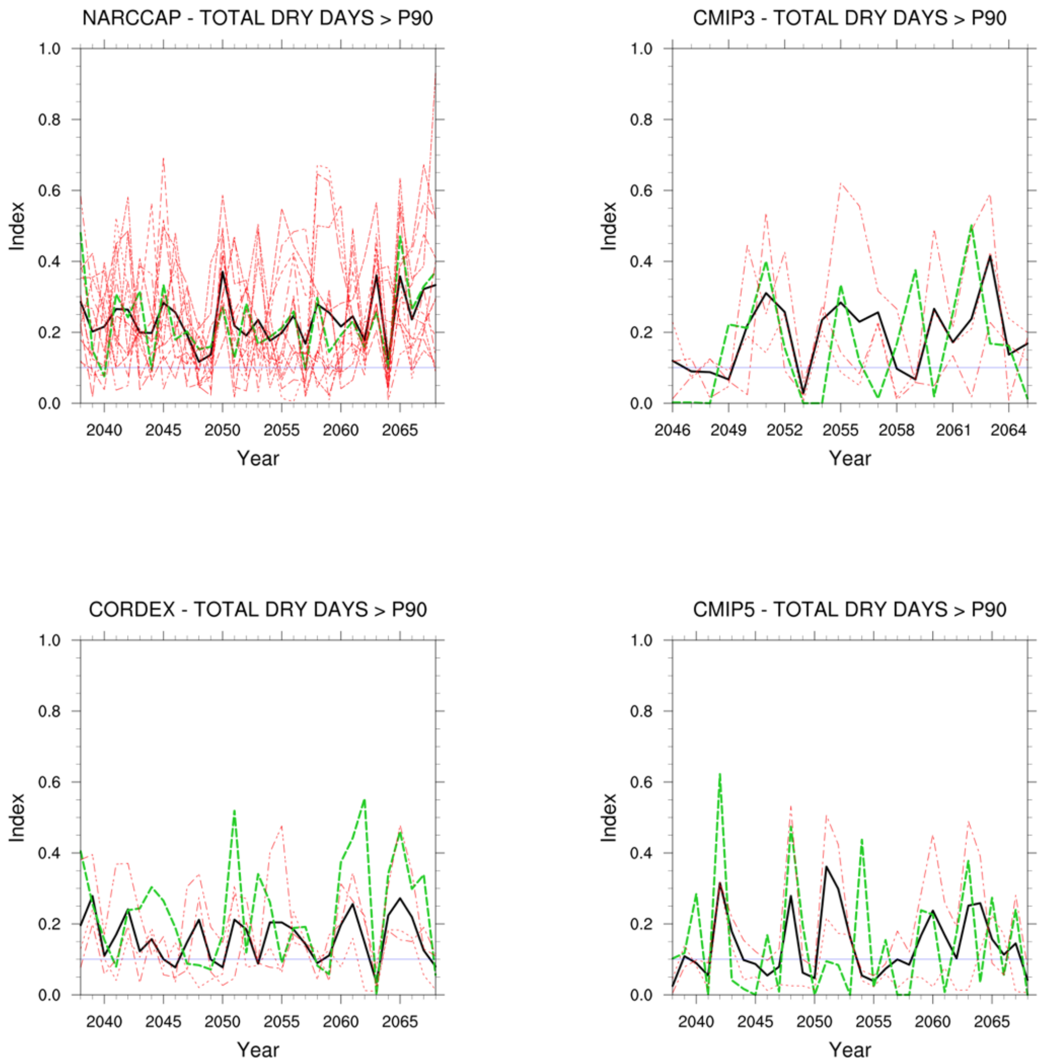

Figure 3.22: Climate Extremes Index (CEI) component TDD90: greater than normal days without precipitation. The date range is 2038 to 2068, except for CMIP3, where the date range is 2046 to 2065. Black lines indicate ensemble mean values for the CONUS, while red lines indicate individual models. The green line represents the ensemble mean for just the Mid-Atlantic region. The blue line indicates the expected value of the component (0.1) for a stationary climate.

Chapter 4

SPATIAL TRENDS

While the index provides a snapshot of the U.S. as a whole, and an effective means of comparing changes over time, it does not on its own provide any spatial information on where these changes are occurring. To examine the spatial patterns of the CEI, we calculate the CEI in the time axis, rather than on the latitude/longitude axes, and show the result on a series of maps. While the original index is a measure of the percentage of gridpoints over the CONUS that experience extremes in each year, the maps in the following section show how many years are extreme at each gridpoint. In both cases, the result is expressed as a proportion, ranging from 0 to 1. In the following section, a value of 0 indicates that gridpoint never exceeded the historic threshold, while a value of 1 indicates that every timestep for that grid cell exceeded the historic threshold. This method of visualizing the CEI over space rather than time is new, and was developed specifically for this study.

As explained in the previous section, the individual components of the CEI are designed to assess both warm and cold extremes, as well as precipitation extremes in both directions (dry and wet). To facilitate visual understanding, common color bars are used across all maps and all indicators: values in orange/red indicate unusually warm conditions, values in blue indicate unusually cool conditions, values in brown indicate unusually dry conditions, and values in green/teal indicate unusually wet conditions, in comparison to their historic baseline values.

4.1 Maximum Temperature

As expected from the CEI values shown in the previous section, maximum temperatures for the future scenario almost never fall below the historic 10^{th} percentile threshold. For NARCCAP (Figure 4.1) three model pairings have consistent values of 0 for every grid point: MM5I-CCSM, CRCM-CGCM3, and RCM3-CGCM3. For CMIP3 (Figure 4.2), both CCSM and GFDL have consistent values of 0 at each grid point, and CGCM3 has only a few values above zero, near Texas. Both of the CMIP5 GCMs (Figure 4.3) have consistent values of zero at all grid points, as does the CanESM2-RCA4 pairing; the EC-EARTH-RCA4 and EC-EARTH-HIRHAM5 pairings show only a few values higher than zero, all close enough to the edge of the map that they could potentially be affected by boundary conditions.

In contrast, while the 90^{th} percentile indicator still shows consistent warming across the entire contiguous US, the magnitude of that warming is very different on the coasts versus the interior. There is one surprisingly consistent pattern across all models: virtually all of them show more extreme changes over the coastlines, and less extreme heating over the interior of the continent, especially the US Midwest. For example, compare the WRFG-CGCM3 to the MM5I-HadCM3 (Figure 4.4): they share neither an RCM nor a GCM boundary forcing, and yet they both produce a very similar distinct J-shape over the center of the U.S. The MM5I-CCSM also shares a similar spatial pattern in the north, although that one does not extend as far south. This would appear to be the opposite of initial expectations; coastlines generally have less extreme temperatures because the ocean acts as a heat sink. While the pattern is not as immediately evident in the CMIP3 models (Figure 4.5), once again we can see a greater severity of relative warming on the coasts, with relatively milder warming in the interior, especially towards the center of the map. The pattern observed in

NARCCAP/CMIP3 is less apparent in the CanESM2 model, due to consistently high warming everywhere (Figure 4.6). However, EC-EARTH does show that same distinctive vertical band over the center of the US, and it carries over into the RCA4 model pairing. While climate models cannot be said to be truly independent of one another, the consistency of this pattern across different RCMs and forcings may be indicative of a physical phenomenon.

Overall, all models are in agreement that both minimum and maximum temperatures will exceed historic thresholds across a majority of the continental United States. This is consistent with findings of the National Climate Assessment, indicating that heat waves are projected to become more intense everywhere across the nation (Walsh et al. 2014). In terms of the unusual Midwestern spatial trend in maximum temperatures, a few possible explanations present themselves. The first possibility is model error. Predictions at the center of RCM domains are less driven by boundary conditions, more driven by model physics, so too-large domains can become decoupled from their boundaries and produce conditions independent of global forcings (Downing et al. 2002). However, this occurs not only in NARCCAP, but also in CORDEX, and in several global models which have no such boundary forcings; let's not stop at the conclusion that the spatial trend is solely a domain error. The CEI is calculated via percentiles, so if the coastlines experience a smaller range of temperatures in the historic time period, it would take a proportionally smaller increase in temperature to exceed the 90^{th} percentile. It could simply be a case of the coasts "catching up" to the interior, while the Midwest is already experiencing extreme heat waves.

A third possibility, however, is related to land cover change and changes in surface energy budget. One study of observed station temperatures from 1910 to 2014 found cooler summer temperature extremes in the Midwest over the 20th century, which they concluded was due to cropland intensification and associated increase in evapotranspiration (Mueller et al. 2012). They found that cooling trends were greatest for the highest temperature percentiles, which is consistent with both greater evapotranspiration and with a reduction in CEI values (Mueller et al. 2012). Another study of agricultural effects on boundary layer processes found significantly lower latent and sensible heat fluxes for simulations of irrigated land, and near-ground temperatures 1.2˚C cooler than the control (Adegoke et al. 2007). On the other hand, in this case, cooler temperatures may not necessarily correlate with an associated decrease in climate-related risk; a study of extreme heat events in Chicago suggested that enhanced evapotranspiration from agriculture led to an increase in dew-point values, and an associated increase in risk to human health from extreme urban heat (Changnon et al. 2003).

As a secondary aspect of the analysis, I wanted to explore whether RCM physics or GCM boundary forcings had a stronger impact on CEI results. In other words, which were more similar: model pairings that shared an RCM, or pairings that shared a GCM? Table 4.1 is a correlation table for the TMAX90 values for all twelve NARCCAP models; as with earlier, NARCCAP was chosen due to the highest number of ensemble members. TMAX10 was excluded, as the high number of zero values resulted in artificially low correlations across all model pairings. For TMAX90, there was universal strong agreement, with correlation values of 0.98 or higher for all model pairings, even those that shared neither an RCM nor a GCM. This is a reflection of how consistent the temperature results were between models; since all NARCCAP models showed a universal large increase in extreme high temperatures, there were simply not enough inter-model differences to determine if RCM physics or GCM boundary forcings had a greater impact.

Table 4.1: TMAX90 correlation table. Cells highlighted in red indicate model pairings that share RCM physics, while cells highlighted in blue indicate model pairings that share GCM boundary forcings.

	1.	2.	3.	4.	5.	6.	7.	8.	9.	10.	11.	12.
1.CRCM-CCSM												
2.CRCM-CGCM3	0.997											
3.ECP2-GFDL	0.990	0.992										
4.ECP2-HadCM3	0.995	0.996	0.989									
5.HRM3-GFDL	0.997	0.998	0.992	0.995								
6.HRM3-HadCM3	0.997	0.997	0.991	0.996	0.997							
7.MM5I-CCSM	0.983	0.979	0.982	0.976	0.978	0.981						
8.MM5I-HadCM3	0.985	0.985	0.989	0.984	0.983	0.985	0.982					
9.RCM3-CGCM3	0.995	0.995	0.991	0.993	0.994	0.996	0.985	0.985				
10.RCM3-GFDL	0.990	0.991	0.995	0.988	0.991	0.992	0.983	0.988	0.992			
11.WRFG-CCSM	0.993	0.992	0.992	0.988	0.992	0.992	0.993	0.988	0.992	0.992		
12.WRFG-CGCM3	0.983	0.981	0.985	0.980	0.979	0.984	0.989	0.990	0.987	0.988	0.990	

4.2 Minimum Temperature

As seen in the previous section with the time series, future patterns for TMIN closely mirrored those for TMAX, but with even greater extremeness. There were very few models with minimum temperatures below the 10^{th} percentile. For TMIN10, seven out of twelve NARCCAP model pairings (Figure 4.7) had constant values of zero: CRCM-CCSM, CRCM-CGCM3, WRFG-CGCM3, RCM3-CGCM3, ECP2-HadCM3, HRM3-HadCM3, and MM5I-HadCM3. All three of the CMIP3 models (Figure 4.8) had consistent values of zero for all grid points. Both of the CMIP5 models (Figure 4.9) had constant values of zero at all grid points, as did the CanESM2-RCA4 pairing; the two EC-EARTH-RCM pairings had only a few values higher than zero, again happening close to the edge of the map.

For TMIN90 (Figures 4.10 through 4.12), as with TMAX90, there is a more or less consistent spatial pattern from model to model. Warming is generally extreme across the entire CONUS, but slightly less so in the northern parts of the country, especially over the Pacific Northwest. As this indicator measures the frequency of years in which minimum temperature exceeds the 90^{th} percentile, this could simply be a reflection of natural climate variation; cold fronts will continue to move over the northern part of the U.S., causing a handful of cold events per year, even as overall temperatures continue to rise.

Table 4.2 shows the correlation table for all twelve NARCCAP models for the TMIN90 indicator. TMIN10 was excluded, as above. Overall correlation rates for TMIN are even higher than for TMAX, with all correlation values at 0.99 or above. As such, it is impossible to draw any conclusions about whether GCM or RCM has a stronger impact on CEI results for temperature; inter-model agreement is simply too high to determine which is the deciding factor. In other words, all models show warming in response to increased greenhouse gases.

Table 4.2: TMIN90 correlation table. Cells highlighted in red indicate model pairings that share RCM physics, while cells highlighted in blue indicate model pairings that share GCM boundary forcings.

	1.	2.	3.	4.	5.	6.	7.	8.	9.	10.	11.	12.
1.CRCM-CCSM												
2.CRCM-CGCM3	0.999											
3.ECP2-GFDL	0.991	0.991										
4.ECP2-HadCM3	0.999	0.999	0.991									
5.HRM3-GFDL	0.998	0.998	0.995	0.998								
6.HRM3-HadCM3	0.999	0.999	0.991	0.999	0.998							
7.MM5I-CCSM	0.996	0.996	0.992	0.996	0.996	0.996						
8.MM5I-HadCM3	0.994	0.994	0.989	0.995	0.992	0.995	0.993					
9.RCM3-CGCM3	0.999	0.999	0.993	0.999	0.998	0.999	0.997	0.995				
10.RCM3-GFDL	0.992	0.992	0.998	0.992	0.995	0.991	0.993	0.990	0.994			
11.WRFG-CCSM	0.997	0.997	0.991	0.997	0.997	0.997	0.996	0.992	0.997	0.992		
12.WRFG-CGCM3	0.999	0.999	0.991	0.998	0.997	0.999	0.996	0.995	0.999	0.991	0.997	

4.3 PDSI

As shown in Figure 4.13, spatial patterns for the PDSI are heterogeneous, and vary from model to model. There is no immediately visible spatial signal, in contrast with the temperature indices. The CMIP3 models (4.14) show slightly more spatial agreement than their NARCCAP counterparts, though not by much; both CCSM and GFDL show a slight tendency towards drought on the eastern half of the US and the west coast, but CGCM3 reverses this, with the largest area of extreme drought over the Rockies. The comparison between GCM and RCM is easier to make with the two side-by-side: as can be seen in Figure 4.15, the RCMs and their driving GCMs have roughly similar spatial patterns, but the patterns in the RCM are more diffuse and heterogeneous, possibly related to the effects of higher horizontal resolution on precipitation patterns. As predicted by Schrier et al. (2011), extreme values of the PDSI are heterogeneous, following individual model patterns of precipitation. While a few potential signals can be seen – a vertical band across the Midwest in the NARCCAP data where the index tends towards drought, for instance – they are not consistent between model groups.

While interpretation of the temperature indices is straightforward, several of the precipitation indices show significant variation in spatial distribution from model to model. To better facilitate interpretation, I created a series of maps intended to show areas of common agreement between multiple models. The maps in Figure 4.16 and 4.20 do not reflect magnitude of changes in the indicators, but only the degree of agreement between models. Each grid cell for each model was assigned a binary value, 0 or 1, indicating whether the value for that cell was unusually wet or unusually dry in comparison to the historic baseline. These binary maps were then averaged together to create a composite map. High values indicate broad consensus between models that the value is higher than 0.1, while low values also indicate broad consensus between models that the value is below 0.1. These values are marked in dark brown and dark teal, respectively, indicating whether the index represents an increase or decrease in precipitation extremes. Mid-range values close to 0.5 indicate that models are divided on whether a particular grid cell has higher or lower values than expected, and these are marked in lighter brown or teal, closer to white. Note that while the NARCCAP had twelve models in its ensemble, CMIP3 and CORDEX had 3 each, and CMIP5 had only two. Hence the possible values for CMIP5 were only 0, 0.5, or 1.

Tables 4.3 and 4.4 show NARCCAP model correlation for the PDSI10 and PDSI90 indicators, respectively. Two things are clear: first, overall correlation for the PDSI is lower than for temperature, with values around 0.7 for PDSI10, and around 0.6 for PDSI90, as compared to values of 0.98 and higher for maximum and minimum temperature. Additionally, there does not appear to be any strong relationship between either GCM or the RCMs that are forced by that particular GCM. Some of the highest correlation values are between model pairings that share neither a GCM nor an RCM: for instance, one of the two highest-correlated model pairings for CRCM-CCSM is MM5I-HadCM3. Overall, models that share boundary forcings appear to be slightly more correlated than those that don't, but it is by no means a clear or universal trend.

The reasons for these two observations – that precipitation patterns in models are less clear and less correlated than temperature – are interrelated, and have to do with the difference in how climate models calculate temperature vs precipitation.

Temperature is a smooth gradient field; it can be calculated at any resolution, and can be comparatively easily interpolated from one grid to another. By contrast, precipitation events frequently happen at scales smaller than a single grid cell, even for RCMs, and thus must be calculated via a combination of explicit model physics and subgrid-scale parameterizations for processes such as convection and cloud physics (Wehner 2012). Climate models are not all wholly independent, and many models use similar physics and parameterization schema; for instance, CRCM and MM5I both use a form of mass flux for their cumulus parameterization (NARCCAP 2008). A full discussion and comparison of precipitation physics between regional models is beyond the scope of this project, but could be a compelling direction for future research.

Table 4.3: PDSI10 correlation table. Cells highlighted in red indicate model pairings that share RCM physics, while cells highlighted in blue indicate model pairings that share GCM boundary forcings.

	1.	2.	3.	4.	5.	6.	7.	8.	9.	10.	11.	12.
1.CRCM-CCSM												
2.CRCM-CGCM3	0.746											
3.ECP2-GFDL	0.726	0.655										
4.ECP2-HadCM3	0.753	0.720	0.711									
5.HRM3-GFDL	0.757	0.713	0.689	0.745								
6.HRM3-HadCM3	0.715	0.718	0.671	0.740	0.714							
7.MM5I-CCSM	0.776	0.694	0.705	0.733	0.716	0.685						
8.MM5I-HadCM3	0.780	0.719	0.699	0.742	0.741	0.732	0.736					
9.RCM3-CGCM3	0.758	0.738	0.688	0.748	0.716	0.724	0.740	0.719				
10.RCM3-GFDL	0.735	0.686	0.662	0.713	0.731	0.691	0.696	0.729	0.712			
11.WRFG-CCSM	0.780	0.728	0.742	0.764	0.728	0.712	0.775	0.759	0.750	0.712		
12.WRFG-CGCM3	0.729	0.720	0.697	0.735	0.714	0.718	0.707	0.713	0.733	0.720	0.735	

Table 4.4: PDSI90 correlation table. Cells highlighted in red indicate model pairings that share RCM physics, while cells highlighted in blue indicate model pairings that share GCM boundary forcings.

	1.	2.	3.	4.	5.	6.	7.	8.	9.	10.	11.	12.
1.CRCM-CCSM												
2.CRCM-CGCM3	0.662											
3.ECP2-GFDL	0.683	0.600										
4.ECP2-HadCM3	0.692	0.665	0.645									
5.HRM3-GFDL	0.676	0.636	0.643	0.692								
6.HRM3-HadCM3	0.672	0.695	0.613	0.658	0.657							
7.MM5I-CCSM	0.709	0.617	0.644	0.664	0.655	0.651						
8.MM5I-HadCM3	0.664	0.657	0.633	0.696	0.702	0.635	0.652					
9.RCM3-CGCM3	0.674	0.699	0.622	0.656	0.635	0.676	0.674	0.666				
10.RCM3-GFDL	0.683	0.651	0.660	0.674	0.673	0.673	0.653	0.662	0.676			
11.WRFG-CCSM	0.721	0.674	0.665	0.685	0.679	0.657	0.693	0.673	0.663	0.676		
12.WRFG-CGCM3	0.683	0.716	0.626	0.675	0.643	0.689	0.648	0.658	0.696	0.672	0.689	

4.4 Extreme Precipitation

As Figure 4.21 shows, the proportion of extreme precipitation is showing more extreme values at a majority of grid cells. There are scattered points of less extreme precipitation (shown in brown) but there is little consensus from model to model on the location of those points, and the predominant trend is increasing extreme precipitation. As expected from the graph of extreme precipitation over time in the previous section, the increase is not dramatic – with most values still at 0.3 or below – but it is consistent. For the CMIP3 models (Figure 4.22), both CCSM and CGCM3 have a mix of more and less extreme precipitation, while GFDL shows a more universal increase in precipitation extremes. In Figure 4.23, both the CMIP5 models, CanESM2 and EC-EARTH, show less extreme precipitation towards the center of the map; as both of these models are global, this trend cannot be attributed to domain size and boundary coupling issues. However, the decrease in extreme precipitation over the Midwest is not seen in the associated RCMs, which return to a diffuse and heterogeneous pattern.

The model agreement maps (Figure 4.24) for extreme precipitation support the conclusion derived from the time series graphs: extreme precipitation is increasing across the majority of the United States. While there is one notable brown region across the center of the CMIP3 map, the large amount of dark teal on all four agreement maps indicates a strong degree of inter-model support. While the change in extreme precipitation is not necessarily large in magnitude, it affects a broad area, and inter-model agreement reflects a high degree of certainty. Likewise, the majority of correlation values between NARCCAP model pairings in Table 4.5 are 0.8 and higher, representing stronger agreement than seen with the PDSI.

One potentially confounding factor is that regional models tend to produce more high intensity precipitation than GCMs. Horizontal resolution greatly affects a model's ability to simulate extreme precipitation; at least one study showed that at grid spacing greater than 50km, extreme precipitation events were significantly lower than observed rates (Wehner 2012). RCMs, with their finer resolution, can better resolve small-scale physical processes and local topography, which theoretically should make them better at reproducing realistic precipitation patterns (Caldwell 2010). However, several studies have shown that reanalysis-forced RCMs tend to significantly overpredict precipitation, especially extreme events, and underpredict frequency (Caldwell 2010, Rauscher et al. 2016). By contrast, GCMs tend to show a "drizzle problem", where global models have a higher precipitation frequency and lower intensity (Mearns et al. 1995, Schoof et al. 2015). This offers a potential explanation as to why the CMIP3 and CMIP5 results show less consistent increases in extreme precipitation than the NARCCAP and CORDEX model groups.

Table 4.5: EPD90 correlation table. Cells highlighted in red indicate model pairings that share RCM physics, while cells highlighted in blue indicate model pairings that share GCM boundary forcings.

	1.	2.	3.	4.	5.	6.	7.	8.	9.	10.	11.	12.
1.CRCM-CCSM												
2.CRCM-CGCM3	0.827											
3.ECP2-GFDL	0.803	0.795										
4.ECP2-HadCM3	0.811	0.802	0.783									
5.HRM3-GFDL	0.796	0.797	0.797	0.801								
6.HRM3-HadCM3	0.797	0.802	0.758	0.772	0.787							
7.MM5I-CCSM	0.826	0.826	0.812	0.808	0.822	0.791						
8.MM5I-HadCM3	0.799	0.799	0.777	0.788	0.771	0.796	0.797					
9.RCM3-CGCM3	0.824	0.795	0.797	0.800	0.802	0.768	0.817	0.795				
10.RCM3-GFDL	0.827	0.807	0.808	0.812	0.819	0.803	0.821	0.806	0.815			
11.WRFG-CCSM	0.850	0.792	0.799	0.811	0.791	0.773	0.828	0.797	0.834	0.836		
12.WRFG-CGCM3	0.833	0.814	0.797	0.801	0.807	0.774	0.823	0.790	0.823	0.820	0.832	

4.5 Days With/Without Precipitation

Unlike the PDSI, the total dry days indicator does show some clear spatial patterns, even if there is still disagreement between models. With some exceptions, the majority of NARCCAP models (shown in Figure 4.25) show a decrease in days with precipitation along the west coast extending into the southwest. Around half of the models also show a similar pattern on the east coast. Visually, RCM seems to be a stronger contributor than GCM for this indicator: the two HRM3 pairings, for instance, both show a decrease in days with precipitation across nearly the entire country, while the other two RCMs paired with the GFDL are both much less severe. With CMIP3 (Figure 4.26), the entire western half of the country shows an increase in years with extremely few precipitation days, in all three models. However, the CGCM3 model shows no reduction in precipitation days in the northwest, instead showing a reduction in precipitation days along the entire east coast. CMIP5 and CORDEX (Figure 4.27) show a clear spatial pattern, although it is slightly different than the pattern shown in CMIP3/NARCCAP. A tendency toward decreased days with precipitation is concentrated in the south for all three RCMs, even when that pattern is not necessarily present in the driving GCMs. And again, several of the models show areas of decreased precipitation days along both the east and west coasts.

When examining model agreement (Figure 4.28) for the total dry days indicator, clear spatial patterns emerge. The west coast is a clear hotspot for reduction in precipitation days, as are parts of the south and southwest, depending on model group. However, parts of the northeast and Mid-Atlantic region also show reduced precipitation days, in all four model groups. While the spatial pattern is less clearly visible on the CMIP5 map, this may be partially attributable to the low number of models in the CMIP5 ensemble. Tables 4.6 and 4.7 show that correlation between NARCCAP models is stronger for the 90th percentile indicator – representing unusually dry years– than for the 10th percentile indicator.

The NARCCAP set of models seems to have strong agreement that extreme years with very few precipitation events will increase across the entire United States, while other model groups do not necessarily show this pattern. As with the total dry days indicator, however, both the west coast and the Mid-Atlantic are highlighted by these maps as potential hotspots for a change in precipitation frequency. Taken in conjunction with the extreme precipitation component, the overall conclusion is that total number of precipitation events per year will decrease, but each individual event will be more intense.

Table 4.6: TDD10 correlation table. Cells highlighted in red indicate model pairings that share RCM physics, while cells highlighted in blue indicate model pairings that share GCM boundary forcings.

	1.	2.	3.	4.	5.	6.	7.	8.	9.	10.	11.	12.
1.CRCM-CCSM												
2.CRCM-CGCM3	0.627											
3.ECP2-GFDL	0.584	0.465										
4.ECP2-HadCM3	0.448	0.462	0.678									
5.HRM3-GFDL	0.499	0.355	0.602	0.373								
6.HRM3-HadCM3	0.450	0.515	0.581	0.642	0.512							
7.MM5I-CCSM	0.634	0.603	0.658	0.534	0.522	0.504						
8.MM5I-HadCM3	0.481	0.539	0.619	0.670	0.481	0.668	0.616					
9.RCM3-CGCM3	0.569	0.615	0.645	0.584	0.551	0.594	0.697	0.607				
10.RCM3-GFDL	0.560	0.377	0.688	0.460	0.656	0.473	0.611	0.463	0.669			
11.WRFG-CCSM	0.657	0.582	0.608	0.524	0.561	0.522	0.776	0.597	0.699	0.653		
12.WRFG-CGCM3	0.599	0.576	0.623	0.562	0.510	0.533	0.738	0.518	0.702	0.650	0.759	

Table 4.7: TDD90 correlation table. Cells highlighted in red indicate model pairings that share RCM physics, while cells highlighted in blue indicate model pairings that share GCM boundary forcings.

	1.	2.	3.	4.	5.	6.	7.	8.	9.	10.	11.	12.
1.CRCM-CCSM												
2.CRCM-CGCM3	0.855											
3.ECP2-GFDL	0.752	0.722										
4.ECP2-HadCM3	0.683	0.764	0.826									
5.HRM3-GFDL	0.749	0.723	0.799	0.705								
6.HRM3-HadCM3	0.722	0.762	0.785	0.770	0.799							
7.MM5I-CCSM	0.848	0.835	0.780	0.727	0.755	0.786						
8.MM5I-HadCM3	0.689	0.757	0.770	0.784	0.809	0.760	0.742					
9.RCM3-CGCM3	0.777	0.846	0.799	0.819	0.775	0.829	0.852	0.796				
10.RCM3-GFDL	0.752	0.702	0.805	0.699	0.837	0.728	0.819	0.770	0.777			
11.WRFG-CCSM	0.802	0.789	0.801	0.742	0.807	0.752	0.871	0.791	0.823	0.842		
12.WRFG-CGCM3	0.715	0.763	0.727	0.718	0.697	0.742	0.846	0.724	0.867	0.762	0.837	

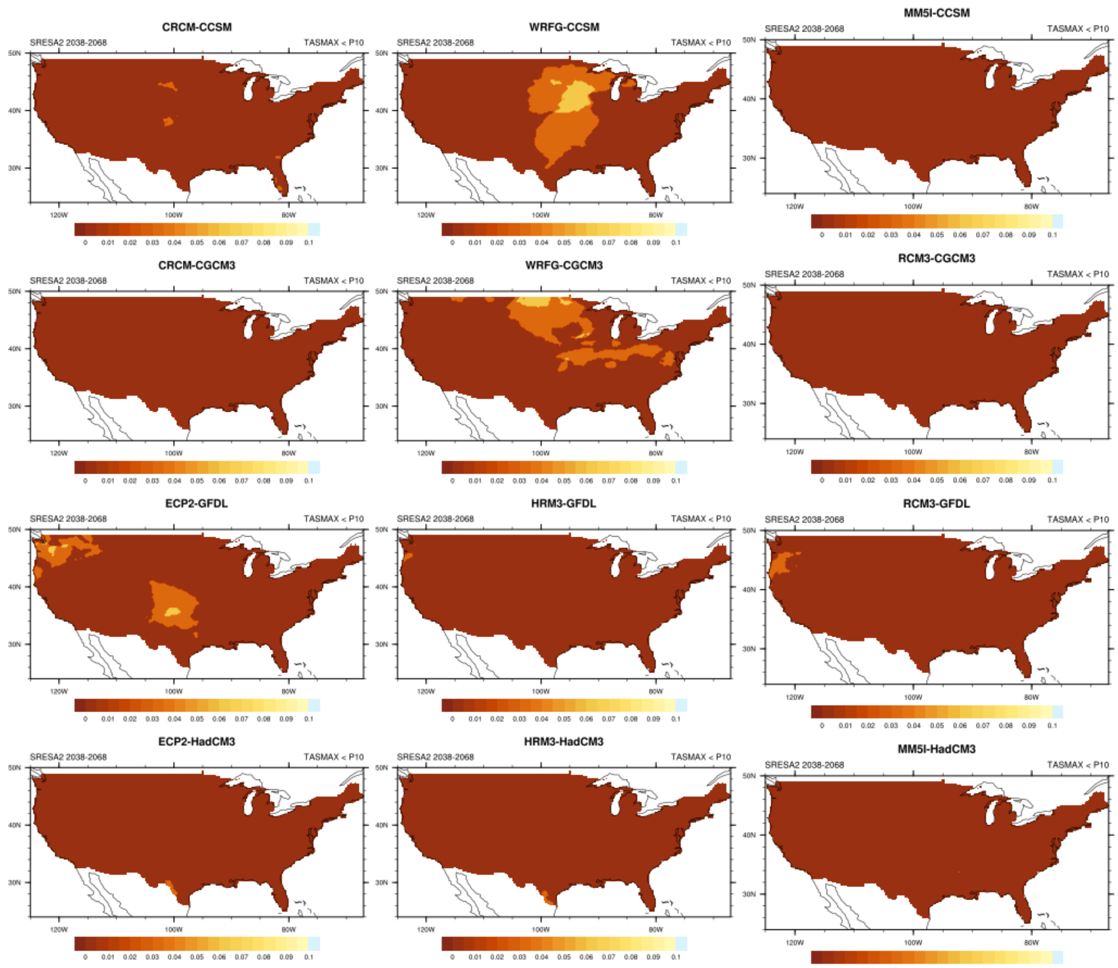

Figure 4.1: Climate Extremes Index (CEI) component TMAX10: maximum temperatures much below normal. The date range is 2038 to 2068. The scale is a dimensionless index: a value of 0 means the value never exceeded the historic threshold, while a value of 1 indicates that the value exceeded the historic threshold for every year of the analysis. NARCCAP model pairings are grouped by GCM in rows, and by RCM in columns.

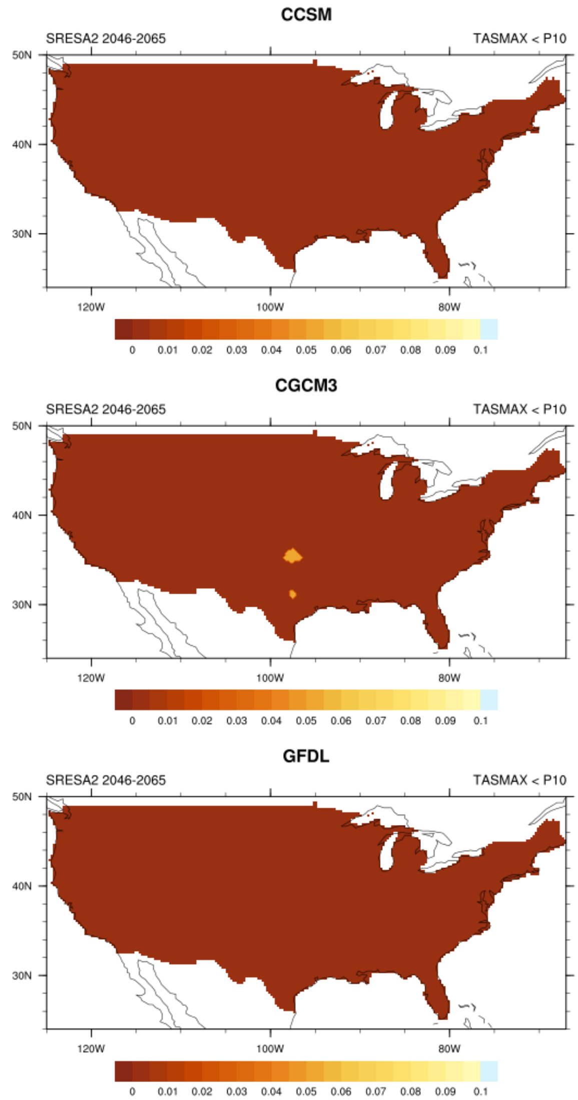

Figure 4.2: Climate Extremes Index (CEI) component TMAX10: maximum temperatures much below normal. The date range is 2046 to 2065. The scale is a dimensionless index: a value of 0 means the value never exceeded the historic threshold, while a value of 1 indicates that the value exceeded the historic threshold for every year of the analysis. All figures are for CMIP3: CCSM on top, CGCM3 in the middle, and GFDL on the bottom.

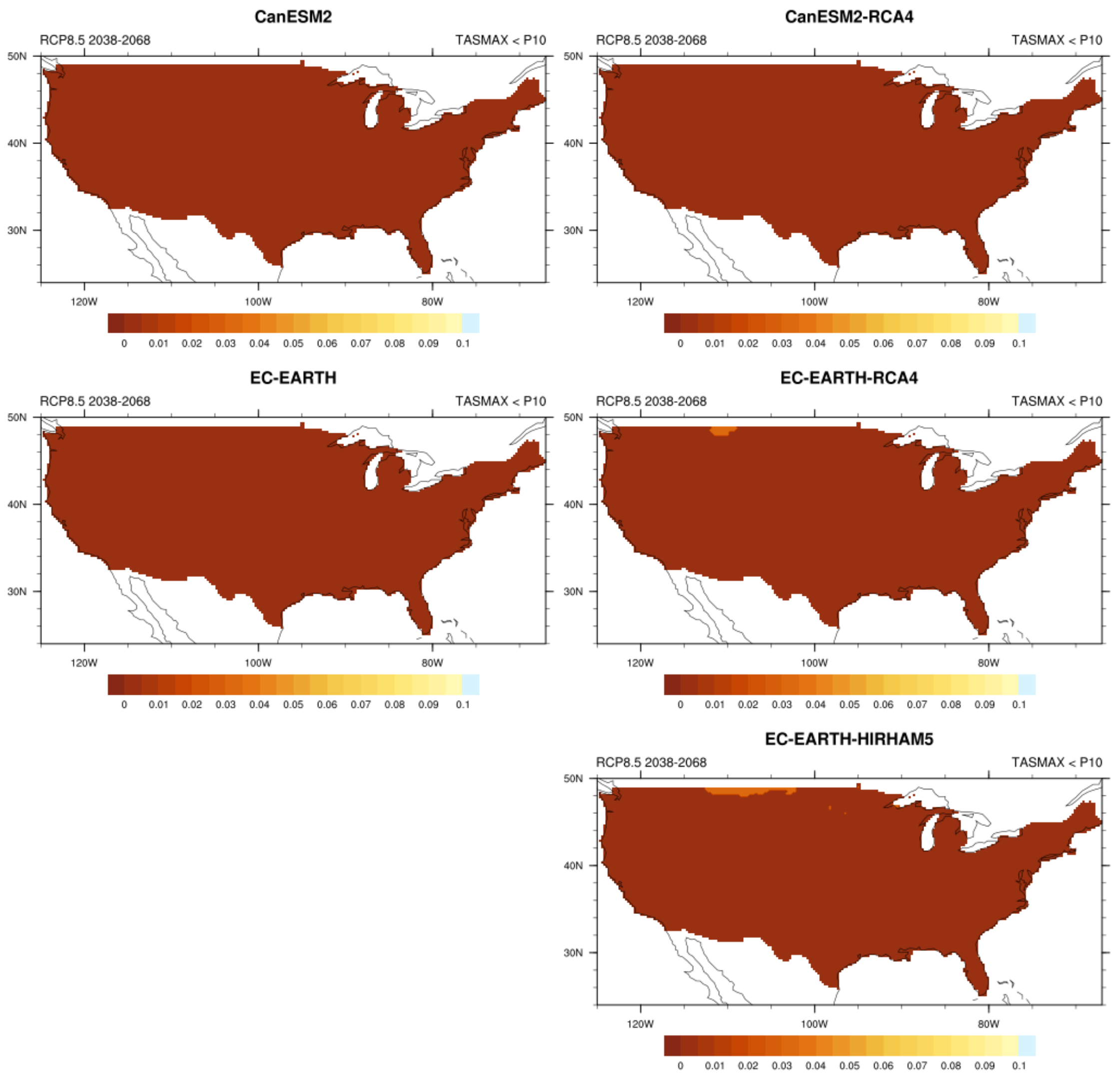

Figure 4.3: Climate Extremes Index (CEI) component TMAX10: maximum temperatures much below normal. The date range is 2038 to 2068. The scale is a dimensionless index: a value of 0 means the value never exceeded the historic threshold, while a value of 1 indicates that the value exceeded the historic threshold for every year of the analysis. Driving GCMs from CMIP5 are on the lefthand side, paired with CORDEX RCMs on the righthand side.

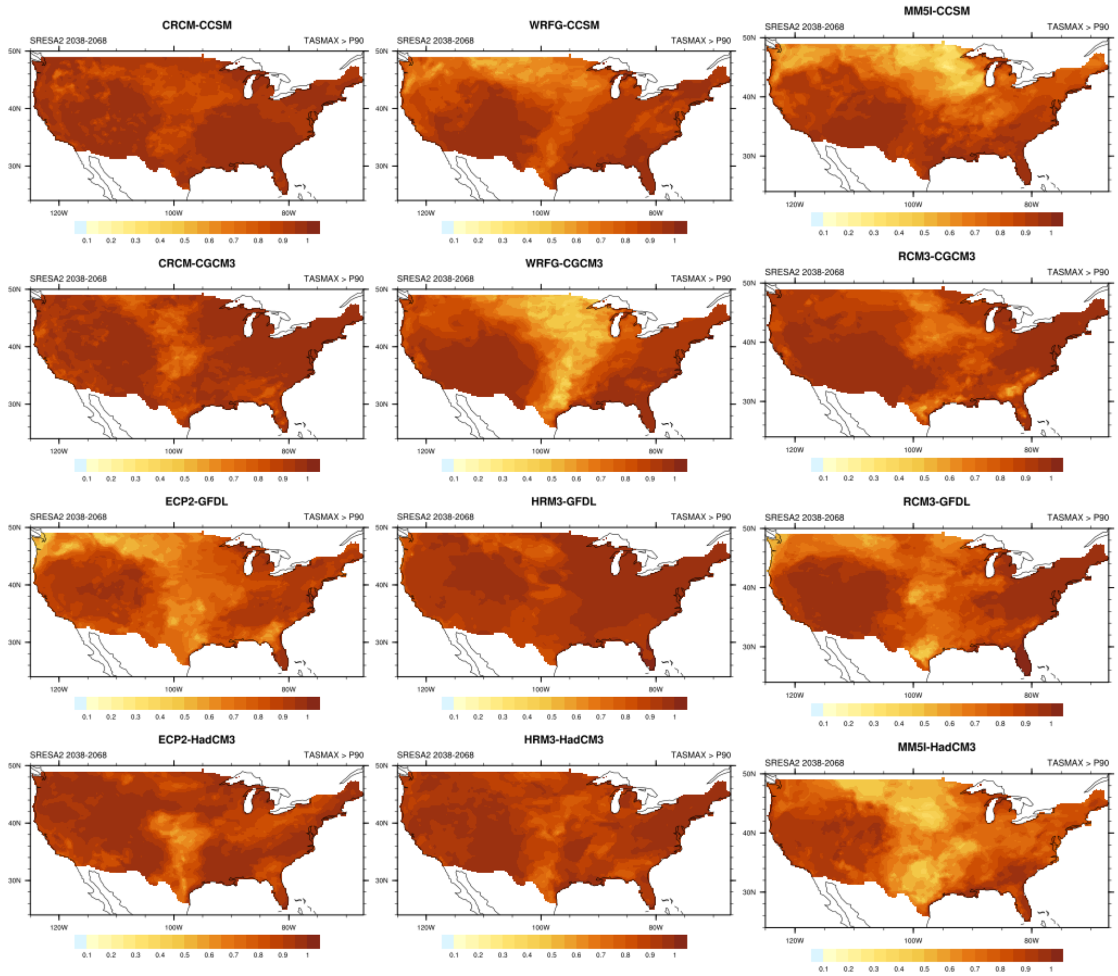

Figure 4.4: Climate Extremes Index (CEI) component TMAX90: maximum temperatures much above normal. The date range is 2038 to 2068. The scale is a dimensionless index: a value of 0 means the value never exceeded the historic threshold, while a value of 1 indicates that the value exceeded the historic threshold for every year of the analysis. NARCCAP model pairings are grouped by GCM in rows, and by RCM in columns.

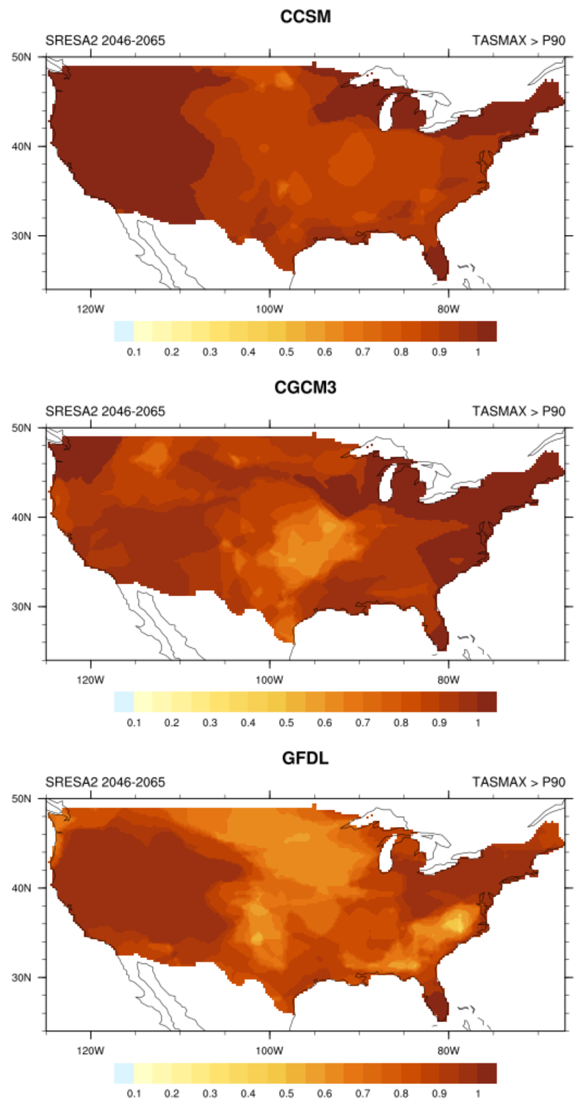

Figure 4.5: Climate Extremes Index (CEI) component TMAX90: maximum temperatures much above normal. The date range is 2046 to 2065. The scale is a dimensionless index: a value of 0 means the value never exceeded the historic threshold, while a value of 1 indicates that the value exceeded the historic threshold for every year of the analysis. All figures are for CMIP3: CCSM on top, CGCM3 in the middle, and GFDL on the bottom.

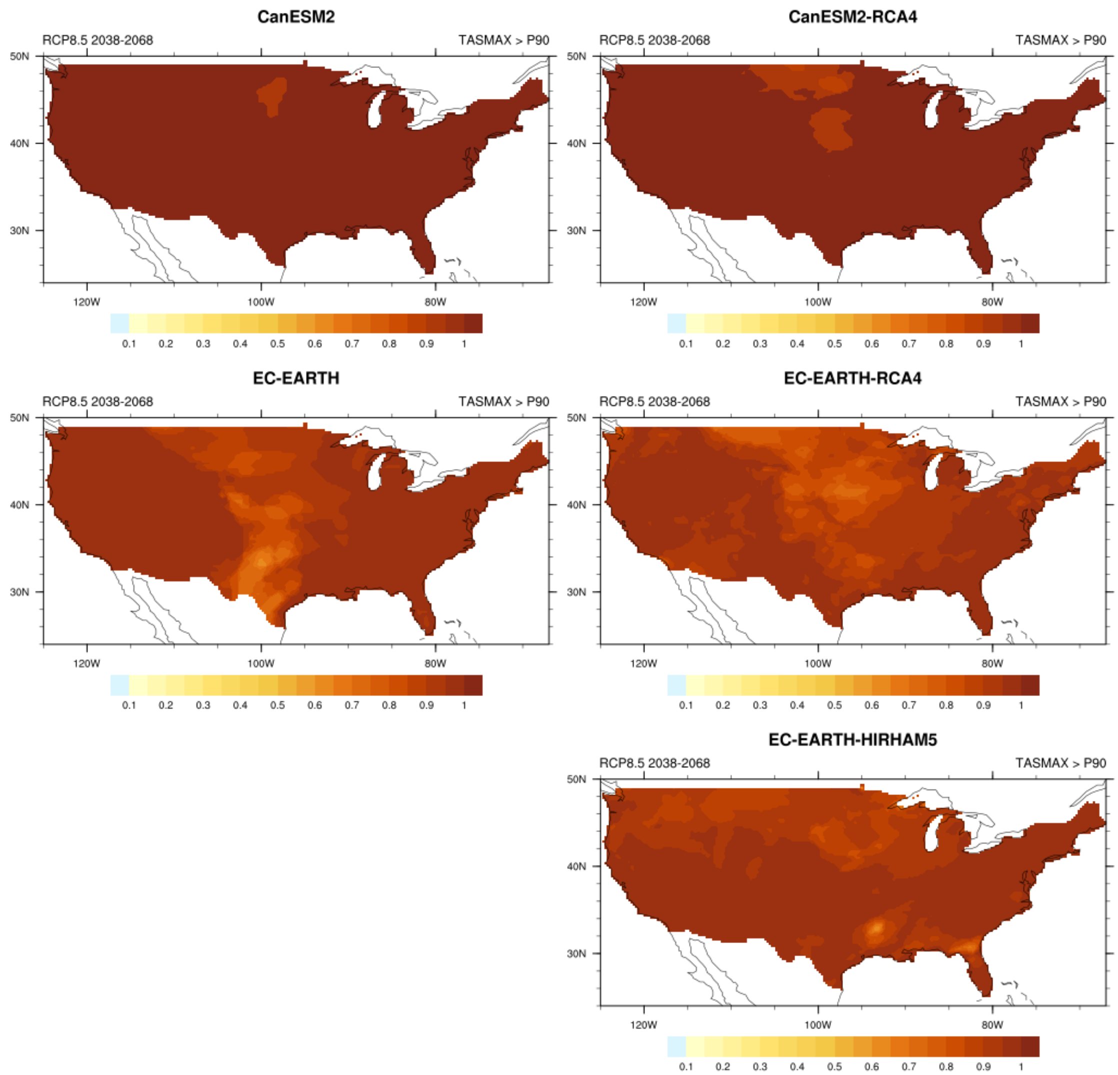

Figure 4.6: Climate Extremes Index (CEI) component TMAX90: maximum temperatures much above normal. The date range is 2038 to 2068. The scale is a dimensionless index: a value of 0 means the value never exceeded the historic threshold, while a value of 1 indicates that the value exceeded the historic threshold for every year of the analysis. Driving GCMs from CMIP5 are on the lefthand side, paired with CORDEX RCMs on the righthand side.

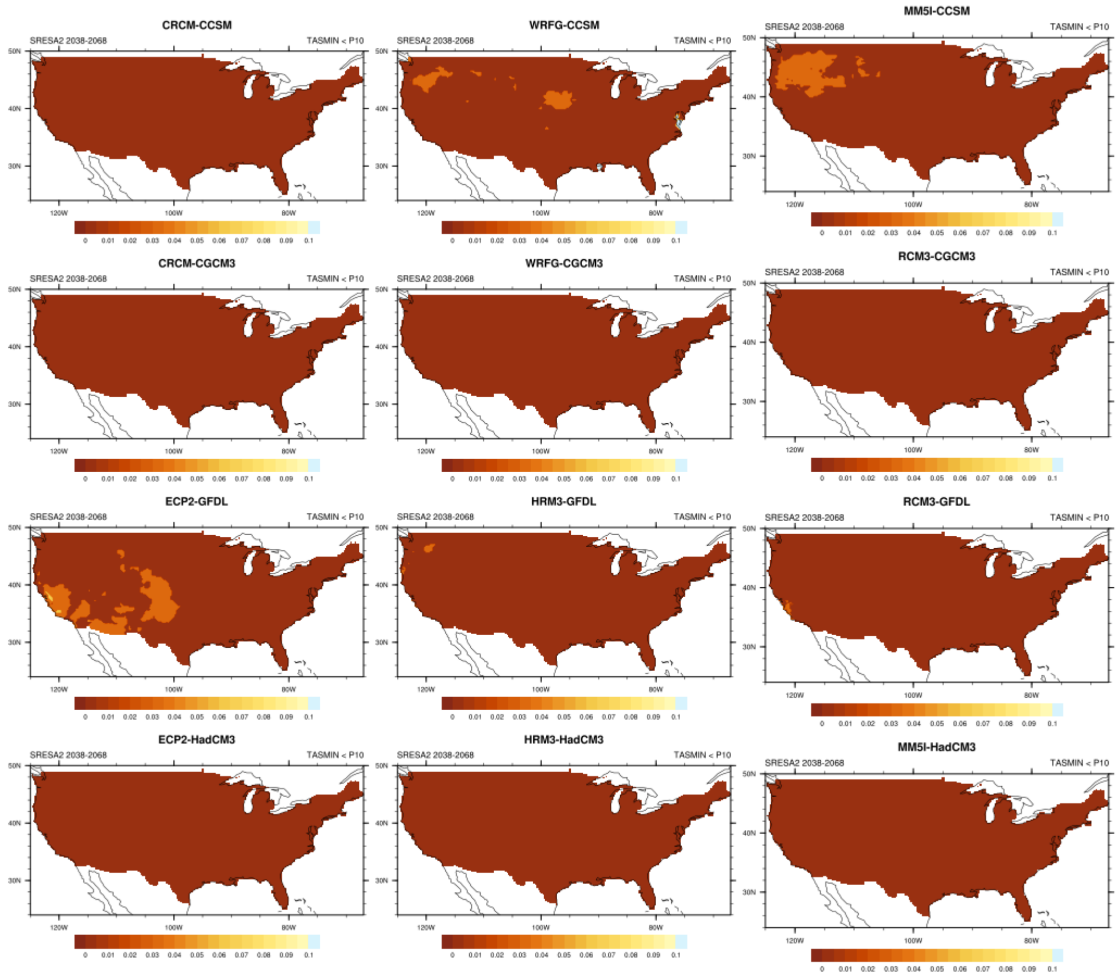

Figure 4.7: Climate Extremes Index (CEI) component TMIN10: minimum temperatures much below normal. The date range is 2038 to 2068. The scale is a dimensionless index: a value of 0 means the value never exceeded the historic threshold, while a value of 1 indicates that the value exceeded the historic threshold for every year of the analysis. NARCCAP model pairings are grouped by GCM in rows, and by RCM in columns.

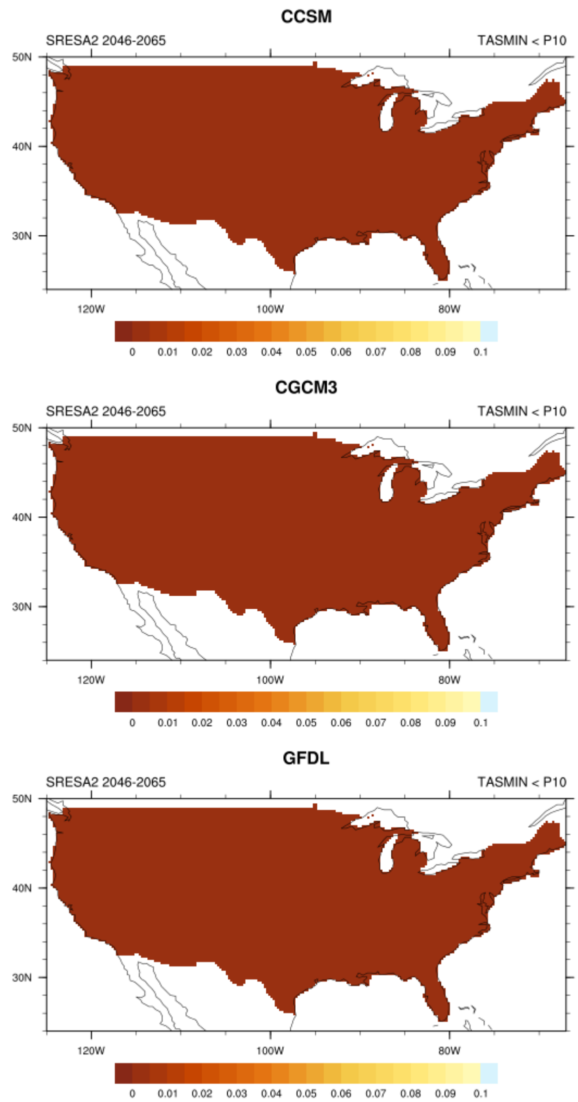

Figure 4.8: Climate Extremes Index (CEI) component TMIN10: minimum temperatures much below normal. The date range is 2046 to 2065. The scale is a dimensionless index: a value of 0 means the value never exceeded the historic threshold, while a value of 1 indicates that the value exceeded the historic threshold for every year of the analysis. All figures are for CMIP3: CCSM on top, CGCM3 in the middle, and GFDL on the bottom.

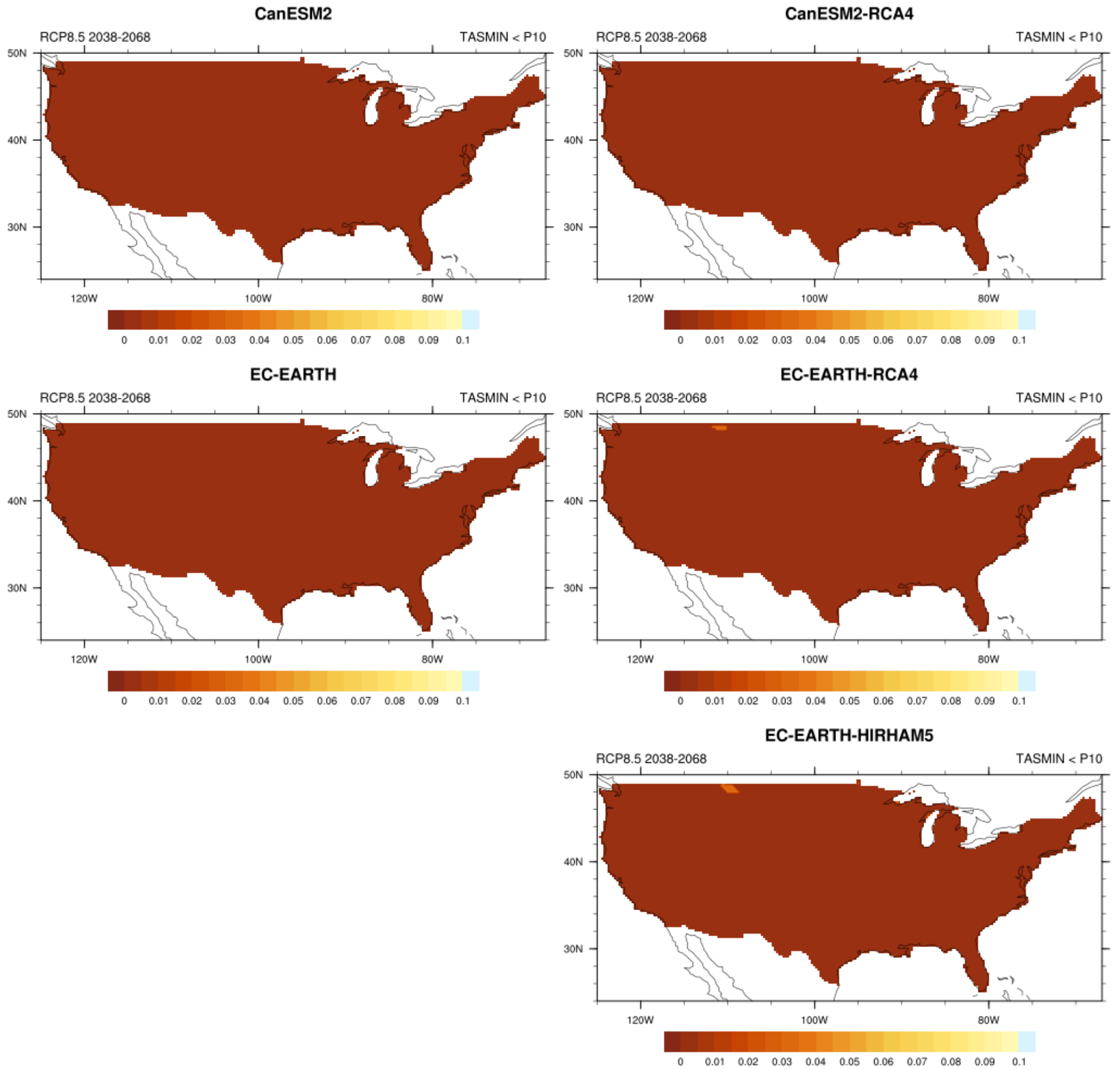

Figure 4.9: Climate Extremes Index (CEI) component TMIN10: minimum temperatures much below normal. The date range is 2038 to 2068. The scale is a dimensionless index: a value of 0 means the value never exceeded the historic threshold, while a value of 1 indicates that the value exceeded the historic threshold for every year of the analysis. Driving GCMs from CMIP5 are on the lefthand side, paired with CORDEX RCMs on the righthand side.

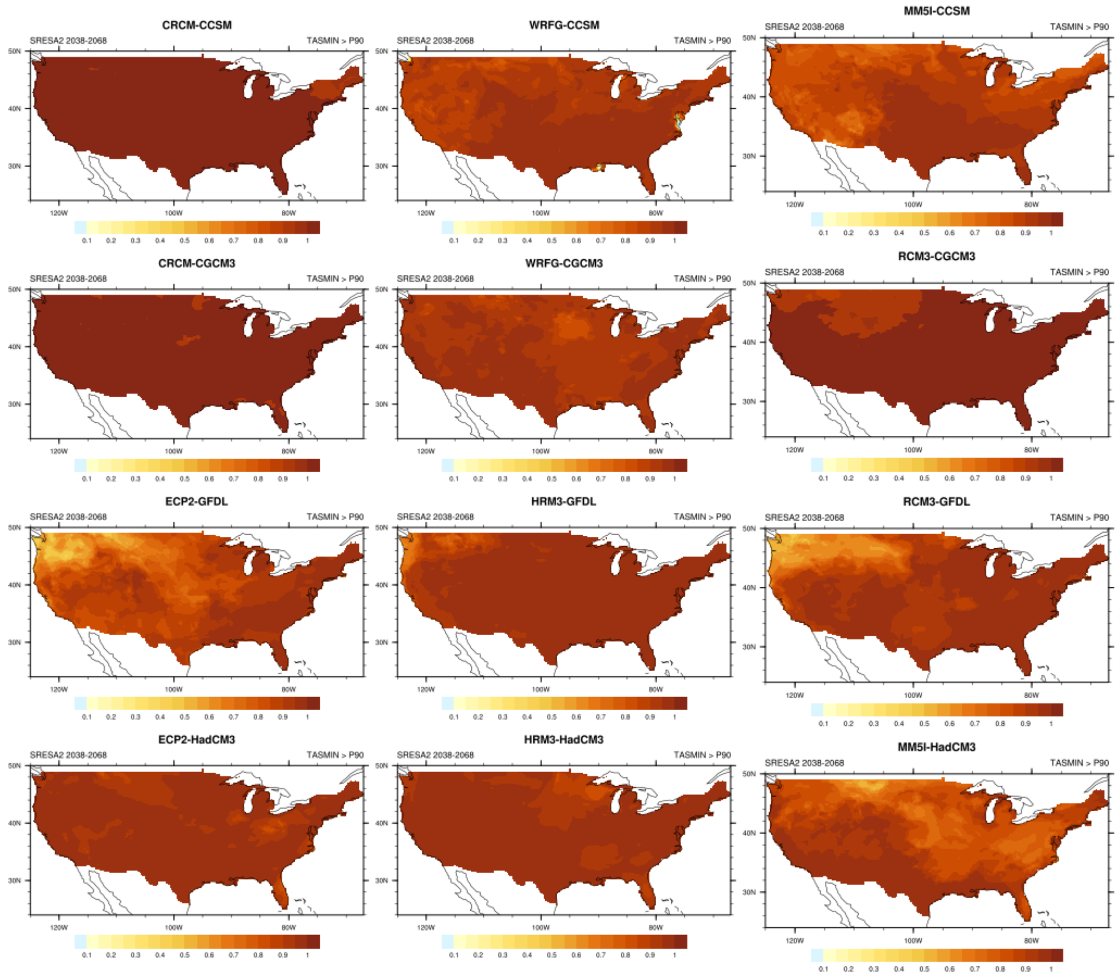

Figure 4.10: Climate Extremes Index (CEI) component TMIN90: minimum temperatures much above normal. The date range is 2038 to 2068. The scale is a dimensionless index: a value of 0 means the value never exceeded the historic threshold, while a value of 1 indicates that the value exceeded the historic threshold for every year of the analysis. NARCCAP model pairings are grouped by GCM in rows, and by RCM in columns.

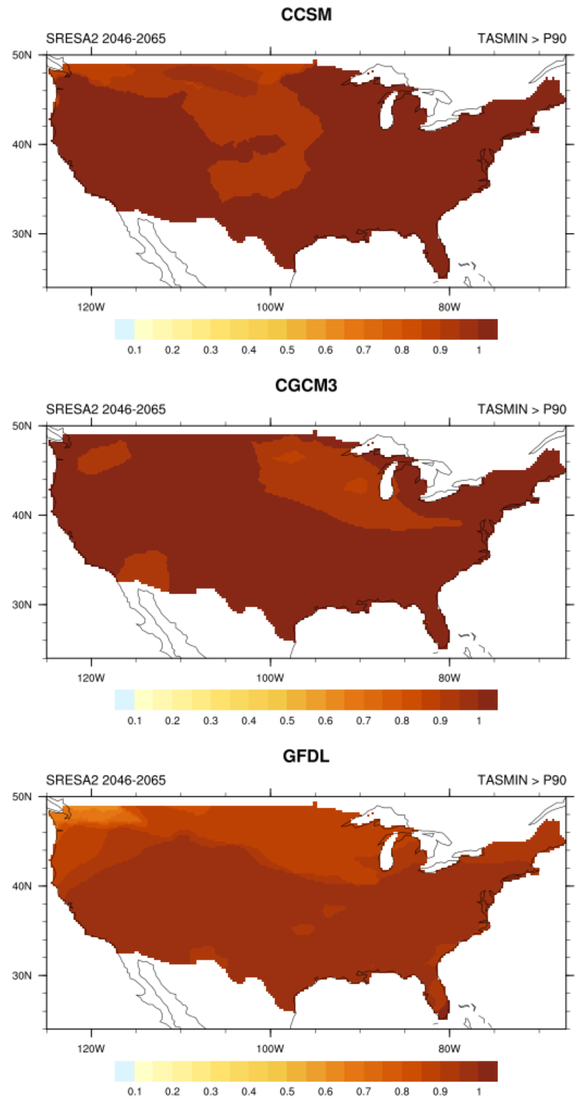

Figure 4.11: Climate Extremes Index (CEI) component TMIN90: minimum temperatures much above normal. The date range is 2046 to 2065. The scale is a dimensionless index: a value of 0 means the value never exceeded the historic threshold, while a value of 1 indicates that the value exceeded the historic threshold for every year of the analysis. All figures are for CMIP3: CCSM on top, CGCM3 in the middle, and GFDL on the bottom.

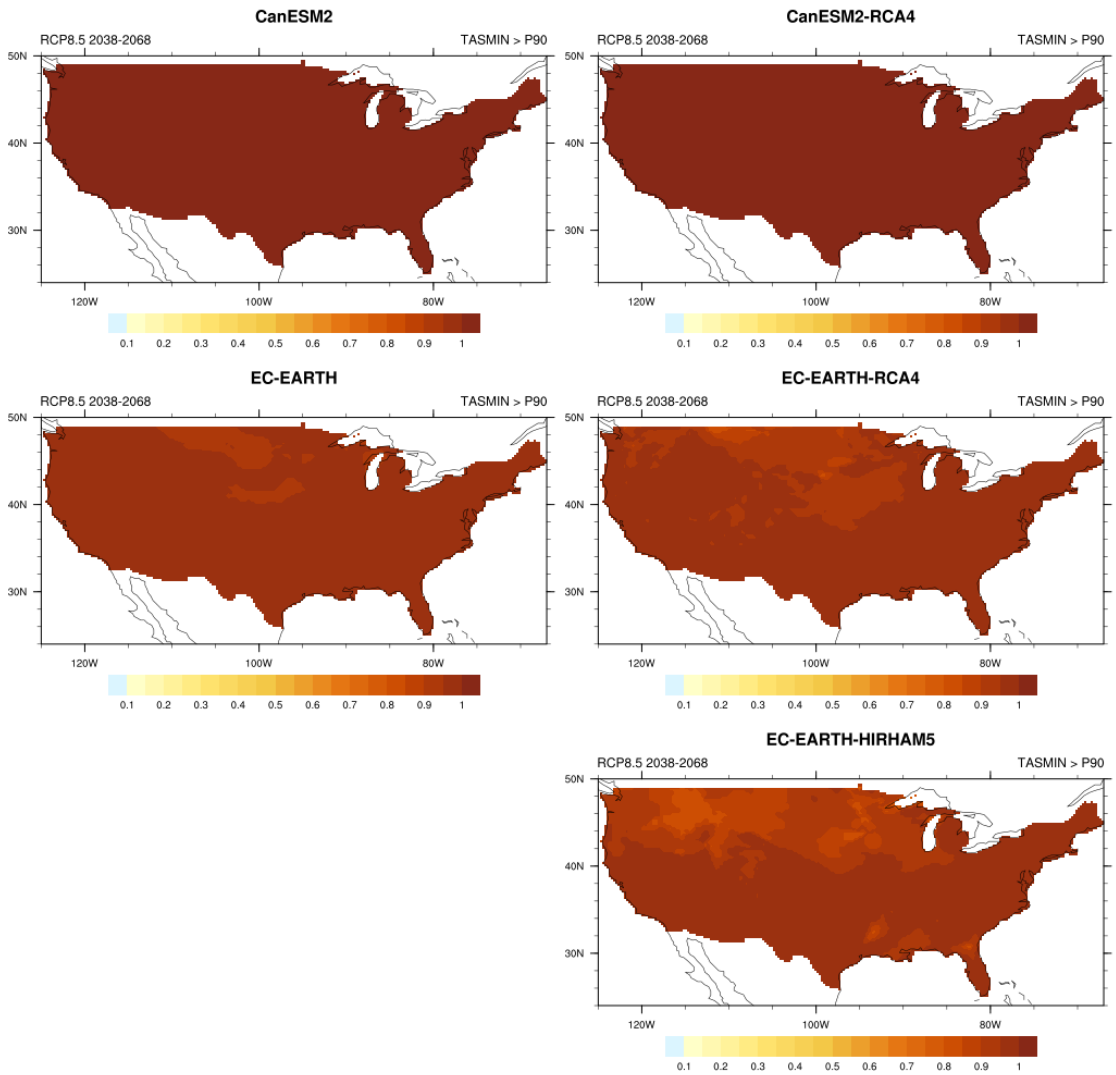

Figure 4.12: Climate Extremes Index (CEI) component TMIN90: minimum temperatures much above normal. The date range is 2038 to 2068. The scale is a dimensionless index: a value of 0 means the value never exceeded the historic threshold, while a value of 1 indicates that the value exceeded the historic threshold for every year of the analysis. Driving GCMs from CMIP5 are on the lefthand side, paired with CORDEX RCMs on the righthand side.

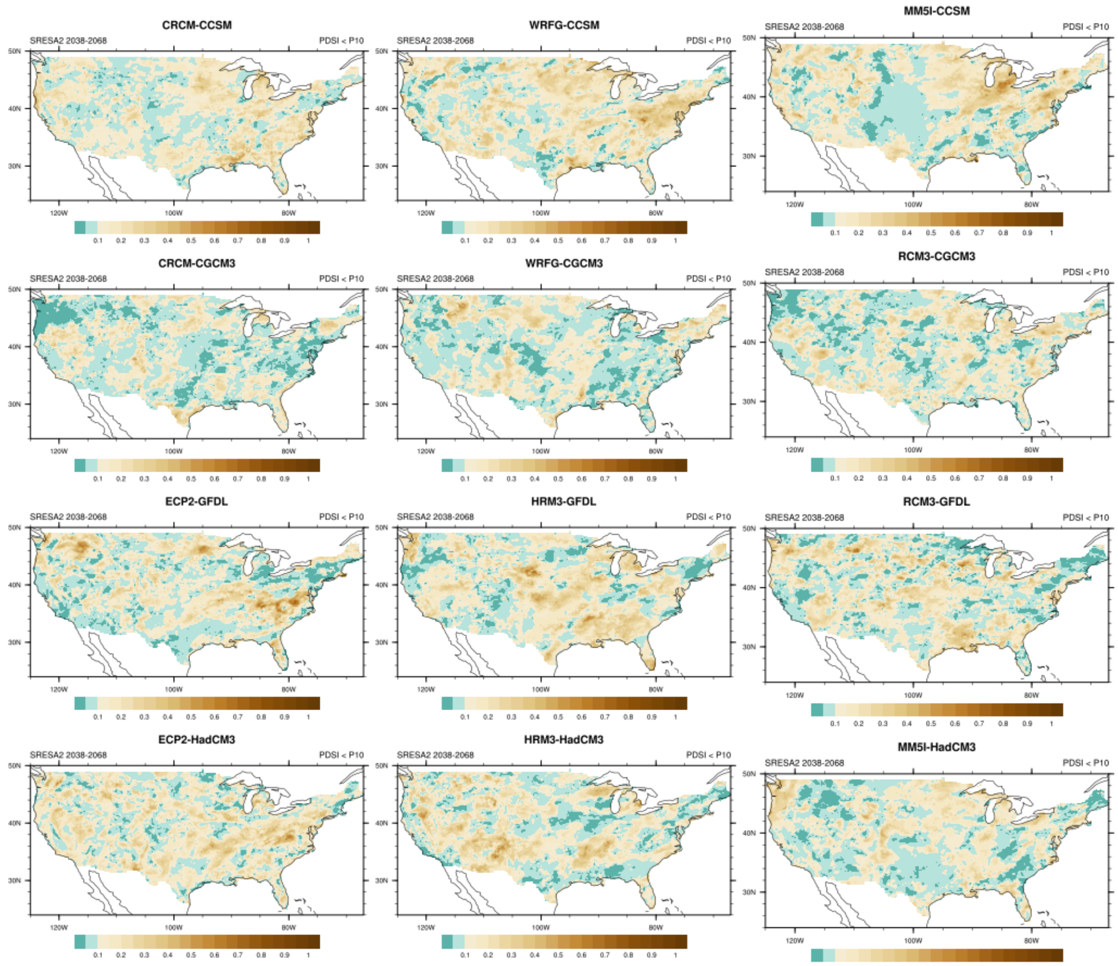

Figure 4.13: Climate Extremes Index (CEI) component PDSI10: strong negative values of the PDSI (indicating severe drought). The date range is 2038 to 2068. The scale is a dimensionless index: a value of 0 means the value never exceeded the historic threshold, while a value of 1 indicates that the value exceeded the historic threshold for every year of the analysis. NARCCAP model pairings are grouped by GCM in rows, and by RCM in columns.

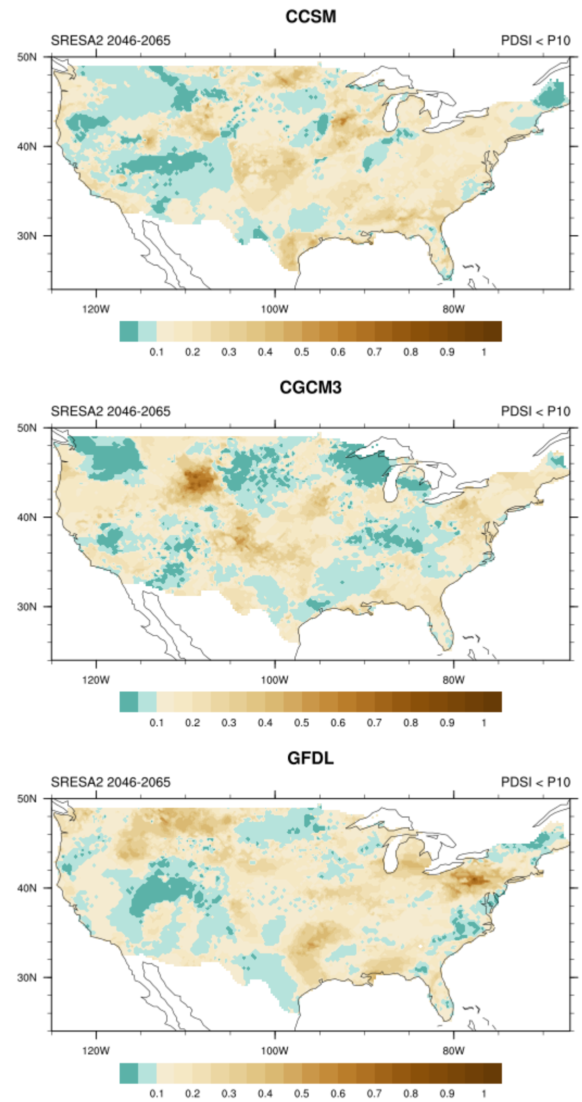

Figure 4.14: Climate Extremes Index (CEI) component PDSI10: strong negative values of the PDSI (indicating severe drought). The date range is 2046 to 2065. The scale is a dimensionless index: a value of 0 means the value never exceeded the historic threshold, while a value of 1 indicates that the value exceeded the historic threshold for every year of the analysis. All figures are for CMIP3: CCSM on top, CGCM3 in the middle, and GFDL on the bottom.

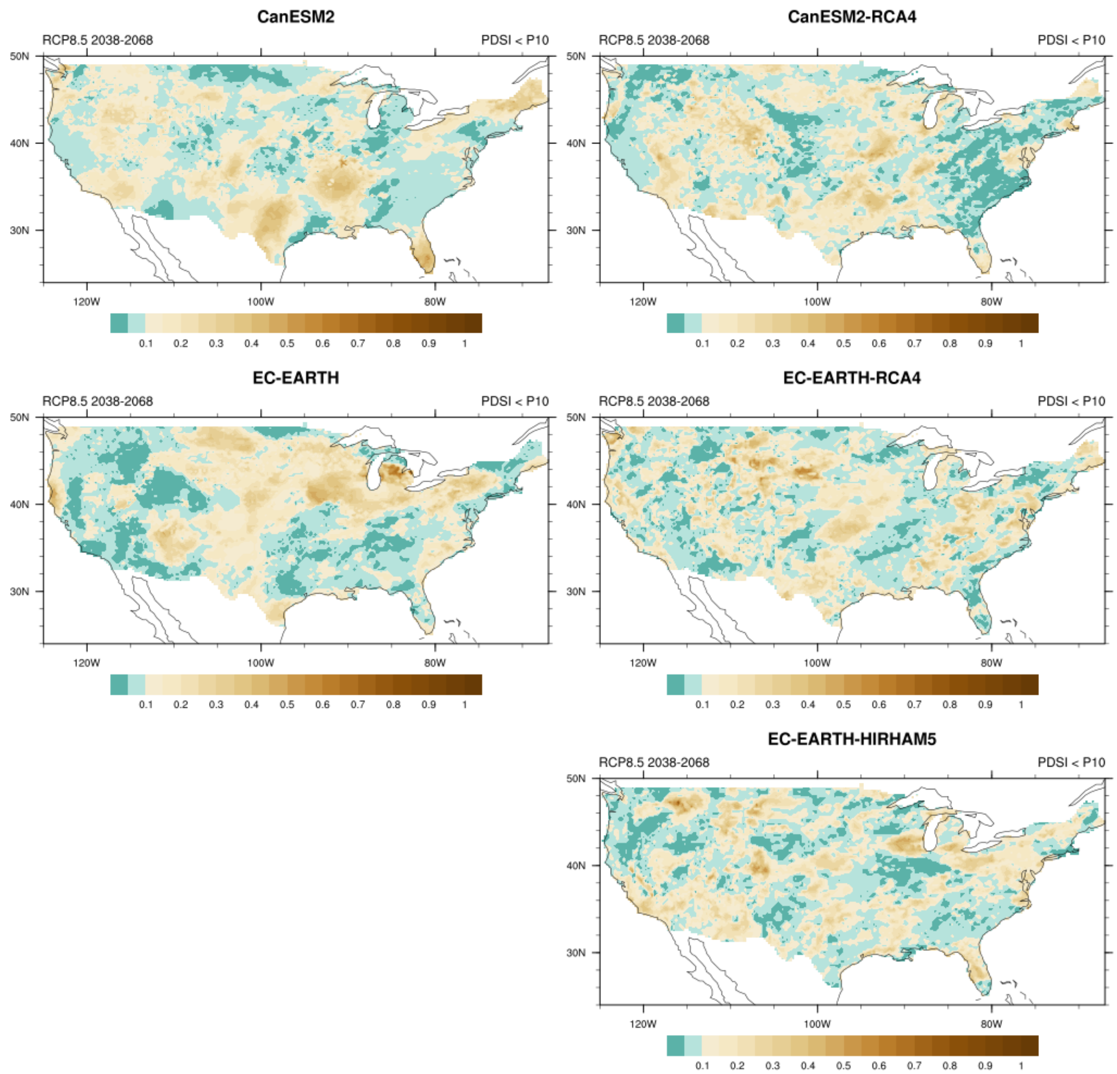

Figure 4.15: Climate Extremes Index (CEI) component PDSI10: strong negative values of the PDSI (indicating severe drought). The date range is 2038 to 2068. The scale is a dimensionless index: a value of 0 means the value never exceeded the historic threshold, while a value of 1 indicates that the value exceeded the historic threshold for every year of the analysis. Driving GCMs from CMIP5 are on the lefthand side, paired with CORDEX RCMs on the righthand side.

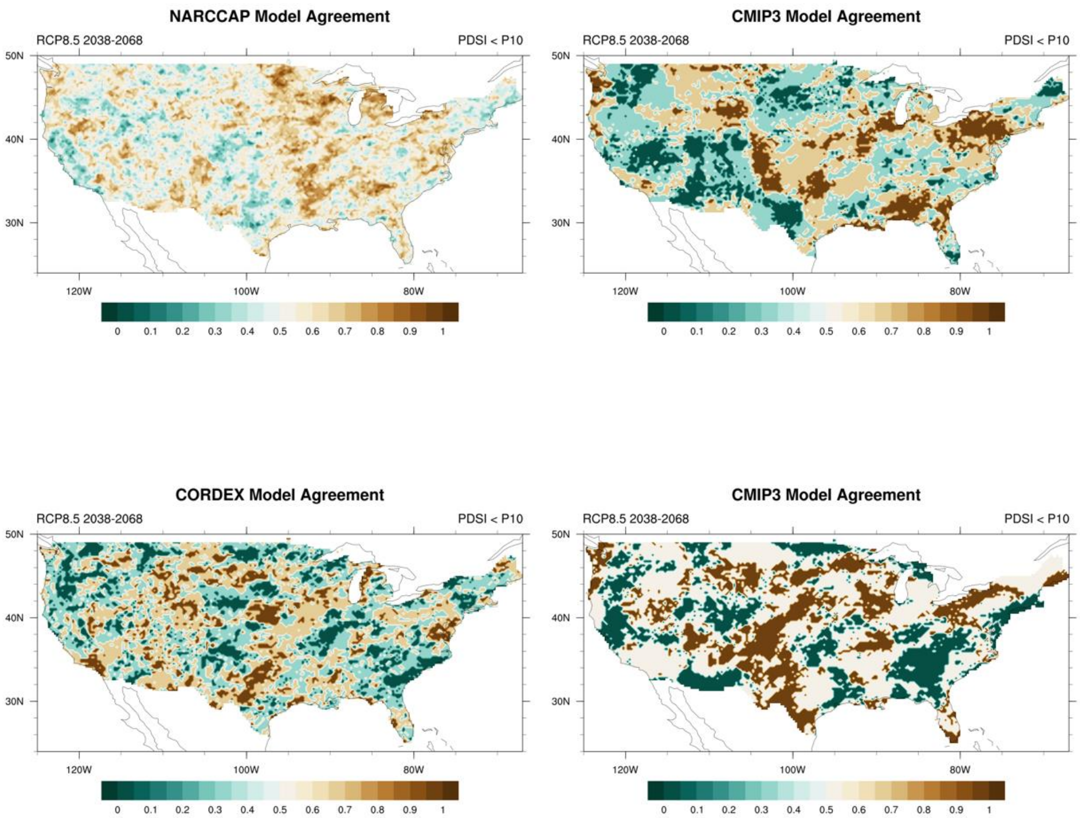

Figure 4.16: Model agreement maps for CEI component PDSI10: strong negative values of the PDSI (indicating severe drought). Color values indicate the direction of model consensus – wetter or drier – while color intensity indicates the strength of agreement.

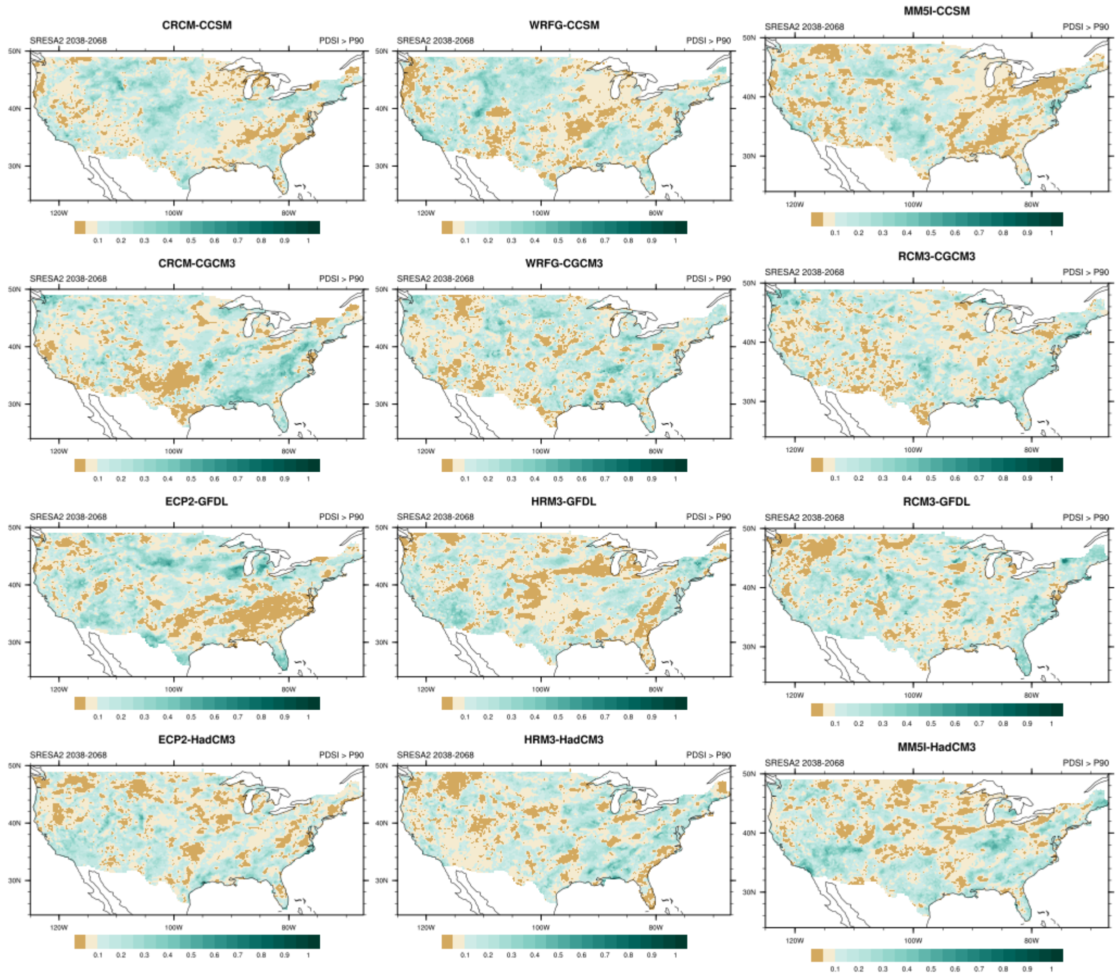

Figure 4.17: Climate Extremes Index (CEI) component PDSI90: strong positive values of the PDSI (indicating severe moisture surplus). The date range is 2038 to 2068. The scale is a dimensionless index: a value of 0 means the value never exceeded the historic threshold, while a value of 1 indicates that the value exceeded the historic threshold for every year of the analysis. NARCCAP model pairings are grouped by GCM in rows, and by RCM in columns.

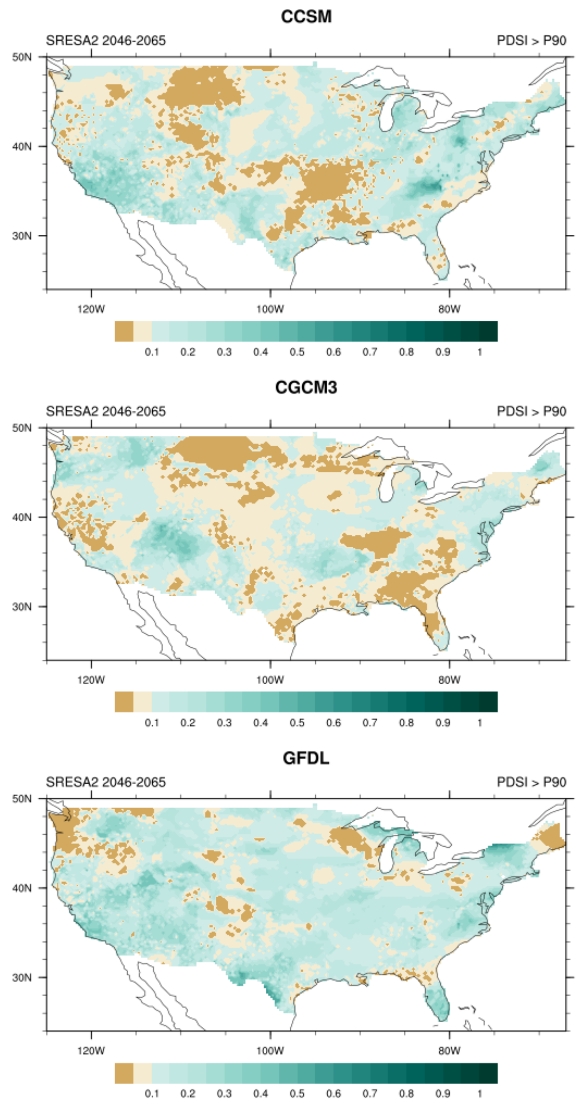

Figure 4.18: Climate Extremes Index (CEI) component PDSI90: strong positive values of the PDSI (indicating severe moisture surplus). The date range is 2046 to 2065. The scale is a dimensionless index: a value of 0 means the value never exceeded the historic threshold, while a value of 1 indicates that the value exceeded the historic threshold for every year of the analysis. All figures are for CMIP3: CCSM on top, CGCM3 in the middle, and GFDL on the bottom.

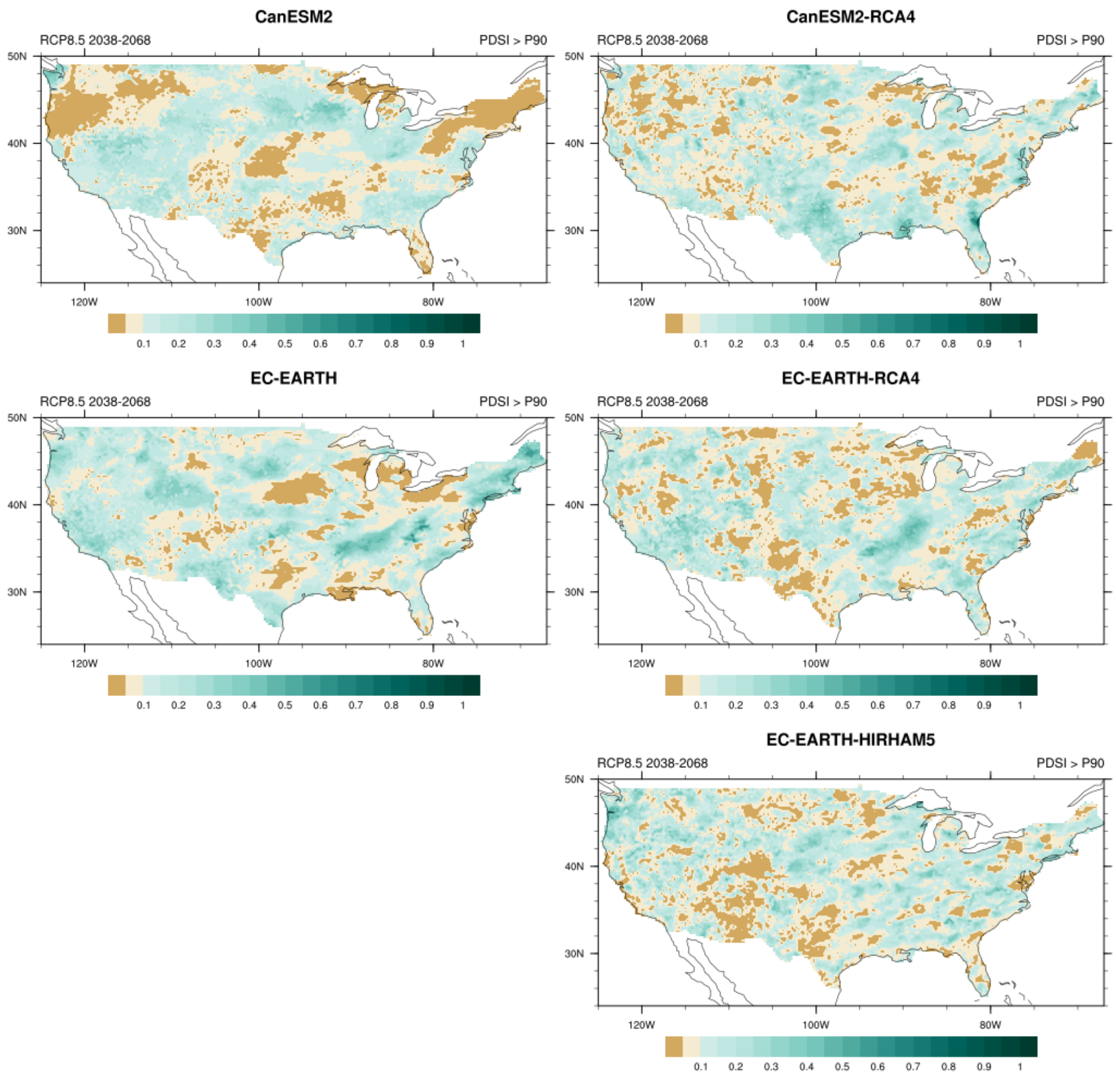

Figure 4.19: Climate Extremes Index (CEI) component PDSI90: strong positive values of the PDSI (indicating severe moisture surplus). The date range is 2038 to 2068. The scale is a dimensionless index: a value of 0 means the value never exceeded the historic threshold, while a value of 1 indicates that the value exceeded the historic threshold for every year of the analysis. Driving GCMs from CMIP5 are on the lefthand side, paired with CORDEX RCMs on the righthand side.

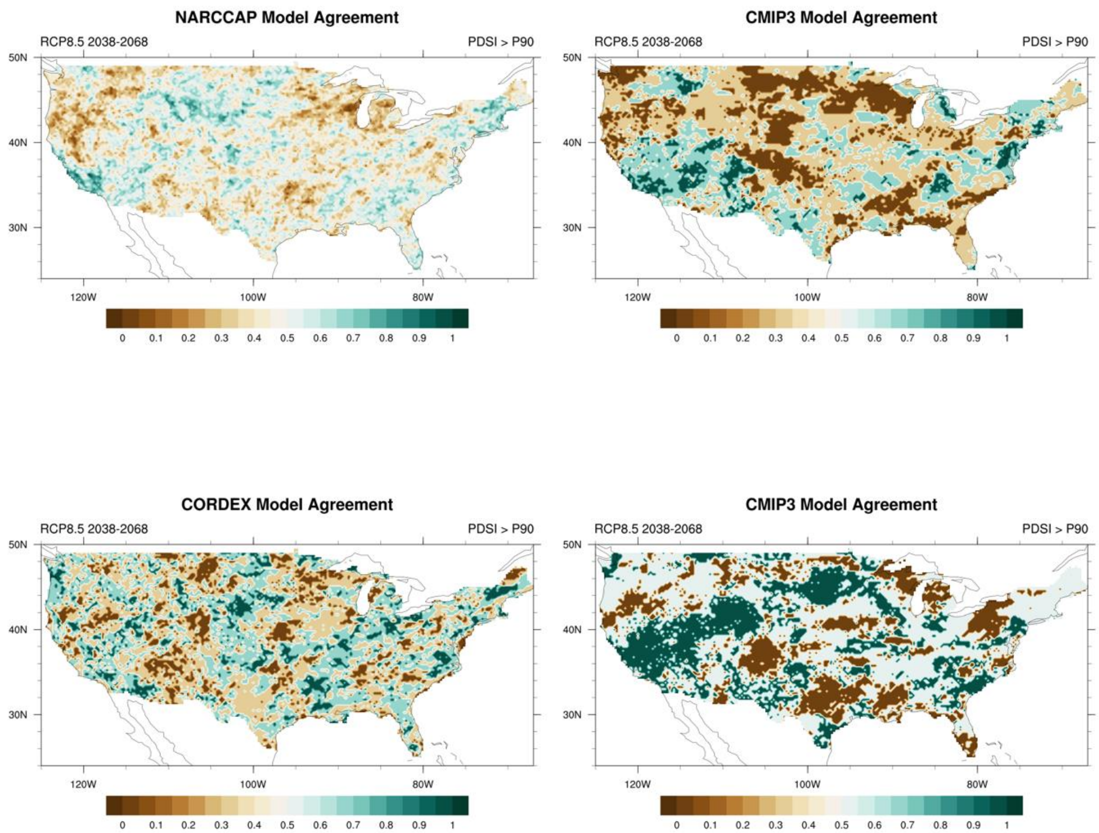

Figure 4.20: Model agreement maps for CEI component PDSI90: strong positive values of the PDSI (indicating severe moisture surplus). Color values indicate the direction of model consensus – wetter or drier – while color intensity indicates the strength of agreement.

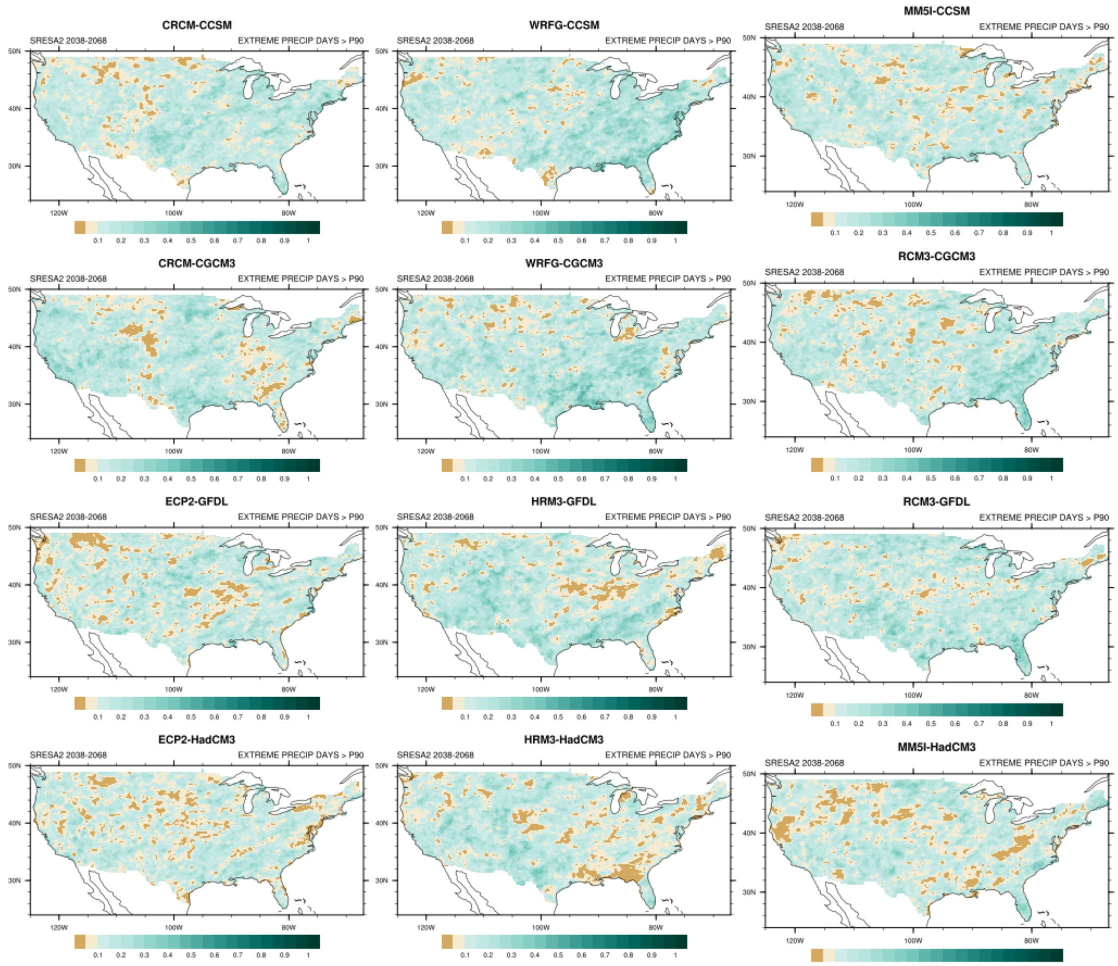

Figure 4.21: Climate Extremes Index (CEI) component ECP90: precipitation derived from extreme 1-day precipitation events. The date range is 2038 to 2068. The scale is a dimensionless index: a value of 0 means the value never exceeded the historic threshold, while a value of 1 indicates that the value exceeded the historic threshold for every year of the analysis. NARCCAP model pairings are grouped by GCM in rows, and by RCM in columns.

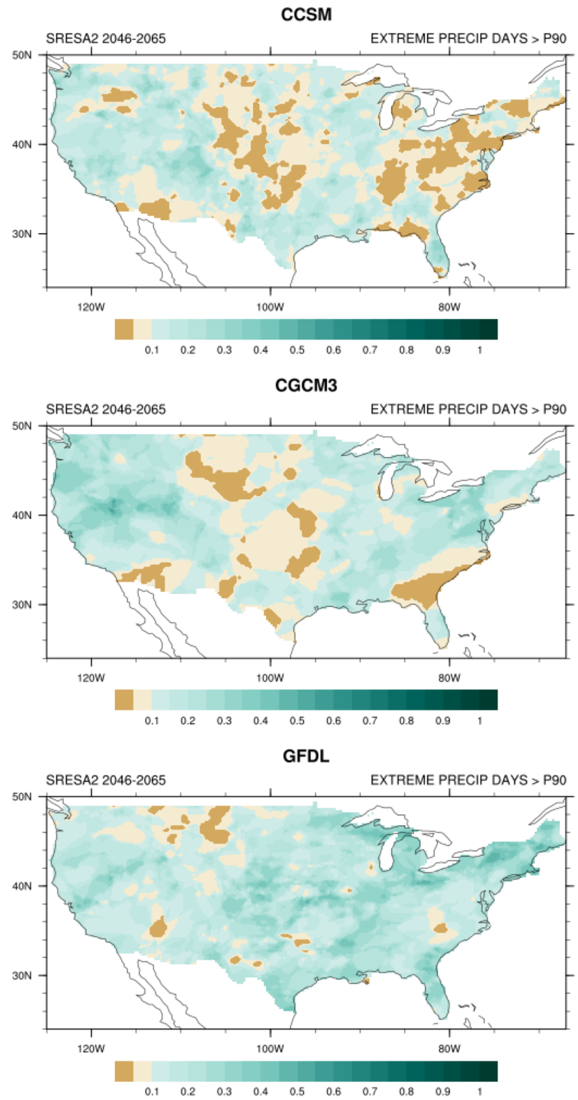

Figure 4.22: Climate Extremes Index (CEI) component ECP90: precipitation derived from extreme 1-day precipitation events. The date range is 2046 to 2065. The scale is a dimensionless index: a value of 0 means the value never exceeded the historic threshold, while a value of 1 indicates that the value exceeded the historic threshold for every year of the analysis. Model pairings are grouped by GCM in rows, and by RCM in columns.

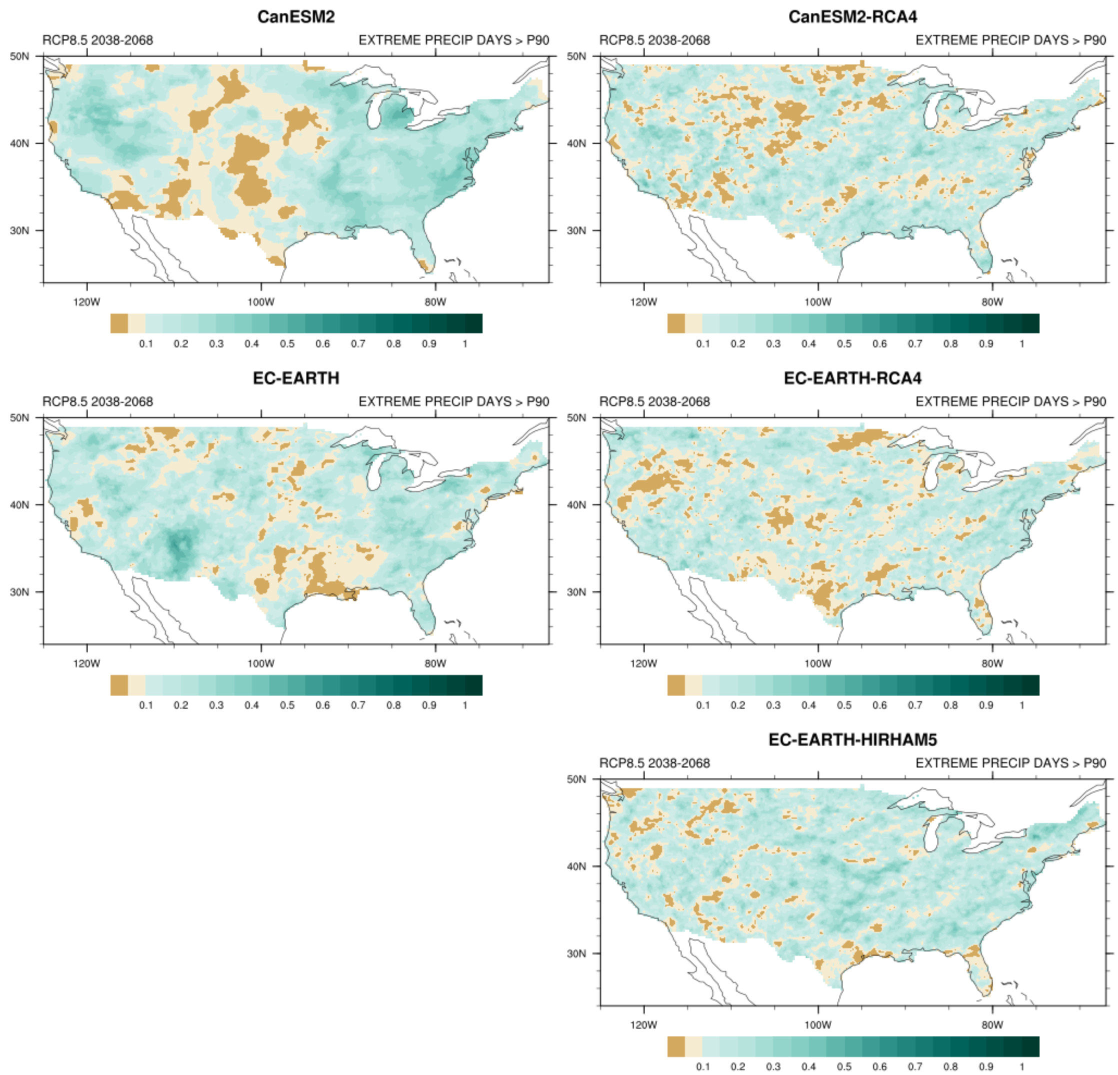

Figure 4.23: Climate Extremes Index (CEI) component ECP90: precipitation derived from extreme 1-day precipitation events. The date range is 2038 to 2068. The scale is a dimensionless index: a value of 0 means the value never exceeded the historic threshold, while a value of 1 indicates that the value exceeded the historic threshold for every year of the analysis. Driving GCMs from CMIP5 are on the lefthand side, paired with CORDEX RCMs on the righthand side.

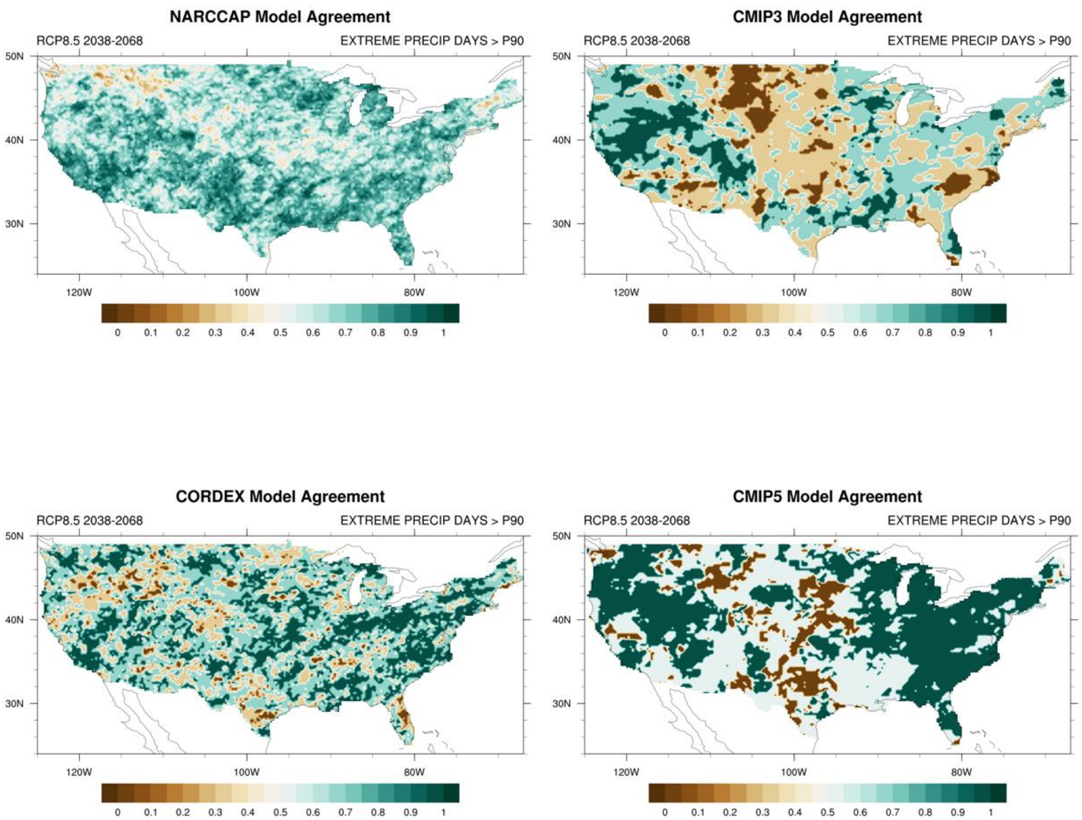

Figure 4.24: Model agreement maps for CEI component ECP90: precipitation derived from extreme 1-day precipitation events. Color values indicate the direction of model consensus – wetter or drier – while color intensity indicates the strength of agreement.

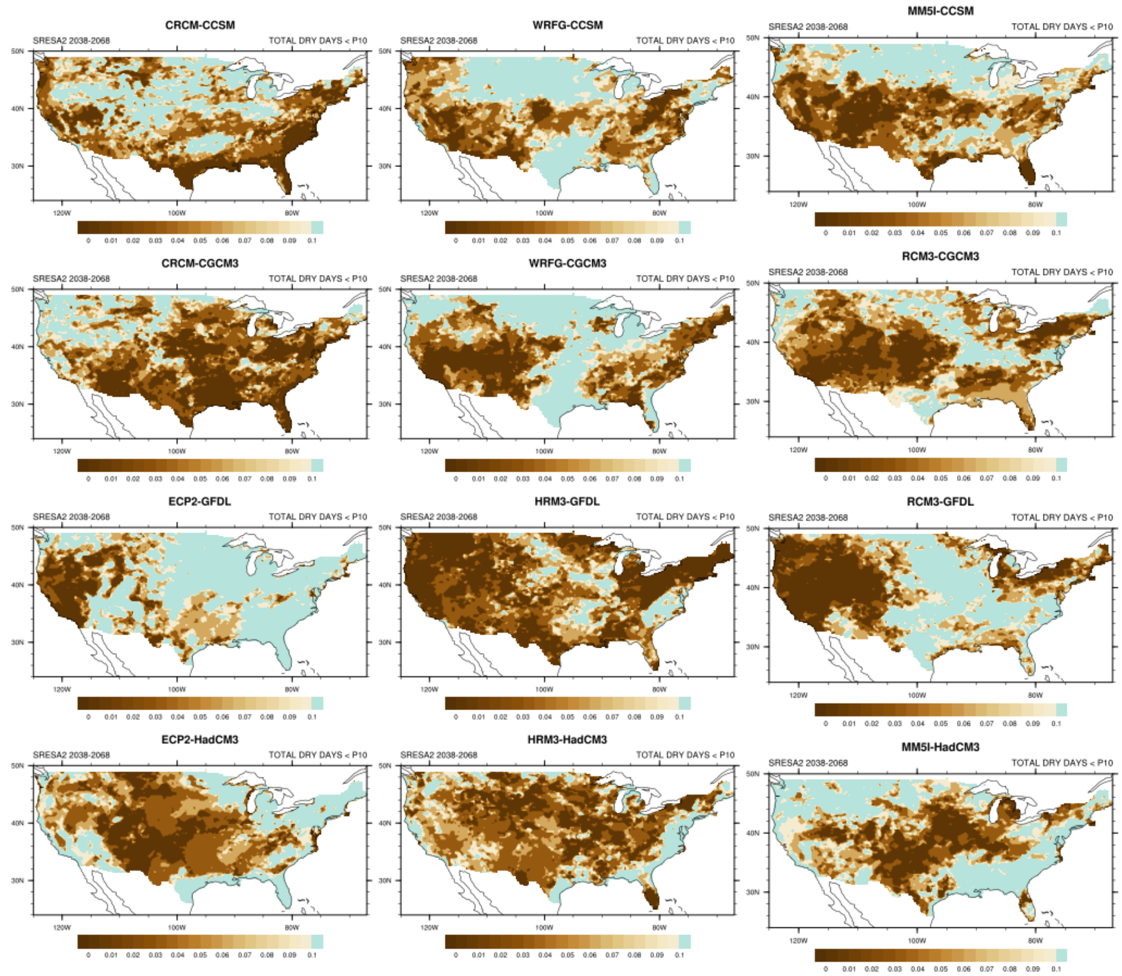

Figure 4.25: Climate Extremes Index (CEI) component TDD10: greater than normal days with precipitation. The date range is 2038 to 2068. The scale is a dimensionless index: a value of 0 means the value never exceeded the historic threshold, while a value of 1 indicates that the value exceeded the historic threshold for every year of the analysis. NARCCAP model pairings are grouped by GCM in rows, and by RCM in columns.

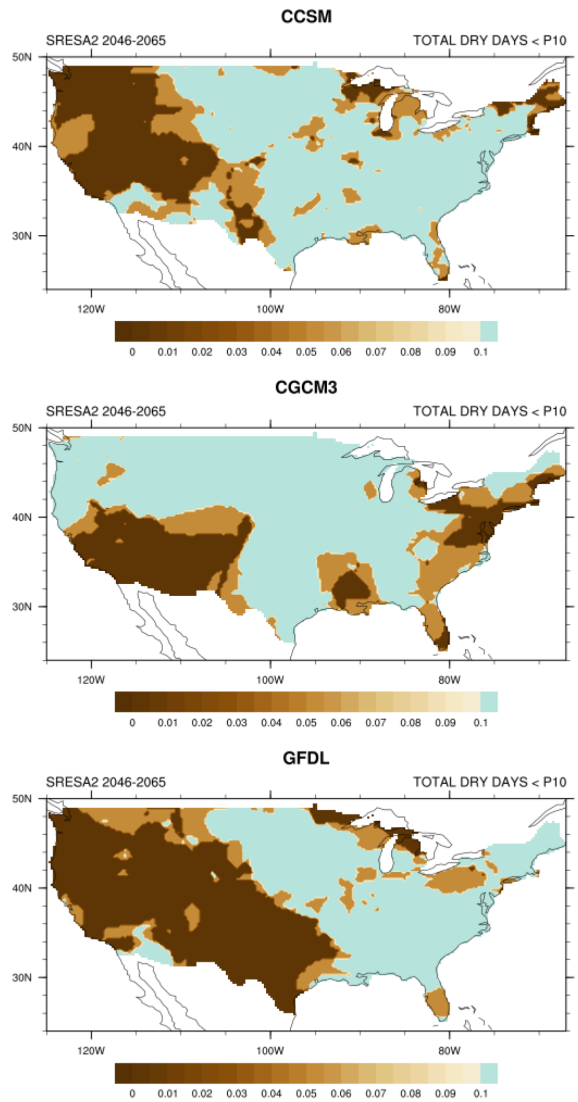

Figure 4.26: Climate Extremes Index (CEI) component TDD10: greater than normal days with precipitation. The date range is 2046 to 2065. The scale is a dimensionless index: a value of 0 means the value never exceeded the historic threshold, while a value of 1 indicates that the value exceeded the historic threshold for every year of the analysis. All figures are for CMIP3: CCSM on top, CGCM3 in the middle, and GFDL on the bottom.

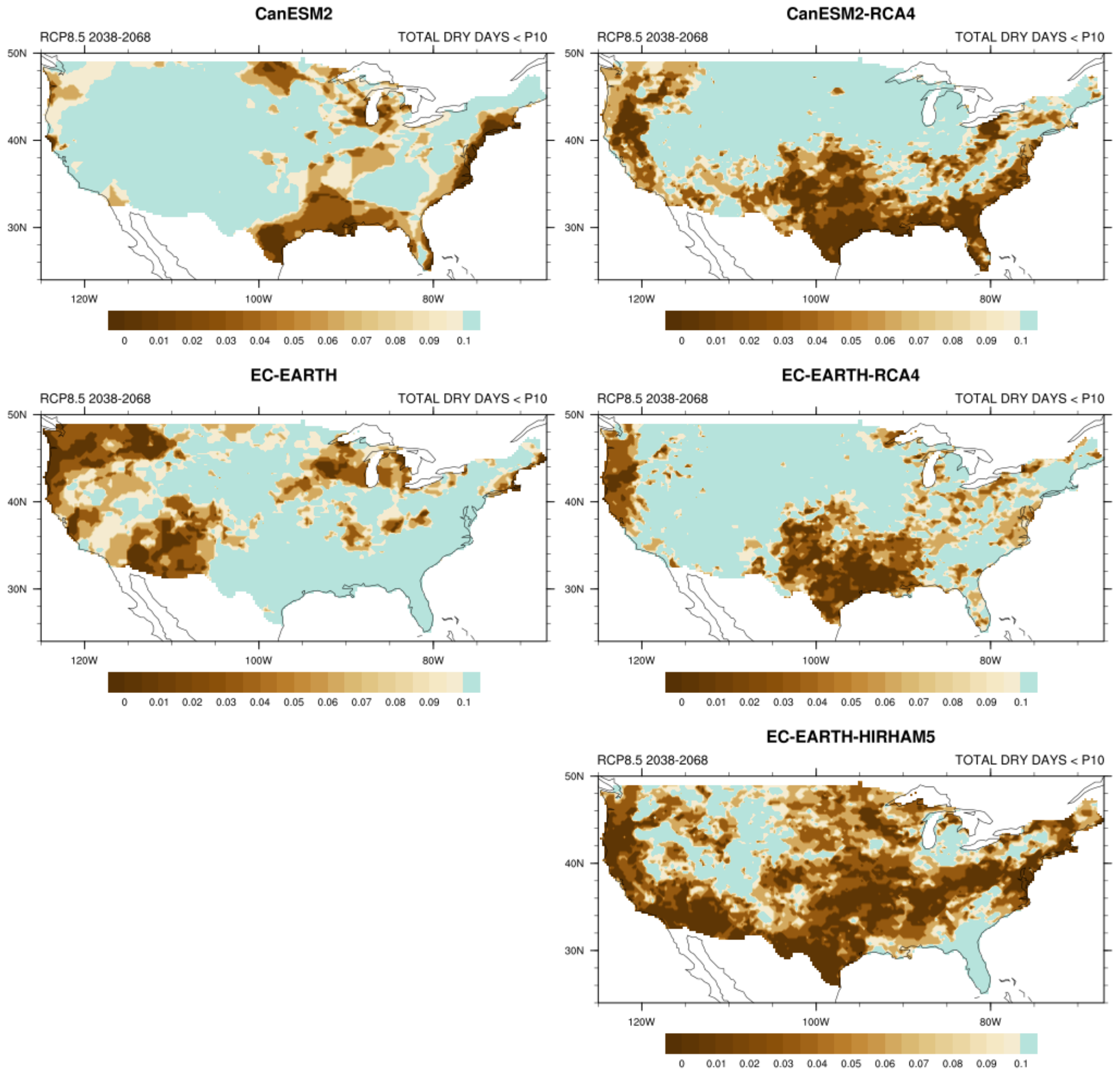

Figure 4.27: Climate Extremes Index (CEI) component TDD10: greater than normal days with precipitation. The date range is 2038 to 2068. The scale is a dimensionless index: a value of 0 means the value never exceeded the historic threshold, while a value of 1 indicates that the value exceeded the historic threshold for every year of the analysis. Driving GCMs from CMIP5 are on the lefthand side, paired with CORDEX RCMs on the righthand side.

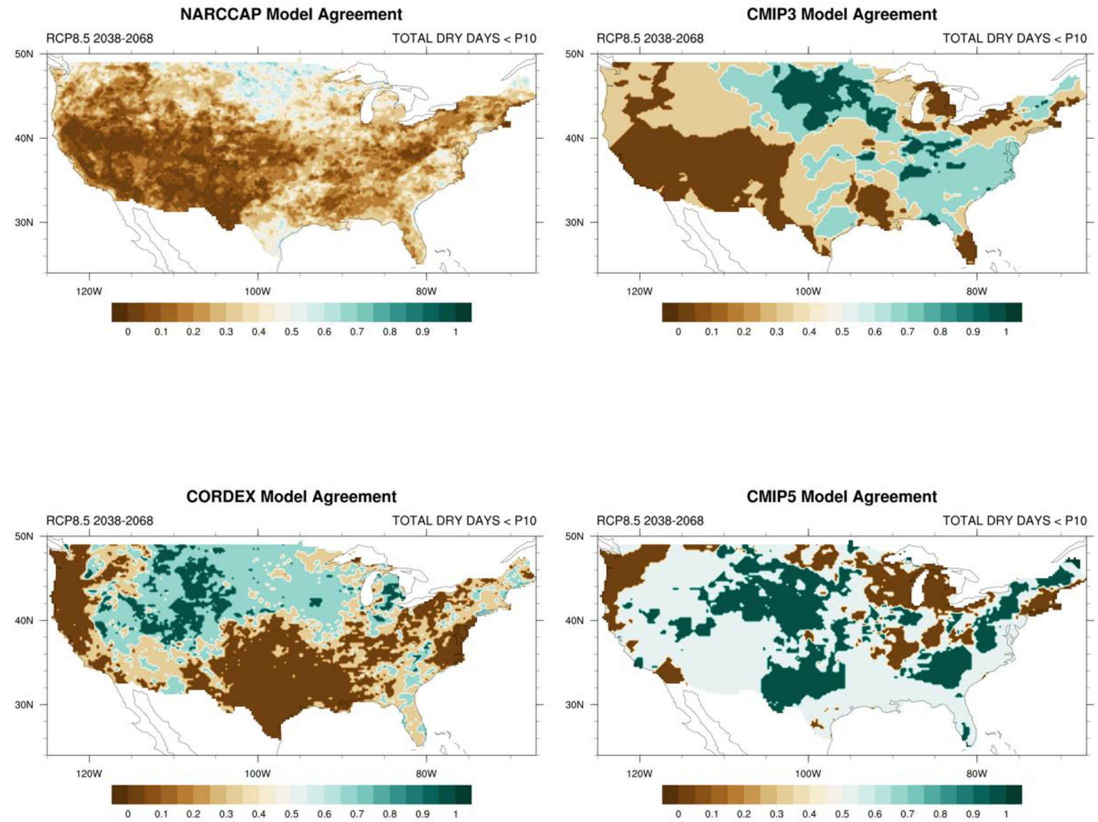

Figure 4.28: Model agreement maps for CEI component TDD10: greater than normal days with precipitation. Color values indicate the direction of model consensus – wetter or drier – while color intensity indicates the strength of agreement.

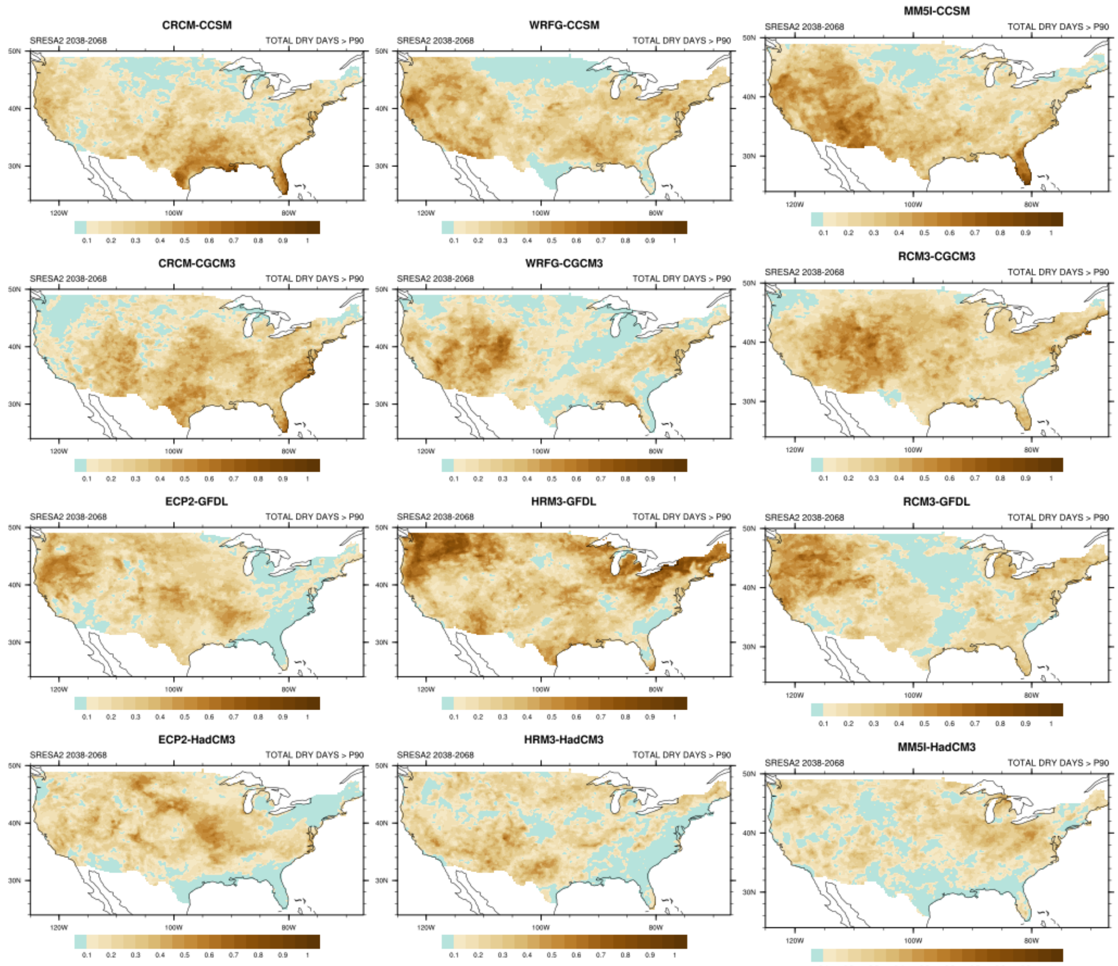

Figure 4.29: Climate Extremes Index (CEI) component TDD90: greater than normal days without precipitation. The date range is 2038 to 2068. The scale is a dimensionless index: a value of 0 means the value never exceeded the historic threshold, while a value of 1 indicates that the value exceeded the historic threshold for every year of the analysis. NARCCAP model pairings are grouped by GCM in rows, and by RCM in columns.

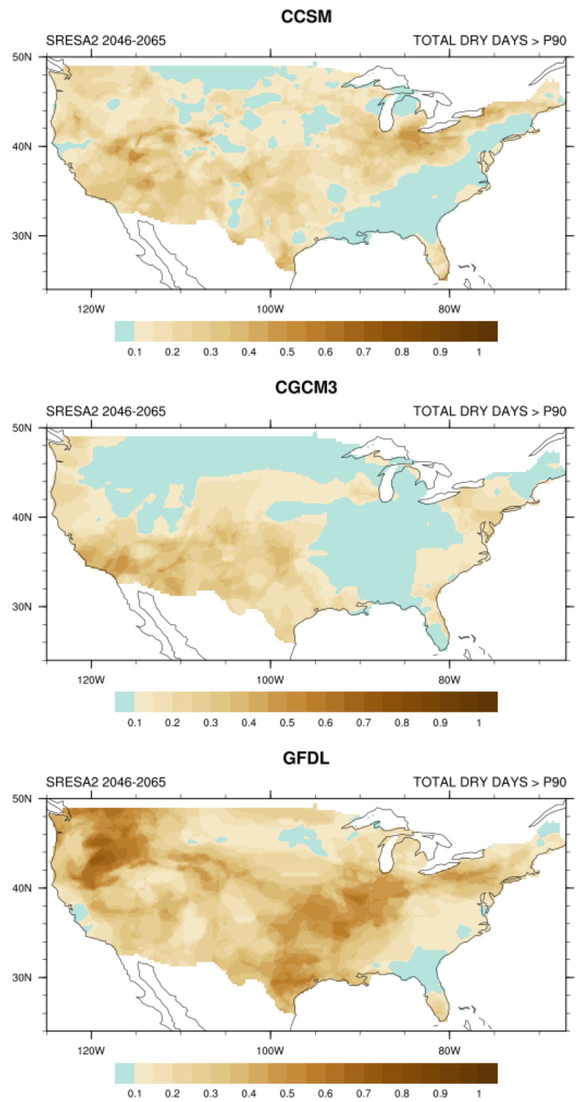

Figure 4.30: Climate Extremes Index (CEI) component TDD90: greater than normal days without precipitation. The date range is 2046 to 2065. The scale is a dimensionless index: a value of 0 means the value never exceeded the historic threshold, while a value of 1 indicates that the value exceeded the historic threshold for every year of the analysis. All figures are for CMIP3: CCSM on top, CGCM3 in the middle, and GFDL on the bottom.

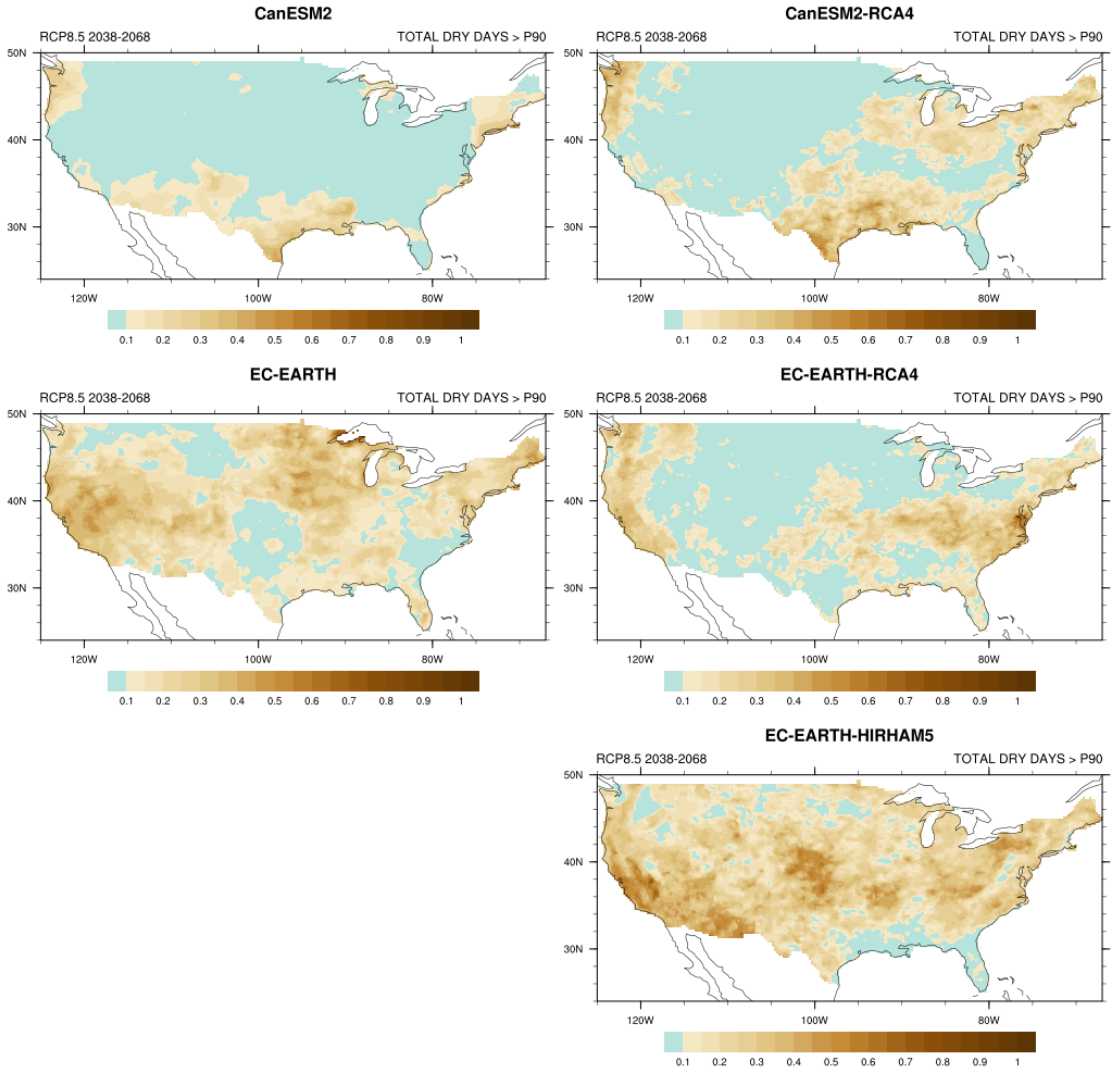

Figure 4.31: Climate Extremes Index (CEI) component TDD90: greater than normal days without precipitation. The date range is 2038 to 2068. The scale is a dimensionless index: a value of 0 means the value never exceeded the historic threshold, while a value of 1 indicates that the value exceeded the historic threshold for every year of the analysis. Driving GCMs from CMIP5 are on the lefthand side, paired with CORDEX RCMs on the righthand side.

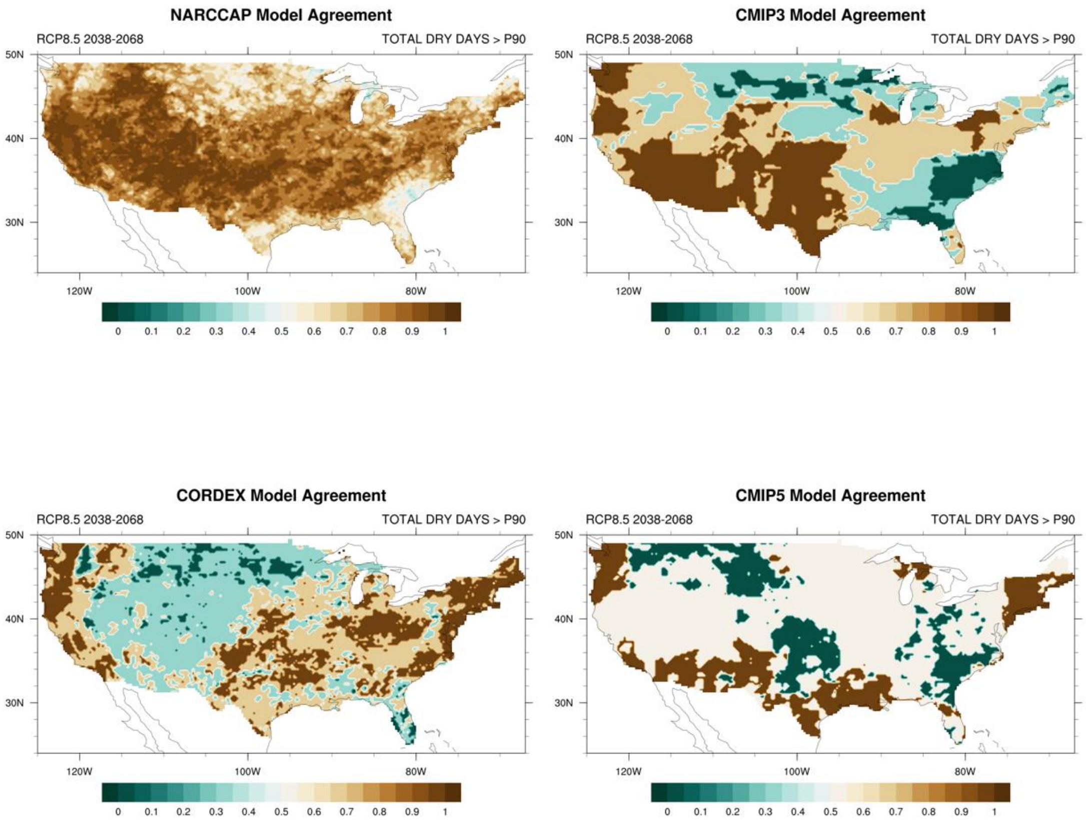

Figure 4.32: Model agreement maps for CEI component TDD90: greater than normal days without precipitation. Color values indicate the direction of model consensus – wetter or drier – while color intensity indicates the strength of agreement.

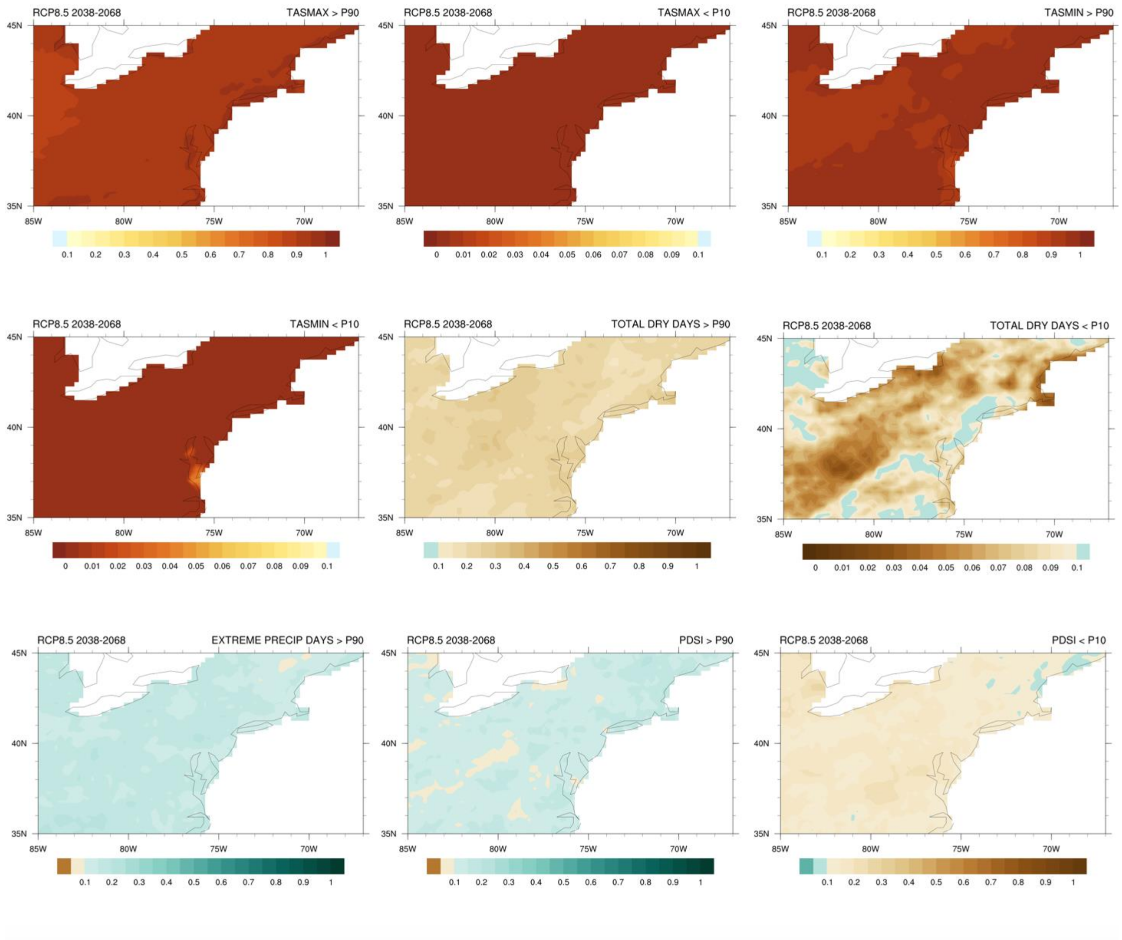

Figure 4.33: The nine components of the CEI, zoomed in over the Mid-Atlantic region. Each figure represents the ensemble mean of all twelve NARCCAP models for each of the components described in previous sections.

Chapter 5

CONCLUSION

Model projections indicate a significant increase in climate extremes across the CONUS, especially in both maximum and minimum temperatures, with historic 90th percentile values becoming commonplace and historic 10th percentile values becoming much rarer. The extreme high values in minimum temperature should be of particular concern to urban planners and public health officials: higher than normal minimum temperatures can lead to greater intensity and lethality of heat waves, as the body does not get a chance to cool down (Changnon et al. 2003). Model projections of precipitation indices are less consistent, but suggest a decrease in total precipitation events, coupled with an increase in precipitation intensity, consistent with previous findings (e,g. Karl et al. 2009, Kunkel et al. 2013, Peterson et al. 2013, Wuebbles et al. 2014).

As mentioned previously, the combined CEI is a measure of what percentage of the CONUS is experiencing climate extremes at any given time. The CEI score alone does not indicate the sign of any given changes in extremes, or which individual indicators are contributing the most to any change in extremes (Gleason et al. 2008). Changes in extreme could indicate changes in mean or variance; thus, it is difficult to draw substantive conclusions about the shape of the overall distribution from the CEI alone (Gleason et al. 2008). Some of this difficulty in interpretation can be ameliorated by examining each individual component in detail, as was shown in previous sections. The increase in 90th percentile temperature extremes, for instance, is clear across all models for both maximum and minimum temperatures. For examining changes in precipitation extremes, however, the spatial averaging inherent in the CEI poses some challenges; as discussed earlier, an overall lack of change could indicate that extremes of both signs are occurring in different locations and being averaged together. The CEI also does not directly assess changes in total monthly or annual precipitation, which could provide valuable context to changes in extreme precipitation and number of days with precipitation.

Additionally, Ye et al. (2017) found that extreme warm years are primarily distinguished from average and cold years by warm nights (night temperatures exceeding the 90^{th} percentile) and that wet years were primarily distinguished from average and dry years by occurrence of heavy precipitation events (events ≥ 10 mm and ≥ 20 mm). The CEI does not specifically distinguish between day and night temperatures, but given scholarship on the health impacts of high nighttime temperatures on the human body (Habeeb et al. 2015, Sarofim et al. 2016) this could be a valuable addition to an examination of climate extremes.

There are some limitations to the results presented here. The reference period used was only 31 years, from 1968 to 1998, the years for which NARCCAP historical experiments were available. This was done in the interest of “apples to apples” comparison, comparing each model only to itself when calculating the 90^{th} percentile threshold. However, the NOAA calculation of the CEI uses the full period of record, from 1910 to the present day, to calculate percentiles. When examining Figure 1.1, the NOAA CEI plot, it would appear that 1960 to 1980 represents a relatively cool and mild period, with maximum temperatures more often falling below the 10^{th} percentile threshold than above the 90^{th}. This may not be a significant issue; for instance, the

NCDC heat index uses 1961-1990 as a base period to calculate their percentile-based thresholds (Habeeb 2015). Still, it represents a departure from the NOAA-calculated CEI that should be noted.

Analysis of spatial correlation between NARCCAP models showed no clear consensus on whether an individual RCM or the GCM boundary forcing contributed more strongly to CEI results. Several pairings showed high correlation despite sharing neither an RCM nor a GCM. One possible avenue for further research would involve a closer examination of individual NARCCAP model attributes: model physics, parameterizations, land cover and soil properties, etc., in order to attribute variations between models to different assumptions.

A study of regional climate models over Europe categorized RCM uncertainty into four different sources: sampling uncertainty, coming from the fact that the climate is estimated over a finite number of years, model uncertainty, reflecting the different physics and parameterization methods between regional models, boundary uncertainty, representing the contribution of the GCM boundaries, and radiative uncertainty, representing that any given IPCC scenario is only one of many possible futures (Déqué et al. 2007). While the scenario (SRES A2/RCP 8.5) and time scale (2038-2068, except for CMIP3) were held as close to constant as possible in this study, Déqué et al. found that the contribution of different sources of uncertainty varied by field, region, and season. While some uncertainty over physical processes can be resolved as gaps in knowledge close, other forms of uncertainty are inherently unknowable; for instance, we as climate scientists cannot perfectly predict how humans will respond to climate change (Foley 2010). We can only provide the tools for stakeholders to make informed decisions about our changing climate.

REFERENCES

Adegoke, J. O., Pielke, R., & Carleton, A. M. (2007). Observational and modeling studies of the impacts of agriculture-related land use change on planetary boundary layer processes in the central U.S. Agricultural and Forest Meteorology, 142(2-4), 203-215. doi:10.1016/j.agrformet.2006.07.013

Barros, A. P., Duan, Y., Brun, J., & Medina, M. A. (2014). Flood Nonstationarity in the Southeast and Mid-Atlantic Regions of the United States. Journal of Hydrologic Engineering J. Hydrol. Eng., 19(10), 05014014. doi:10.1061/(asce)he.1943-5584.0000955

Brody SD, Zahran S, Maghelal P, Grover H, Highfield WE. The Rising Costs of Floods: Examining the Impact of Planning and Development Decisions on Property Damage in Florida. Journal of the American Planning Association. 2007;73(3):330-345. doi:10.1080/01944360708977981.

Caldwell, P. (2010). California Wintertime Precipitation Bias in Regional and Global Climate Models. Journal of Applied Meteorology and Climatology, 49(10), 2147-2158. doi:10.1175/2010jamc2388.1

Canning-Clode, J., Fowler, A. E., Byers, J. E., Carlton, J. T., & Ruiz, G. M. (2011). ‘Caribbean Creep’ Chills Out: Climate Change and Marine Invasive Species. PLoS ONE, 6(12). doi:10.1371/journal.pone.0029657

CCSP, 2009: *Coastal Sensitivity to Sea-Level Rise: A Focus on the Mid-Atlantic Region*. A report by the U.S. Climate Change Science Program and the Subcommittee on Global Change Research. [James G. Titus (Coordinating Lead Author), K. Eric Anderson, Donald R. Cahoon, Dean B. Gesch, Stephen K. Gill, Benjamin T. Gutierrez, E. Robert Thieler, and S. Jeffress Williams (Lead Authors)]. U.S. Environmental Protection Agency, Washington D.C., USA, 320 pp.

CDC (2015). “Lyme Disease: Data and Statistics.” Retrieved July 12, 2016, from http://www.cdc.gov/lyme/stats/index.html

Changnon, D., Sandstrom, M., & Schaffer, C. (2003). Relating changes in agricultural practices to increasing dew points in extreme Chicago heat waves. Climate Research, 24, 243-254. doi:10.3354/cr024243

CMIP (2010). "Overview." Retrieved September 11, 2016, from http://cmip-pcmdi.llnl.gov/

Cook, B. I., Smerdon, J. E., Seager, R., & Coats, S. (2014). Global warming and 21st century drying. Climate Dynamics, 43(9-10), 2607-2627. doi:10.1007/s00382-014-2075-y

CORDEX (2013). "CORDEX." Retrieved from http://www.cordex.org/

Curtis, S. (2007). The Atlantic multidecadal oscillation and extreme daily precipitation over the US and Mexico during the hurricane season. Clim Dyn Climate Dynamics, 30(4), 343-351. doi:10.1007/s00382-007-0295-0

Daly, C, Halbleib, M, Smith, JI, Gibson, WP, Doggett, MK, Taylor, GH, Curtis, J, Pasteris, PP (2008). Physiographically sensitive mapping of climatological temperature and precipitation across the conterminous United States. International Journal of Climatology 28:2031–2064, doi:10.1002/joc.1688, URL http://dx.doi.org/10.1002/joc.1688528

Déqué, M., Rowell, D.P., Lüthi, D. et al. Climatic Change (2007) 81(Suppl 1): 53. https://doi-org.udel.idm.oclc.org/10.1007/s10584-006-9228-x

Diffenbaugh, N. S., Giorgi, F., & Pal, J. S. (2008). Climate change hotspots in the United States. Geophys. Res. Lett. Geophysical Research Letters, 35(16). doi:10.1029/2008gl035075

Donat, M. G., Alexander, L. V., Yang, H., Durre, I., Vose, R., Dunn, R. J., . . . Kitching, S. (2013). Updated analyses of temperature and precipitation extreme indices since the beginning of the twentieth century: The HadEX2 dataset. Journal of Geophysical Research: Atmospheres, 118(5), 2098-2118. doi:10.1002/jgrd.50150

Downing, T., Butterfield, R., Bindi, M., Brooks, R., Carter, T., Delécolle, R., . . . Wolf, J. (2002). Scaling Methods in Regional Integrated Assessments: From Points Upward and from Global Models Downwards. Integrated Assessment, 3(2-3), 167-187. doi:10.1076/iaij.3.2.167.13570

Ezer, T., & Atkinson, L. P. (2014). Accelerated flooding along the U.S. East Coast: On the impact of sea-level rise, tides, storms, the Gulf Stream, and the North Atlantic Oscillations. *Earth's Future*, 2(8), 362-382. doi:10.1002/2014ef000252

Foley, A. (2010). Uncertainty in regional climate modelling: A review. Progress in Physical Geography, 34(5), 647-670. doi:10.1177/0309133310375654

Gallant, A. J., Karoly, D. J., & Gleason, K. L. (2014). Consistent Trends in a Modified Climate Extremes Index in the United States, Europe, and Australia. Journal of Climate J. Climate, 27(4), 1379-1394. doi:10.1175/jcli-d-12-00783.1

Gleason, K. L., Lawrimore, J. H., Levinson, D. H., Karl, T. R., & Karoly, D. J. (2008). A Revised U.S. Climate Extremes Index. Journal of Climate J. Climate, 21(10), 2124-2137. doi:10.1175/2007jcli1883.1

Habeeb, D., Vargo, J., & Stone, B. (2015). Rising heat wave trends in large US cities. Natural Hazards, 76(3), 1651-1665. doi:10.1007/s11069-014-1563-z

Heim, R. R. (2002). A Review of Twentieth-Century Drought Indices Used in the United States. Bulletin of the American Meteorological Society, 83(8), 1149-1165. doi:10.1175/1520-0477(2002)083<1149:arotdi>2.3.co;2

Hirsch, R. M., 2011: A perspective on nonstationarity and water management. J. Amer. Water Resour. Assoc., 47, 436–446.

Hirsch, R. M., and K. R. Ryberg, 2012: Has the magnitude of floods across the USA changed with global CO2 levels? Hydrol. Sci. J., 57, 1–9.

Hodgkins, G. A., 2010: Historical changes in annual peak flows in Maine and implications for floodfrequency analyses. U.S. Geological Survey Scientific Investigations Rep. 2010-5094, 38 pp. [Available online at http://pubs.usgs.gov/sir/2010/5094/pdf /sir2010-5094.pdf.]

Hoerling, M. P., Eischeid, J. K., Quan, X., Diaz, H. F., Webb, R. S., Dole, R. M., & Easterling, D. R. (2012). Is a Transition to Semipermanent Drought Conditions Imminent in the U.S. Great Plains? Journal of Climate, 25(24), 8380-8386. doi:10.1175/jcli-d-12-00449.1

Horton, R., G. Yohe, W. Easterling, R. Kates, M. Ruth, E. Sussman, A. Whelchel, D. Wolfe, and F. Lipschultz, 2014: Ch. 16: Northeast. Climate Change Impacts in the United States: *The Third National Climate Assessment*, J. M. Melillo, Terese (T.C.) Richmond, and G. W. Yohe, Eds., U.S. Global Change Research Program, 16-1-nn.

IPCC, 2001: Climate Change 2001: The Scientific Basis. Contribution of Working Group I to the Third Assessment Report of the Intergovernmental Panel on Climate Change [Houghton, J.T., Y. Ding, D.J. Griggs, M. Noguer, P.J. van der Linden, X. Dai, K. Maskell, and C.A. Johnson (eds.)]. Cambridge University Press, Cambridge, United Kingdom and New York, NY, USA, 881pp.

IPCC (2014). “Scenario Process For AR5.” Retrieved August 02, 2016, from http://sedac.ipcc-data.org/ddc/ar5_scenario_process/RCPs.html

Jacobi, J., Perrone, D., Duncan, L. L., & Hornberger, G. (2013). A tool for calculating the Palmer drought indices. Water Resources Research Water Resour. Res., 49(9), 6086-6089. doi:10.1002/wrcr.20342

Karl, T. R., Knight, R. W., Easterling, D. R., & Quayle, R. G. (1996). Indices of Climate Change for the United States. Bulletin of the American Meteorological Society, 77(2), 279-292. doi:10.1175/1520-0477(1996)0772.0.co;2

Karl, T. R., J. M. Melillo, and T. C. Peterson, Eds., 2009: Global Climate Change Impacts in the United States. Cambridge University Press, 188 pp.

Kunkel, K. E., and Coauthors, 2013: Monitoring and understanding changes in extreme storm statistics: State of knowledge. Bull. Amer. Meteor. Soc., 94, 499–514.

Lu, J., Sun, G., Mcnulty, S. G., & Amatya, D. M. (2005). A Comparison Of Six Potential Evapotranspiration Methods For Regional Use In The Southeastern United States. Journal of the American Water Resources Association, 41(3), 621-633. doi:10.1111/j.1752-1688.2005.tb03759.x

Maurer, E.P., A.W. Wood, J.C. Adam, D.P. Lettenmaier, and B. Nijssen, 2002, A Long-Term Hydrologically-Based Data Set of Land Surface Fluxes and States for the Conterminous United States, J. Climate 15(22), 3237-3251

Mearns, L.O., Giorgi F, McDaniel L, Brodeur CS (1995) Analysis of daily variability and diurnal range of temperature in a nested regional climate model: comparison with observations and dou- bled CO_2 results. Clim Dyn 11:193–209

Mearns, L.O., et al., 2007, updated 2014. The North American Regional Climate Change Assessment Program dataset, National Center for Atmospheric Research Earth System Grid data portal, Boulder, CO.

Moglen, G. E., & Vidal, G. E. (2014). Climate Change and Storm Water Infrastructure in the Mid-Atlantic Region: Design Mismatch Coming? Journal of Hydrologic Engineering J. Hydrol. Eng., 19(11), 04014026. doi:10.1061/(asce)he.1943-5584.0000967

Monaghan, A. J., Moore, S. M., Sampson, K. M., Beard, C. B., & Eisen, R. J. (2015). Climate change influences on the annual onset of Lyme disease in the United States. Ticks and Tick-borne Diseases, 6(5), 615-622. doi:10.1016/j.ttbdis.2015.05.005

Mueller, N. D., Butler, E. E., Mckinnon, K. A., Rhines, A., Tingley, M., Holbrook, N. M., & Huybers, P. (2015). Cooling of US Midwest summer temperature extremes from cropland intensification. Nature Climate Change, 6(3), 317-322. doi:10.1038/nclimate2825

Najjar, R., Walker, H., Anderson, P., Barron, E., Bord, R., Gibson, J., . . . Swanson, R. (2000). The potential impacts of climate change on the mid-Atlantic coastal region. Climate Research Clim. Res., 14, 219-233. doi:10.3354/cr014219

Nakićenović, N. (2000). Special report on emissions scenarios: A special report of Working Group III of the Intergovernmental Panel on Climate Change. Cambridge: Cambridge University Press.

NARCCAP (2008). "About NARCCAP." Retrieved from http://www.narccap.ucar.edu/about/index.html

Ning, L., & Bradley, R. S. (2015). Winter Climate Extremes over the Northeastern United States and Southeastern Canada and Teleconnections with Large-Scale Modes of Climate Variability*. Journal of Climate J. Climate, 28(6), 2475-2493. doi:10.1175/jcli-d-13-00750.1

Ning, L., Mann, M. E., Crane, R., Wagener, T., Najjar, R. G., & Singh, R. (2012). Probabilistic Projections of Anthropogenic Climate Change Impacts on Precipitation for the Mid-Atlantic Region of the United States*. Journal of Climate J. Climate, 25(15), 5273-5291. doi:10.1175/jcli-d-11-00565.1

NOAA (2015). "U.S. Climate Extremes Index (CEI): Introduction." Retrieved from https://www.ncdc.noaa.gov/extremes/cei/introduction

National Weather Services (2012). "Heat Safety Tips." Retrieved from http://www.nws.noaa.gov/os/heat/index.shtml

Palmer, W. C., 1965: Meteorological drought. U.S. Department of Commerce Weather Bureau Research Paper 45, 58 pp.

Peterson, T. C., Heim, R. R., Hirsch, R., Kaiser, D. P., Brooks, H., Diffenbaugh, N. S., . . . Wuebbles, D. (2013). Monitoring and Understanding Changes in Heat Waves, Cold Waves, Floods, and Droughts in the United States: State of Knowledge. Bull. Amer. Meteor. Soc. Bulletin of the American Meteorological Society, 94(6), 821-834. doi:10.1175/bams-d-12-00066.1

Peterson, T. C., and Coauthors, 2008: Why weather and climate extremes matter. Weather and Climate Extremes in a Changing Climate. Regions of Focus: North America, Hawaii, Caribbean, and U.S. Pacific Islands, T. R. Karl et al., Eds., U.S. Climate Change Science Program and the Subcommittee on Global Change Research, 11–33

Polsky, C., Allard, J., Crane, R., & Yarnal, B. (2000). The Mid-Atlantic Region and its climate: Past, present, and future. Climate Research Clim. Res., 14, 161-173. doi:10.3354/cr014161

Rauscher, S. A., Pal, J. S., Diffenbaugh, N. S., & Benedetti, M. M. (2008). Future changes in snowmelt-driven runoff timing over the western US. Geophys. Res. Lett. Geophysical Research Letters, 35(16). doi:10.1029/2008gl034424

Sallenger, A.H., Doran, K.S., and Howd, P.A., 2012: Hotspot of accelerated sea level rise on the Atlantic coast of North America. *Nature Climate Change*, **2**, 884-888. doi:10.1038/nclimate1597

Sarofim, M.C., S. Saha, M.D. Hawkins, D.M. Mills, J. Hess, R. Horton, P. Kinney, J. Schwartz, and A. St. Juliana, 2016: Ch. 2: Temperature-Related Death and Illness. The Impacts of Climate Change on Human Health in the United States: A Scientific Assessment. U.S. Global Change Research Program, Washington, DC, 43–68. http://dx.doi.org/10.7930/J0MG7MDX

Schoof, J. T., & Robeson, S. M. (2016). Projecting changes in regional temperature and precipitation extremes in the United States. Weather and Climate Extremes, 11, 28-40. doi:10.1016/j.wace.2015.09.004

Schrier, G. V., Jones, P. D., & Briffa, K. R. (2011). The sensitivity of the PDSI to the Thornthwaite and Penman-Monteith parameterizations for potential evapotranspiration. Journal of Geophysical Research, 116(D3). doi:10.1029/2010jd015001

Sheffield, J., Wood, E. F., & Roderick, M. L. (2012). Little change in global drought over the past 60 years. Nature, 491(7424), 435-438. doi:10.1038/nature11575

Smith, J. A., M. L. Baeck, G. Villarini, and W. F. Krajewski, 2010: The hydrology and hydrometeorology of flooding in the Delaware River basin. J. Hydrometeor., 11, 841–859.

State of Delaware (2014). “Delaware Geography.” Retrieved July 11, 2016, from http://delaware.gov/topics/facts/geo.shtml

Strzepek, K., Yohe, G., Neumann, J., & Boehlert, B. (2010). Characterizing changes in drought risk for the United States from climate change. Environ. Res. Lett. Environmental Research Letters, 5(4), 044012. doi:10.1088/1748-9326/5/4/044012

Taylor, K.E., R.J. Stouffer, G.A. Meehl: An Overview of CMIP5 and the experiment design.” Bull. Amer. Meteor. Soc., 93, 485-498, doi:10.1175/BAMS-D-11-00094.1, 2012.

Thornton PE, Running SW, White MA (1997) Generating surfaces of daily meteorolog- 673 ical variables over large regions of complex terrain. Journal of Hydrology 190:214–251, 674 doi:10.1016/S0022-1694(96)03128-9, URL http://www.sciencedirect.com/science/ 675 article/pii/S0022169496031289

UCAR (2011). “Climate Modelling.” Retrieved July 11, 2016, from http://scied.ucar.edu/longcontent/climate-modeling

Villarini, G., and J. A. Smith, 2010: Flood peak distributions for the eastern United States. Water Resources., 46, W06504, doi:10.1029/2009WR008395.

Wang, L., & Chen, W. (2013). A CMIP5 multimodel projection of future temperature, precipitation, and climatological drought in China. International Journal of Climatology Int. J. Climatol., 34(6), 2059-2078. doi:10.1002/joc.3822

Walsh, J., D. Wuebbles, K. Hayhoe, J. Kossin, K. Kunkel, G. Stephens, P. Thorne, R. Vose, M. Wehner, J. Willis, D. Anderson, S. Doney, R. Feely, P. Hennon, V. Kharin, T. Knutson, F. Landerer, T. Lenton, J. Kennedy, and R. Somerville, 2014: Ch. 2: Our Changing Climate. Climate Change Impacts in the United States: The Third National Climate Assessment, J. M. Melillo, Terese (T.C.) Richmond, and G. W. Yohe, Eds., U.S. Global Change Research Program, 19-67. doi:10.7930/J0KW5CXT.

Wehner, M. F. (2012). Very extreme seasonal precipitation in the NARCCAP ensemble: model performance and projections. Climate Dynamics, 40(1-2), 59-80. doi:10.1007/s00382-012-1393-1

Wells, N., Goddard, S., & Hayes, M. J. (2004). A Self-Calibrating Palmer Drought Severity Index. Journal of Climate, 17(12), 2335-2351. doi:10.1175/1520-0442(2004)017

Wuebbles, D., Meehl, G., Hayhoe, K., Karl, T. R., Kunkel, K., Santer, B., ... Sun, L. (2014). CMIP5 climate model analyses: Climate extremes in the United States. Bulletin of the American Meteorological Society, 95(4), 571-583. DOI: 10.1175/BAMS-D-12-00172.1

Ye, J., Y. Gong, F. Zhang, J. Ren, X. Bai, and Y. Zheng, 0: Which temperature and precipitation extremes best explain the variation of warm vs. cold years and wet vs. dry years?. J. Climate, 0, https://doi.org/10.1175/JCLI-D-17-0377.1